Electronic Structure and Nonadiabatic Dynamics in the Photoisomerization of Polyenes

Masakatsu Ito

Doctor of Philosophy

Department of Structural Molecular Science,
School of Mathematical and Physics Science,
The Graduate University for Advanced Studies,

1996 (School Year)

Contents

List of Tables

List of Figures

Acknowledgments

This study has been carried out under the direction of Professor Iwao Ohmine at the Institute for Molecular Science (IMS) and Nagoya University since 1992. Electronic structure calculations were performed with the package programs, MOLPRO94, GAUSSIAN94, GAMESS and MELD. The other programs were newly developed to construct the model Hamiltonian, perform the nonadiabatic dynamics simulation, and analyze the result. Most programming, calculations and analyses were held on HP9000/735,J,K.

I wish to take this opportunity to express my sincere thanks to Professor Iwao Ohmine, for his supervising my research, discussing with me, and encouraging me. We have discussed the way of investigation in front of the white board, and the discussion with him and the other members of his group have shown me how the theoretical chemists find out the points from complex phenomena.

I am obliged to Professor Keitaro Yoshihara, Dr. Hrvoje Petek, and Mr. Kaoru Ohta for their valuable discussion on the spectroscopies of polyenes. Their experiments stimulated me to perform the simulation of the nonadiabatic dynamics. I am glad to thank Professor Bryan E. Kohler. He responded to my inquiry and without his experiments, the present studies would be totally misled.

I would like to thank Prof. Nobuaki Koga for the discussion on the construction of the σ bond force field.

I am indebted to Dr. Tamiki Komatsuzaki, Dr. Shoji Takada, Dr. Shinji

Saito and Dr. Masakazu Matsumoto for their warm support and their comments on my work. Dr. Komatsuzaki taught me the technique and the underlying philosophy of the parameter fitting, and he installed the least square fitting program which helped me to construct the model Hamiltonian. When we were at IMS, Dr. Takada drove his car to take us to a supper almost everyday. And until the midnight we enjoyed talking about various topics. Dr. Saito has kindly answered to my various inquiries. He showed his classical trajectory program to me and his explanation for it is very helpful to me in developing my semiclassical trajectory program. Dr. Matsumoto helped me to enjoy the object-oriented programming (C++) and X Window programming. The discussion with him is helpful to me to invent the various algorithms.

I also thank Mr. Kosuke Doga and Mr. Kensuke Iwahashi for their help to arrange the programming environment.

At the end, I wish to express my sincere gratitude to my parent, Masao and Reiko, for their warm encouragement and unchangeable supports.

Chapter 1

General Introduction

Polyenes are versatile compounds with linear conjugated chain of carbon atoms joined by alternating double and single bonds. Long polyenic chains appear in many important organic molecules, including light-harvesting chromophore, vitamins, fatty acid and antibiotics. Their diverse reactivities with the special selectivities are intriguing subjects of investigations. The fundamental importance of ultra fast cis-trans isomerization in photochemistry is distinctive. Biologically, photoisomerization plays a major role in the visual system and the photosynthetic bacteria. [1, 2]

In the Born-Oppenheimer description, the investigation of the ultra fast photoisomerization process involves two steps. The first step is to deal with static aspect of the electronic structure of the polyene chromophore. The electronic structure calculations are performed to obtain the potential energy surfaces (PES) and the nonadiabatic couplings involved in the isomerization. Locating the funnel of PES with intense nonadiabatic coupling is of special importance. We then need to analyze the nonadiabatic dynamics of the process as the second step. When the system approaches the locus where the potential energies of two or more electronic states get mutually very close, it yields the mixing of these adiabatic electronic states. This mixing is described as the nonadiabatic transition. The nonadiabatic dynamics simulation is needed to the relaxation mechanism and the time evolution of the state

occupation probability.

The photoisomerization dynamics is multidimensional in nature. The electronic structure and the dynamics should be treated in multi-dimensional conformational space. The polyene isomerization involves simultaneous multi-π bond torsions and many electronic configuration state functions are necessary to describe the electronic structures. Until recently, the full multi-dimensionality has not be taken accounted in almost all trajectory calculations. The isomerization shifts the conjugated π bonding character and thus alters the electronic structures of the low lying states. To describe these states, a careful choice of the electronic configurations in the configuration interaction (CI) method is required.

Along the whole isomerization paths, the π-electron states of polyenes are specified as either Ag or Bu symmetry which are of the irreducible representation of the planar polyene with the C_{2h} symmetry. There are three low lying states involved in the photoisomerization, 1^1Ag, 1^1Bu, and 2^1Ag. The 1^1Bu state is optically allowed at the planar geometry while the 2^1Ag state is optically forbidden. Although the lowest excited state at the planar geometry is the 1^1Bu state in the simple molecular orbital (MO) description, the experiments and theoretical investigations have revealed that the 2^1Ag state locates below the 1^1Bu state in polyenes. [3, 4, 5, 6, 7, 8]

There have been numerous investigations to study the mechanism of the polyene photoisomerization. A proposed mechanism is; the isomerization of ethylene or very short polyenes proceeds through 1^1Bu state, which degenerates with an ionic ^1Ag state and becomes so called a sudden polarization state at 90° C=C twisted geometry and then decays to the ground state. The hydrogen migration path at 90° C=C twisted geometry was also proposed. [9] Another mechanism suggested is that a polyene is initially excited to the optically allowed 1^1Bu state, then makes a rapid transition

to 2^1Ag state through the efficient internal conversion, and finally decays to the ground state by a nonadiabatic transition. Recent experiments have shown that the internal conversion from 1^1Bu to 2^1Ag is very fast (in tens of femto seconds).[10] This internal conversion occurs so fast that the polyene structure is still being nearly planar. The polyene then stays on the 2^1Ag state until it makes the nonadiabatic transition into the ground state (1^1Ag). Thus the 2^1Ag, and 1^1Ag states dominantly control the photoisomerization process. Recently Yoshihara and his coworkers have performed the ultra-fast time resolved flash photolisys on polyenes both in the condensed phase and in the jet-cooled condition and examined the mechanism of the internal conversion and the intramolecular vibrational relaxation in the hexatriene photoisomerization.[11, 12] The observed delayed response of their transient absorption signals in the condensed-phase shows that the vibrational energy redistribution in the 2^1Ag state occurs in less than 500 fs and this redistribution is due to the intrinsic nature of the excited state rather than the solvent-induced interaction. They attributed the first component of transient bleach recovery signals to the internal conversion from 2^1Ag to 1^1Ag and concluded that it occurs in $\sim$ 1 ps. The second component is attributed to the vibrational relaxation process in 1^1Ag and the process occurs in 15 $\sim$ 20 ps.

By using a model calculation, Zerbetto and Zgierski have proposed that a nonadiabatic transition from 2^1Ag to 1^1Ag is induced by the CC torsions.[13] Robb and his coworkers have proposed that the triple CC torsion which leads to the conical crossing of 2^1Ag to 1^1Ag states is the major path to yield a very fast nonadiabatic transition. [14, 15, 16] Their complete active space self consistent field(CASSCF)/4-31G calculation have scanned an entire conformational space over all three CC bond torsional degrees, and found that 2^1Ag degenerates with 1^1Ag at the conformations where three CC bonds are

partially twisted. [14]

Numerous ab-initio calculations have performed on the potential surfaces of butadiene, and the various isomerization paths have been proposed. [9, 13, 14, 15, 17] These decay mechanisms must play an important role also in photoisomerization processes of longer polyenes. The fluorescence measurement of octatetraene and its derivatives by Peteck et al. showed that there exists a very fast disposal channel at about $2000cm^{-1}$ above the bottom of the 2^1Ag planar minimum. [11] This disposal channel was also attributed to the fast internal conversion from 2^1Ag to 1^1Ag state at a triply twisted CC bond conformation. [16] Kohler et al. have suggested that there exist adiabatic CC torsional isomerization paths on the 2^1Ag surface not involving the nonadiabatic transition. [18]

In this thesis, we focus our attention on the dynamical aspects of this internal conversion process from 2^1Ag to 1^1Ag of s-trans butadiene, especially the intramolecular mode dynamics promoting this conversion. We examine the multidimensional nature of the 2^1Ag and 1^1Ag potential energy surfaces and their nonadiabatic coupling in detail. We develop a model Hamiltonian describing these two covalent states and perform the trajectory calculations including the nonadiabatic transitions. In order to investigate various isomerization paths, the model Hamiltonian is simple enough for the efficient evaluation of the potential energy surfaces and the nonadiabatic coupling. Besides, the model must include all internal degrees of the molecule in order to treat the energy relaxation dynamics properly.

There have been considerable numbers of studies on model Hamiltonians.[19, 20, 21, 23, 24, 25] Malrieu, Maynau and coworkers have investigated the potential energy surfaces for the CC bond stretching and torsion by employing Heisenberg Hamiltonian.[19, 20, 21, 22] Bernardi et al. transformed the CASSCF wavefunction into the Heitler-London valence bond space via the

construction of an effective Hamiltonian.[24] Based on this simplified model, they could allocate the locus where 2^1Ag degenerates with 1^1Ag.[26] They also combined their Valence Bond (VB) model with Molecular Mechanics (MM) force field to optimize the geometry [25] and investigate the relaxation dynamics from the excited state of Benzene and Azulene[27, 28]. In the present calculation, we employ a similar model; a VB Hamiltonian is used to describe the localized π orbital interactions and is combined with the σ orbital description by a modified MM force field method.

A considerable number of calculations have been performed to investigate the photoisomerization processes of polyenes including nonadiabatic transitions [29, 30, 31, 32, 33, 34] ; the Golden-rule model of Gelber, Free and Rice [29], the phenomenological damped oscillator model of Bagchi, Fleming and Oxtoby [30], and the surface-hopping trajectory of rhodopsin by Warshel and his coworkers [31]. Since these treatments are often based on models which only include a part of internal molecular degrees of freedom, they might not fit to treat the irreversible character in the nonadiabatic transitions of the polyene photoisomerization processes, as indicated by the study of Domcke and collaborators. [34]

In this thesis we investigate the photoisomerization dynamics of polyene by generating the model Hamiltonian yielding the realistic potential energies and nonadiabatic coupling vectors. The CASSCF/DZ+d calculation is used to evaluate the 1^1Ag and 2^1Ag potential energies at various conformations in order to fit the parameters in the model Hamiltonian. The CASSCF level calculation is required to balance the description of these states along isomerization paths.

In part I of this thesis, we develop the model Hamiltonian based on the VB description of the π bond. The nature of the 1^1Ag and 2^1Ag PES along various isomerization paths is examined by using the model Hamiltonian.

The shape of each PES is interpreted in terms of the simple configurational interactions in the model Hamiltonian. The results are compared with the ab-initio calculation.

Potential energy surfaces of butadiene, hexatriene and octatetraene and the nonadiabatic couplings of butadiene are analyzed in detail.

In part II, we investigate the photoisomerization dynamics of butadiene by using the model Hamiltonian, which is parametrized in the full dimension with the ab-initio potential energies and nonadiabatic coupling vectors. The mechanisms of the nonadiabatic transition and the energy relaxation in the isomerization dynamics are analyzed in detail.

Bibliography

[1] B.S. Hudson, B.E. Kohler and K. Schulten, in Excited States, edited by E.C. Lim (Academic, New York, 1982), Vol. 6, p. 1. ; G. Orlandi, F. Zerbetto and M.Z. Zgierski, Chem. Rev. 91, 867 (1991)

[2] M. Mimuro and T. Katoh, Pure Appl. Chem. 63, 123 (1991); R.R. Bierge, Biochim. Biophys. Acta 293, 1016 (1990); H.J.C. Jacobs and E. Havinga, in Advances in Photochemistry, Vol. 11, edited by J.N. Pitts, Jr., G.S. Hammond, K. Gollnick and D. Grosjean (Willy, New York, 1979), p. 305.

[3] B.R. Hudson, B.E. Kohler, Chem. Phys. Lett. 14, 299 (1972); B.R. Hudson, B.E. Kohler, J. Chem. Phys. 59, 4984 (1973)

[4] K. Schulten, I. Ohime, and M. Karplus, J. Chem. Phys. 64, 4422 (1976)

[5] I. Ohmine, M. Karplus, and K. Schulten, J. Chem. Phys. 68, 2298 (1978)

[6] K. Schulten and M. Karplus, Chem. Phys. Lett. 14, 305 (1972); K. Schulten, Thesis, Harvard University, March 1974

[7] J. Koutecky, J. Chem. Phys. 47, 1501 (1967)

[8] T.H. Dunning, Jr., R. P. Hosteny, and I. Shhavitt, J. Am. Chem. Soc. 95, 5067 (1973)

[9] I. Ohmine, J. Chem. Phys. 83, 2348 (1985)

[10] M.O.Trulson and R.A.Mathies, J.Phys.Chem. 94, 5741 (1990); D.L.Phillips et al., ibid. 97,1800 (1993); X. Ci and A.B. Myers, J.Chem.Phys. 92, 4708 (1990); X. Ci and A.B. Myers, ibid. 96, 6433 (1992); C.C. Hayden and D.W. Chandler, ibid. 99 ,7897 (1995); P.O. Anderson and T. Gillbro, ibid. 103, 2509 (1995); K. Ohta, Y. Naitoh, K. Saitow, K. Tominaga, N. Hirota and K. Yoshihara, Chem. Phys. Lett. 256, 629 (1996);

[11] H. Petek, A.J. Bell, R.L. Christensen and K. Yoshihara, J. Chem. Phys. 96, 2412 (1992); H. Petek, A.J. Bell, K. Yoshihara, B.A. Tounge and R.L. Christensen, ibid. 98, 3777 (1993)

[12] K. Ohta, Y. Naitoh, K. Saitow, K. Tominaga, N. Hirota and K. Yoshihara, Chem. Phys. Lett. 256, 629 (1996);

[13] F. Zerbetto and M. Z. Zgierski, J. Chem. Phys. 93, 1235 (1990)

[14] M. Olivucci, I. N. Ragazos, F. Bernardi and M. A. Robb, J. Am. Chem. Soc. 115, 3710 (1993)

[15] P. Celani, F. Bernardi, M. Olivucci and M. A. Robb, J. Chem. Phys. 102, 5733 (1995)

[16] P. Celani, M. Gravelli, S. Ottani, F. Bernardi, M.A. Robb and M.Olivucci, J.Am.Chem.Soc. 117, 11584 (1995)

[17] M.Aoyagi, Y. Osamura and S. Iwata, J. Chem. Phys. 83, 1140 (1985)

[18] B. E. Kohler, Chem. Rev. 93, 41 (1993);

[19] J.P. Marlrieu and D. Maynau, J.Am.Chem.Soc. 104,3021 (1982); D. Maynau and J.P. Malrieu, ibid. 104, 3029 (1982)

[20] M. Said, D. Maynau, J.P. Malrieu and M.A.G.Bach, J.Am.Chem.Soc. 106, 571 (1984); M. Said, D. Maynau and J.P. Malrieu, ibid. 106, 580 (1984)

[21] G. Treboux, D. Maynau and J.P. Malrieu, J.Phys.Chem. 99 , 6417 (1995)

[22] P.Durand and J.P. Malrieu, Adv.Chem.Phys. 76,321(1987)

[23] A. Warshel in, 'MODERN THEORETICAL CHEMISTRY',Vol. 7, p133, eds.G. A. Segal, PLENUM PRESS,NEW YORK AND LONDON

[24] F. Bernardi, M. Olivucci, J. J. W. McDouall and M. A. Robb, J. Chem. Phys. 89, 6365 (1988)

[25] F. Bernardi, M. Olivucci and M. A. Robb, J. Am. Chem. Soc. 114, 1606 (1992)

[26] F. Bernardi, S. De, M. Olivucci and M.A. Robb, J.Am.Chem.Soc. 112,1737 (1990)

[27] B.R. Smith, M.J. Bearpark, M.A. Robb, F. Bernardi and M. Olivucci, Chem.Phys.Lett. 242, 27 (1995)

[28] M.J. Bearpark, F. Bernardi, S. Clifford, M. Olivucci, M.A. Robb, B.R. Smith and T. Vreven, J.Am.Chem.Soc. 118, 169 (1996)

[29] W. M. Gelbart, K. F. Freed and S. A. Rice, J. Chem. Phys. 52, 2460 (1970)

[30] B. Bagchi, G. R. Fleming and D. W. Oxtoby, J. Chem. Phys. 78, 7375 (1983)

[31] A. Warshel, Z. T. Chu and J. K. Hwang, Chem. Phys. 158, 303 (1991)

[32] G. J. M. Dormans, G. C. Groenenboo and H. M. Buck, J. Chem. Phys. 86, 4895 (1987)

[33] M. Perisco, J. Am. Chem. Soc. , 102 , 7839 (1980)

[34] L. Seiner and W. Domcke Chem. Phys. 186, 27 (1994) ; H. Köppel, W. Domcke and L. S. Cederbaum, Advan. Chem. Phys. 57, 59 (1984) ; R. Schnider, W. Domcke and H. Köppel, J. Chem. Phys. 92, 1045 (1990)

Part I

Electronic Structure of Low Lying Singlet States

Chapter 2

Introduction

To understand the mechanism of polyene photoisomerization processes, a detailed knowledge of the electronic structures and the potential energy surfaces of the polyene molecules is required. The shape of the potential energy surfaces such as the position of minima, funnels, and barriers is the key factor to determine the isomerization paths including the nuclear tunneling and the nonadiabatic transition. The nonadiabatic transitions take place near the intersection among the potential energy surfaces.

The photoisomerization dynamics is strongly controlled by the internal conversion process. It is known that butadiene and hexatriene has much shorter fluorescence lifetime than octatetraene. The 2^1Ag state planar conformations of butadiene and hexatriene are not stable and thus undergoes a facile CC torsion followed by the nonadiabatic transition, while that of octatetraene is stable. The octatetraene has the longest fluorescence lifetime among all linear polyenes.

Numerous ab-initio calculations have performed on the potential surfaces of butadiene, and the various isomerization paths which causes the large nonadiabatic transition have been proposed.[1, 2, 3, 5, 4] The CASSCF/4-31G calculation of M. Olivucci et. al. have scanned an entire conformational space over all three CC bond torsional degrees, and found that 2Ag degenerates with 1Ag at the conformations where three CC bonds are partially

twisted.[3, 5]

Recently ultra-fast time resolved experiments have found the existence of the strong excess energy dependence in the fluorescence and the internal conversion rates of hexatriene. Petek et al. have demonstrated that cis-hexatriene has a nonradiative decay channel involving an activation energy between 71.3 and 157.7 cm^{-1}, Ohta et al. have measured the transient bleach signals of trans-hexatriene and shown that the internal conversion from 2^1Ag to 1^1Ag takes place within $\sim$ 1 ps.

These experiments suggest that hexatriene in 2^1Ag state isomerizes with only a very small activation energy to the conformation where the energy gap between 2^1Ag and 1^1Ag is quite small and thus the facile nonadiabatic transition can take place. Olivucci et al. have used the CASSCF/4-31G or DZ+d and CASPT2 calculations to demonstrate that the conformation responsible for the facile nonadiabatic transition involves three partially twisted CC bonds and a sharp "kink" at a $-(CH)_3-$ segment in the middle of the molecules.[6]

By the florescence measurement of all trans-octatetraene and its derivatives, Petek et al. showed that Octatetraene also has an very fact internal conversion channel with a considerable activation energy barrier ($\sim$ $2200cm^{-1}$) above the 2^1Ag planar minimum ,[7] yielding the longest fluorescence lifetime among all polyenes. Kohler et al. have suggested that Z/E-photoisomerization yield of octatetraene is explained on the basis of the adiabatic CC torsional isomerization paths on the 2^1Ag state. [8]

An extensive ab-initio calculation does provide the precise potential energy surfaces, but its wavefunction involves numerous determinants, which is hard to interpret in a simple physical picture. If one requires some explanation, reduction of information must be necessary. Such a rational reduction of information is a goal of theoretical chemistry, and this must proceed through

physical grounded simplified schemes.

The π system in the ethylene molecule can be described through a simple model as a prototype of a π bond. The σ electrons are treated only at the SCF level, having a nonpolarizable time-averaged charge distribution. For describing the π electron, we use here only a pair of nonorthogonal atomic orbitals (Fig.2.1).

The ethylene photoisomerization process is well described by the simplified 3×3 Hamiltonian.[9] Although the MO picture without the configuration interaction quantitatively fails to predict the ethylene isomerization from the planar conformation, it is still possible to understand the roughly shape of the potential energy curves (Fig.2) by considering the MO energies alone.

Figure 2.1: Localized π orbitals as the minimum basis for the π system

A valence bond based picture also gives similar interpretation, and a considerable number of dynamic simulation [10, 11, 12, 13, 14, 15] has been performed to investigate the photoisomerization process of ethylene like molecules on the basis of this picture. The sudden polarization and the hydrogen migration at the 90° twisted conformation is easily interpreted by this picture though no realistic dynamical simulation including these processes has been performed so far.

This picture bases on the electronic state correlation along a reaction path is useful for many other reactions. For example, the ground state selectivities of pericyclic reactions are well explained on this picture, i.e. Woodward-Hoffman rule.[16]

This picture is, however, not well applicable for a description of the polyene

photoisomerization dynamics, since a large number of configurations are involved in the polyene electronic states. Instead, numerous studies based on various model Hamiltonians have been performed to describe the potential energy surface (PES) of the polyene electronic states.[17, 18, 19, 20, 21, 22] The models are generally parametrized from experimental data or ab-initio calculations. They would involve the semi-empirical Hamiltonians of solid state physics (Hüchel, Hubbard, Pariser-Parr-Pople (PPP), Heisenberg, our VB type Hamiltonian, $\cdots$). The effective Hamiltonian is also useful for the rational reduction of information obtained from the ab-initio calculations. The term 'effective Hamiltonian' denotes for Hamiltonian obtained by projecting a exact wavefunction onto a finite model space. The corresponding theory is well established and various practical procedures are well documented.

Malrieu and Maynau applied the quasi-degenerate many body perturbation theory to the VB-CI matrix and the procedure result in a very simple Heisenberg Hamiltonian dominated by effective exchange interaction between adjacent atoms.[17] They have investigated the potential energy surfaces for the CC bond stretching and torsion of the polyene molecule by employing this Hamiltonian.[17, 18, 19, 23] Bernardi et al. transformed the CASSCF wavefunction into the Heitler-London valence bond space by constructing an effective Hamiltonian.[21] They used the resulting Heitler-London parameters Q and K_{ij} for a posteriori rationalization of the bonding effects in molecular structures. In particular, their procedure enabled the diabatization of the adiabatic potential surface in a rigorous way. Based on this simplified model, they could allocate the locus where 2^1Ag degenerates with 1^1Ag.[24]

They also combined their Valence Bond (VB) model with Molecular Mechanics (MM) force field to optimize the geometry [22] and investigate the relaxation dynamics from the excited state of Benzene and Azulene[25, 26].

In the present work, we employ a similar Heisenberg model; a VB Hamil-

tonian is used to describe the localized π orbital interactions and is combined with the σ orbital description by a modified MM force field method. We have examined if the Heisenberg Hamiltonian can describe the electronic structure of various isomerized polyene conformations. For longer polyenes, many VB structures are necessary to describe the electronic states and numerous isomerization paths exist. We have found that various features of the polyene potential energy surfaces are easily rationalized in this model. Especially for s-trans butadiene we can construct the model Hamiltonian which is accurate enough to be used in a nonadiabatic dynamics simulation. For hexatriene, we only examine the Heisenberg model to fit PES along the CC isomerizations. The SA-CASSCF calculation is used to evaluate the 1^1Ag and 2^1Ag potential energies at various conformations in order to fit the parameters in the model Hamiltonian. The CASSCF level calculation is needed for the balanced description of these states along the isomerization paths. The characteristics of octatetraene PES is also analyzed by the ab-initio calculation.

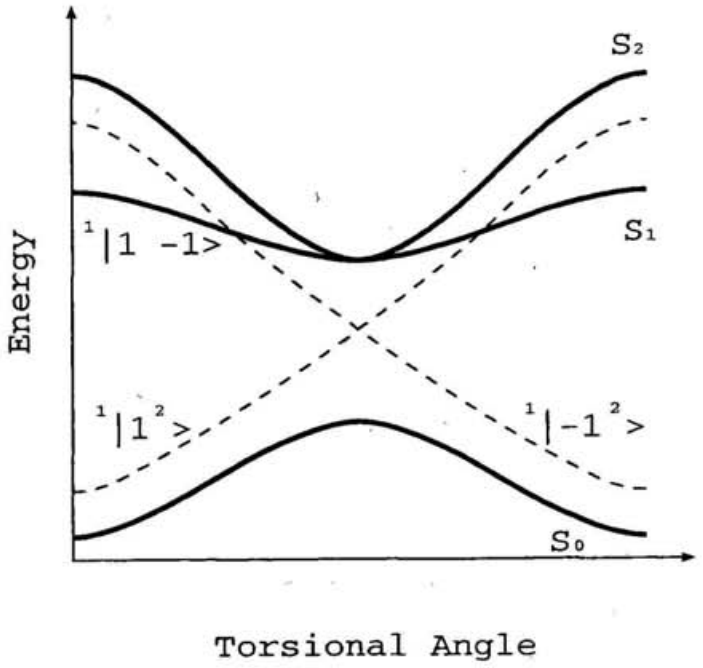

Figure 2.2: State diagram for ethylene as a function of the torsional angle. $^1|1^2>$ is the ground state configuration with the bonding orbital $|1>$ doubly occupied. $^1|1\ -\ 1>$ is the singly excited configuration where one electron is in the bonding orbital $|1>$ and the other is in the anti-bonding orbital $|-1>$. $^1|1^2>$ is the doubly excited configuration.

Chapter 3

Model Hamiltonian

The model electronic Hamiltonian consists of the π and σ parts. [27]

$$\mathbf{H} = \mathbf{H}_{\pi} + V_{\sigma}\mathbf{I} \tag{3.1}$$

The π part describing the π electronic structure change along the isomerization is approximated by Heisenberg Hamiltonian. The σ part is assumed to be independent of the π part, and a simple function of the internal molecular degrees of freedom.

3.1 Description of 1Ag and 2Ag states

Heisenberg Hamiltonian is based on the VB description of the electronic wave functions.[17, 18, 19, 23] Since 1^1Ag and 2^1Ag states are covalent states, their electronic wavefunctions along the isomerization are approximately expanded with neutral VB bases and the effect of ionic VB bases is effectively incorporated into the model Hamiltonian through the spin dependent interaction.

In a system with four π electrons, there are two ways of the spin coupling to construct a singlet spin function [28](Fig.3.1), the perfect pairing φ_1^{VB} which dominates in the 1^1Ag state at the planar conformation and so called the double triplets φ_2^{VB} which dominates in the 2^1Ag state;

$$\varphi_1^{VB} = \frac{1}{2}(|1\bar{2}3\bar{4}| - |1\bar{2}\bar{3}4| - |\bar{1}23\bar{4}| + |\bar{1}2\bar{3}4|) , \tag{3.2}$$

$$\varphi_2^{VB} = \frac{1}{2\sqrt{3}}(2|12\bar{3}\bar{4}| - |1\bar{2}3\bar{4}| - |1\bar{2}\bar{3}4| - |\bar{1}23\bar{4}| - |\bar{1}2\bar{3}4| + 2|\bar{1}\bar{2}34|) . \quad (3.3)$$

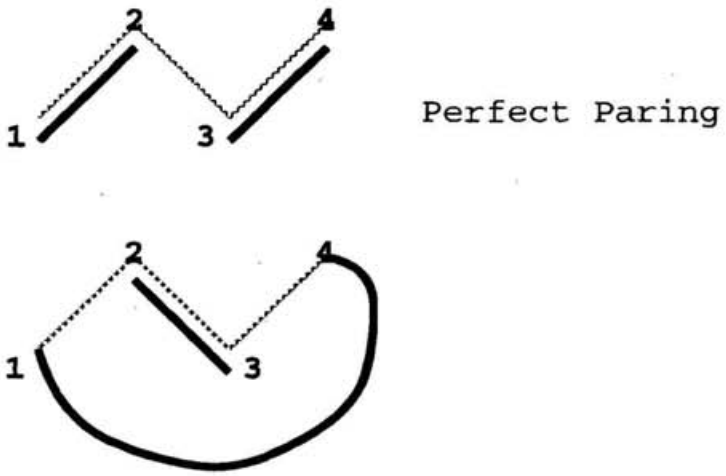

Figure 3.1: Two spin couplings to construct a singlet spin function

3.2 The Effective Interactions in the Model Hamiltonian

The model Hamiltonian accounts for effective interactions among a pair of the π electrons on i'th and the j'th carbon atoms in the neutral VB bases with the interaction strength $g_{i,j}$. The numbering of carbon atoms are shown in Fig.3.2.

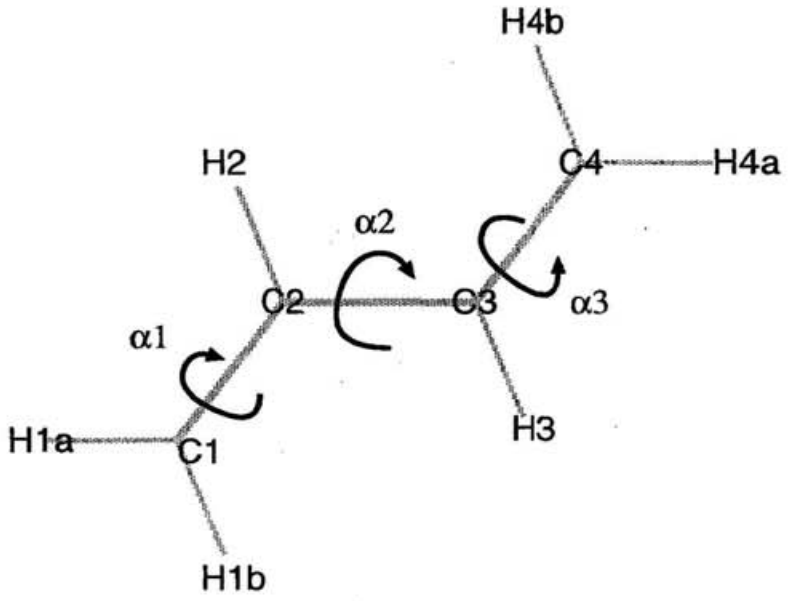

Figure 3.2: Numbering of atoms and torsions

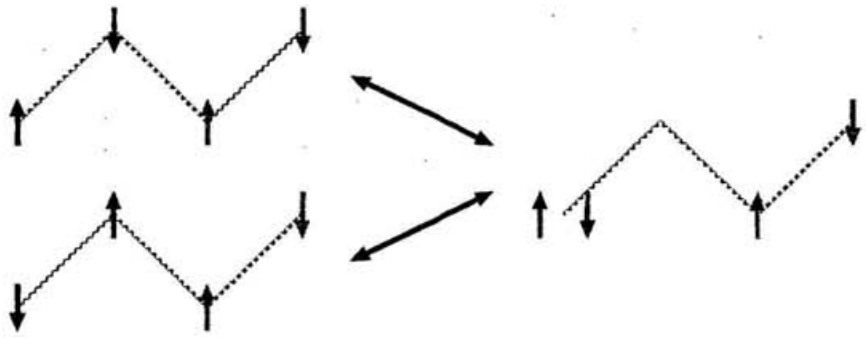

The parallel spins in a neutral VB base cannot interact with an ionic VB base, that is, an electron can not jump into an orbital occupied by an electron with the same spin, and thus the model Hamiltonian includes only the interactions among anti-parallel spins,

$$\begin{aligned}\mathbf{H}_\pi &= \sum_{i<j} g_{i,j}(\mathbf{a}_i^\dagger \mathbf{a}_{\bar{j}}^\dagger \mathbf{a}_{\bar{j}} \mathbf{a}_i + \mathbf{a}_i^\dagger \mathbf{a}_j^\dagger \mathbf{a}_j \mathbf{a}_{\bar{i}} - \mathbf{a}_i^\dagger \mathbf{a}_j^\dagger \mathbf{a}_j \mathbf{a}_{\bar{i}} - \mathbf{a}_{\bar{i}}^\dagger \mathbf{a}_j^\dagger \mathbf{a}_{\bar{j}} \mathbf{a}_i) \\ &= \sum_{i<j} g_{i,j}(|i\bar{j}\rangle\langle i\bar{j}| + |\bar{i}j\rangle\langle\bar{i}j| - |i\bar{j}\rangle\langle\bar{i}j| - |\bar{i}j\rangle\langle i\bar{j}|) \ . \end{aligned} \tag{3.4}$$

We assume that this Hamiltonian contains the two terms, the interaction between the neighboring orbitals ($\mathbf{H}_\pi^0$) and that between the next neighbors ($\mathbf{H}_\pi^1$),

$$\mathbf{H}_\pi = \mathbf{H}_\pi^0 + \mathbf{H}_\pi^1 \ . \tag{3.5}$$

The neighbor interaction contribution to the Hamiltonian elements are represented in VB basis (Eq.3.2 and 3.3) as

$$H_{\pi\,1,1}^0 = g_{1,2} + g_{3,4} \ , \tag{3.6}$$

$$H_{\pi\,1,2}^0 = -\frac{g_{2,3}}{\sqrt{3}} \ , \tag{3.7}$$

$$H_{\pi\,2,2}^0 = \frac{2g_{2,3} - g_{1,2} - g_{3,4}}{3} \ . \tag{3.8}$$

$g_{i,i+1}$ is assumed to be a product of functions of individual internal degrees and its functional form is determined by the nature of the bonding character, mainly related to the C_iC_{i+1} stretching and the C_iC_{i+1} torsion. It is thus assumed to be given by

$$g_{i,i+1} = g_i^0 \ \exp(-\mu_i r_i^{CC}) \ (\frac{1}{2} + k_i^{c2} \cos 2\alpha_i + k_i^{c4} \cos 4\alpha_i) \tag{3.9}$$

where r_i^{CC} is the distance and α_i is a torsional angle of the C_iC_{i+1} bond.

The parameterized Hamiltonian only including the neighbor interaction are fitted with the CASSCF/DZ+d energies to well reproduce the excitation energy changes and the potential energy surface landscape when the CCC bond angles are not so small.

It was found that the CCC bending yields a significant contribution to the 2^1Ag energy when all three CC bonds are partially twisted. This is due to a large orbital overlap between the next neighbor π orbitals at this conformation as shown in Fig.3.3. To take account this effect, the Hamiltonian must include the next neighbor interactions.

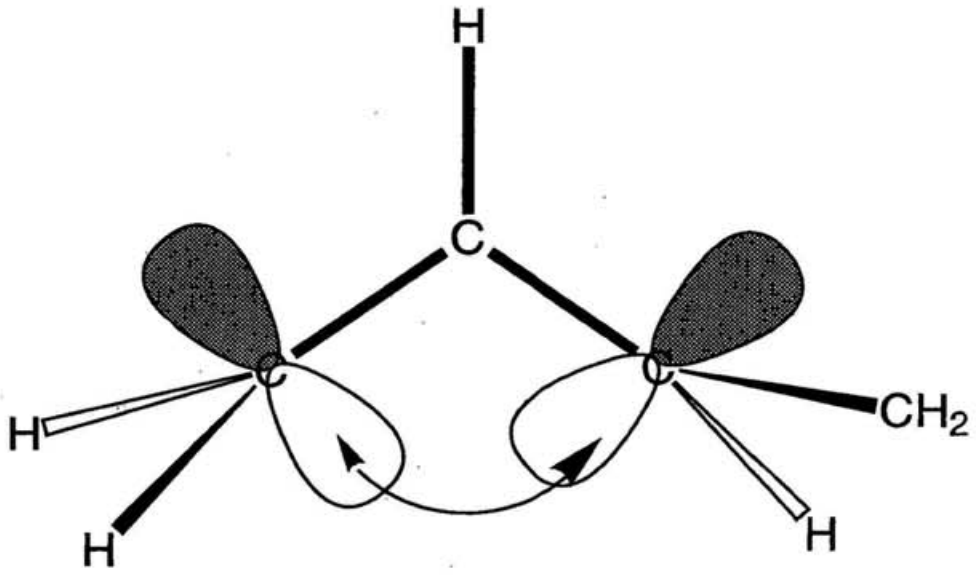

Figure 3.3: Next neighbor interaction between 1,3 localized π orbitals

The Hamiltonian matrix elements for the next neighbor interactions in VB basis are

$$H^1_{\pi 1,1} = 0\,, \tag{3.10}$$

$$H^1_{\pi 1,2} = \frac{g_{1,3}+g_{2,4}}{\sqrt{3}}\,, \tag{3.11}$$

$$H^1_{\pi 2,2} = \frac{2(g_{1,3}+g_{2,4})}{3}\,. \tag{3.12}$$

We use an ad hoc function to represent $g_{i,i+2}$ which satisfies the following conditions. The bending and torsional angle dependence must be taken into account. As the nodal properties of the localized π orbitals, the sign of their overlap changes at a small bending angle θ; the interaction is zero at that bending angle. Furthermore, the interaction must also be small

if the geometry is far from the triple twisted conformation; these requirements are implemented by multiplication of the attenuating terms, $\sin^4\theta_i$ and $\sin^2\alpha_i \sin^2\alpha_{i+1}$. The functional form of the next neighbor interaction is thus assumed to be

$$g_{i,i+2} = (a_i + b_i\cos\theta_i + c_i\cos^2\theta_i + d_i\cos^3\theta_i)\sin^4\theta_i \ \sin^2\alpha_i \sin^2\alpha_{i+1} \ . \quad (3.13)$$

3.3 The σ bond potential function

The σ bond potential function is assumed to be the sum of the functions of individual internal molecular degrees,

$$\begin{aligned} V_\sigma \ = \ & \sum_i V_i^{CH\,stretch}(r_i^{CC}) + \sum_i V_i^{CC\,stretch}(r_i^{CH}) + \sum_j V_j^{bend}(\theta_j) + \\ & \sum_k V_k^{torsion}(\alpha_k) + \sum_l V_l^{out\,of\,plane}(\chi_l) + \sum_m V_m^{Lennard-Jones}(r_m^{nonbonded}) \end{aligned} \quad (3.14)$$

The Morse potential is used for the CC stretching,[29]

$$V^{CC\,stretch}(r_i^{CC}) = D_i^{CC}(\exp(-2\eta_i^{CC}(r_i^{CC} - r_i^{CC,eq})) - 2\exp(-\eta_i^{CC}(r_i^{CC} - r_i^{CC,eq}))) \ . \quad (3.15)$$

$r_i^{CC,eq}$ corresponds to the equilibrium CC bond length when the C_iC_{i+1} π bond is completely broken.

the harmonic potential is used for the CH stretching.[29]

$$V^{CH\,stretch}(r_i^{CH}) = k_i^{CH}(r_i^{CH} - r_i^{CH,eq})^2 \quad (3.16)$$

$r_i^{CH,eq}$ corresponds to the equilibrium CH bond length.

The potentials related to angles are expanded in the Fourier series[30], and only the dominant terms are retained,

$$V^{bend}(\theta_i) = k^{bend}(1 + \cos\theta_i)^2 \ , \quad (3.17)$$

$$V^{torsion}(\alpha_i) = k^{torsion}\cos 2\alpha_i \ , \quad (3.18)$$

$$V^{out\ of\ plane}(\chi_i) = k^{out\ of\ plane} \cos \chi_i \ . \tag{3.19}$$

For the non-bonded interaction separated by three or more bonds, the Lennard-Jones potential is used whose parameters are adopted from the force field of Kollman et al. [31]

3.4 Parameter fitting

To fit the parameters in the model Hamiltonian (Eqs.3.9, 3.13, 3.15, 3.16, 3.17, 5.3, and 3.19), from the ab-initio calculations, a nonlinear least square fitting procedure in the program SALS[32] is employed.

3.4.1 Conformation Sampling

The potential energies at various conformations are calculated by state averaged complete active space self consistent filed (SA-CASSCF) with Dunning-Huzinaga double-ζ + d-type polarization function basis set (DZ+d). [33] MOLPRO94 [34] is employed for these calculations. The active space of butadiene comprises four π electrons and four π orbitals (4e,4o). For a balanced description of 1^1Ag and 2^1Ag states, the state average orbitals with the equal weight are used. This level of calculation yields a fairly good agreement with more extensive calculations in potential energies of 1^1Ag and 2^1Ag states. [5].CASSCF in GAUSSIAN94[35] is mainly employed for the geometry optimization. Sampled conformations are; Twisting CC bonds along the various isomerization paths with relaxing CC bond lengths generates 513 conformations which include the planar s-trans, the planar s-cis conformations, and conformations with a 90° twisted CC bond, with two 90° twisted CC bonds, and with three 90° twisted CC bonds. Stretching CC bonds ranging from 1.25$\mathring{A}$ to 1.65$\mathring{A}$ for each state generates 239 conformations.

For determining the parameters of the next neighbor interaction (Eq.3.13), we arbitrary select 11 conformations with triply twisted CC bonds and with

small excitation energies. Bending CCC of these conformations generates 603 conformations. The CCC bending ranges from 70° to 150°. As total, we generate 1355 conformations for the π parameters fit. In these conformations, the bond angles (H-C-C, H-C-H etc.) and CH bond lengths are fixed as the average of 1^1Ag and 2^1Ag equilibrium values at the planar conformations obtained by CASSCF/DZ+d

3.4.2 The nonlinear least square fit

The parameters of the π part are estimated from the excitation energies calculated at sampled conformations, generated by twisting and stretching the CC bonds and bending the CCC angles, i.e. by varying those inducing large π electron energy changes.

We employ the SALS program [32] to perform the nonlinear least square fit, in which the square sum of the deviation of the excitation energies

$$S(\kappa) = \sum_i (\Delta E_i^{ab} - \Delta E_i^{model})^2$$

is minimized. Here, κ is the set of π parameters. ΔE_i^{ab} is the excitation energy at the i'th conformation calculated by SA-CASSCF/DZ+d and ΔE_i^{model} is the excitation energy calculated by the model Hamiltonian.

To determine the parameters of the σ part, we use the averaged energies of 1^1Ag and 2^1Ag states evaluated by SA-CASSCF/DZ+d at various conformations (see Appendix A. for the parameter fitting).

In addition to the conformations used for the π parameter fit, further sample conformations are generated to fit the parameters of CH stretching, bending, and out-of-plane bending in the neighbor of the s-trans conformation. The nonlinear least square fitting procedure is used for determining the σ parameter, where the square sum of the deviations of the averaged energies of the 1^1Ag and 2^1Ag states among 1558 conformations is minimized.

The parameters thus obtained are listed in Table 3.1 and 3.2

Table 3.1: π parameters. Values are in the atomic unit.

g_1^0	-2.01
g_2^0	-0.0835
μ_1	1.18
μ_2	0.0840
k_1^{c2}	0.523
k_2^{c2}	0.530
k_1^{c4}	-0.191
k_2^{c4}	-0.138
a_1	-0.0633
b_1	-0.0190
c_1	-0.126
d_1	-0.00887

Table 3.2: σ parameters. Values are in the atomic unit.

$D^{C1=C2}$	0.0920
D^{C2-C3}	3.73
$\eta^{C1=C2}$	1.68
η^{C2-C3}	0.908
$r^{C1=C2,eq}$	2.68
$r^{C2-C3,eq}$	2.71
k^{C1-H1a}	0.372
$k^{C2-H2,eq}$	0.364
$r^{C1-H1a,eq}$	2.07
$r^{C2-H2,eq}$	2.07
$k^{H1a-C1-C2}$	0.0665
$k^{C1-C2-C3}$	0.0668
$k^{H2-C2-C3}$	0.0718
$k^{torsion}$	-0.001016
$k^{out\,of\,plane}$	0.0320

Chapter 4

Potential Energy Surfaces and Nonadiabatic Coupling of s-trans butadiene

4.1 Model Eigen Energies and Nonadiabatic couplings

The eigen state of the model Hamiltonian are expanded with the VB bases $\varphi_i^{VB}(\mathbf{R}(t))$ and are determined by the diagonalization.

$$\phi_n(\mathbf{r}, \mathbf{R}(t)) = \sum_i C_{in} \varphi_i^{VB}(\mathbf{R}(t)) \ , \tag{4.1}$$

$$\mathbf{H}(\mathbf{r}, \mathbf{R}(t)) \phi_n(\mathbf{r}, \mathbf{R}(t)) = E_i \, \phi_n(\mathbf{r}, \mathbf{R}(t)) \ . \tag{4.2}$$

The nonadiabatic coupling vectors are obtained by differentiating the time-independent Schrödinger equation. Since the wave function is expanded with the VB bases (Eqs.4.1), the coupling consists of two terms,

$$\langle \phi_m | \frac{\partial}{\partial R} | \phi_n \rangle = \sum_i C_{im}^* \frac{\partial C_{in}}{\partial R} + \sum_i \sum_j C_{im}^* \langle \varphi_i^{VB} | \frac{\partial}{\partial R} | \varphi_j^{VB} \rangle C_{jn} \ . \tag{4.3}$$

The first term is readily calculated by the equation which resembles the Hellmann-Feynman theorem,

$$\sum_i C_{im}^* \frac{\partial C_{in}}{\partial R} = \frac{1}{E_m - E_n} \sum_{i,j} C_{im}^* \frac{\partial H_{\pi ij}}{\partial R} C_{jn} \ . \tag{4.4}$$

Evaluation of the second term requires the knowledge of the conformational dependencies of the VB base φ_i^{VB}. This term is, however, in general very small and can be neglected because the nonadiabatic coupling strength is proportional to the abrupt change of the wavefunction, but the nature of the VB bases only changes gradually along the isomerization. Many ab-initio calculations indeed show that the orbital term, corresponding the second term, is generally much smaller than the first term (CI term). We thus use only first term in the following model calculation.

4.2 Interpretation on the characteristic of the 1^1Ag and the 2^1Ag potential energy curves

4.2.1 Torsional isomerization

In order to examine the quality of the model Hamiltonian obtained, potential energy curves calculated by the present model and SA-CASSCF along various CC torsions are plotted in Fig.4.1. We can see that the potential curves of the model Hamiltonian are in a very good agreement with SA-CASSCF curves in almost all isomerization paths. In these figures the CC bond lengths are optimized along given CC torsions. The bonds angles (H-C-C, H-C-H etc.) and CH bond lengths are fixed as the average of 1^1Ag and 2^1Ag equilibrium values at the planar conformations obtained by SA-CASSCF/DZ+d.

The present model gives simple interpretation on the characteristic of the 1^1Ag and the 2^1Ag potential energy curves and their nonadiabatic coupling along the CC torsional isomerization, considering only the neighbor interaction in 2 *times*2 Hamiltonian.

In the parameter set of Eq.3.9, the term $\cos 2\alpha$ dominates $\cos 4\alpha$ as seen

in Table 3.1 of Appendix A, and thus

$$g_{i,i+1} \sim -b_i \frac{1 + cos2\alpha_i}{2} , \tag{4.5}$$

$$b_i = -g_i^0 \exp(-\mu \bar{r}_i^{CC}) \ (b_i > 0) ,$$

where α_i is the torsional angle of C_iC_{i+1} bond. The π bonding strength gradually decreases from the maximum at $\alpha_i = 0°$ to zero at $\alpha_i = 90°$. Substituting this to Eqs.3.10-3.12, we can predicts the 1^1Ag and 2^1Ag potential curves along various CC isomerization paths.

When a double bond ($C_1 = C_2$ or $C_3 = C_4$) is twisted to 90° from the planar conformation, $H^0_{\pi\,1,1}$, the VB energy of φ_1^{VB} increases by about $b_{C=C}$, while $H^0_{\pi\,2,2}$, the energy of φ_1^{VB} decreases by about $b_{C=C}/3$. Consequently, the 1^1Ag state energy rapidly increases while the 2^1Ag state energy slightly decreases as seen Fig.4.1(b).

When the single bond $C_2 - C_3$ is twisted, $H^0_{\pi\,2,2}$ significantly increases by about $2/3\, b_{C-C}$ and $H^0_{\pi\,1,1}$ slightly increase because the C-C bond becomes longer (see Fig.4.1(a)), whereas the coupling $H^0_{\pi\,1,2}$ decreases. This is indeed reflected to the 2^1Ag and the 1^1Ag potential energy curves. It is noted that single bond twisting causes the largest unstabilization among the all combination of bond twistings (Table 4.1). It is also noted, however, the agreement between our model and SA-CASSCF is poor in the 2^1Ag state potential energy at this 90° C-C bond twisted conformation. It may be attributed that the ionic component, not included in our model, becomes important when the 2^1Ag state approaches upper singlet states and mixes with their ionic characters. This does not much affect our dynamics simulation because the trajectories of 2^1Ag state in the simulation scarcely reach such high energy conformations.

When the two double bonds are twisted but the single bond is not, since the energy of the VB bases, $H^0_{\pi\,2,2}$ stabilizes about $2/3\, b_{C=C}$, $H^0_{\pi\,1,1}$ unstabi-

lizes about $2b_{C=C}$ and they mutually cross, but the coupling element $H^0_{\pi 1,2}$ remains to be significant. It thus yields a strong avoid crossing; the adiabatic 2^1Ag potential surface is largely separated from the adiabatic 1^1Ag potential surface even near at 90° C=C twisted conformation. (see Fig.4.1(d) and (e)). It is noted that the torsions alone can not cause the SA-CASSCF potential energy difference between the disrotatory and conrotatory paths of two double bond torsions, and our VB model does not predict the electronic structure difference between the disrotatory and conrotatory paths of two double bond torsions (Figs.4.1(d) and (e), and Table 4.1). Although the reaction selectivity between these paths in the excited state is not completely elucidated, the fully geometry relaxation along these paths might anticipate the disrotatory propensity.[3, 5]

When a single bond and two double bonds are simultaneously twisted, $H^0_{\pi 2,2}$ (thus the 2^1Ag state energy) slightly increases whereas $H^0_{\pi 1,1}$ (thus the 1^1Ag state energy) rapidly increases, whereas the coupling element $H^0_{\pi 1,2}$ about diminishes; 2^1Ag nearly degenerates with 1^1Ag states nearly at the triply twisted conformation.

(a) C-C twisting

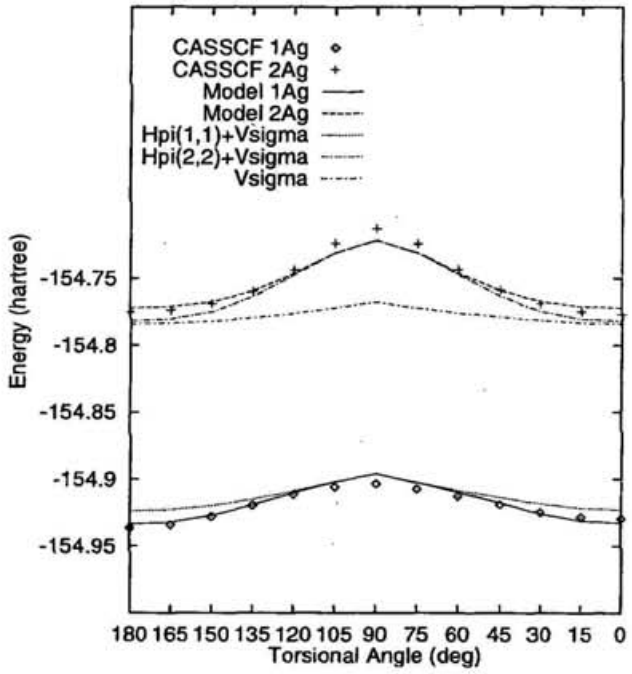

(b) C=C twisting

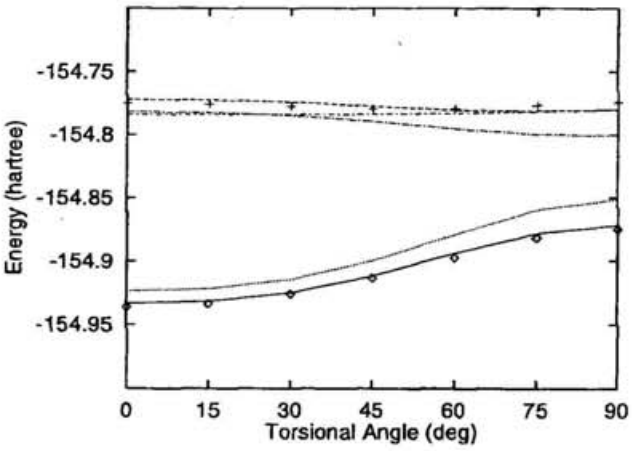

(c) C=C C-C simultaneous twisting

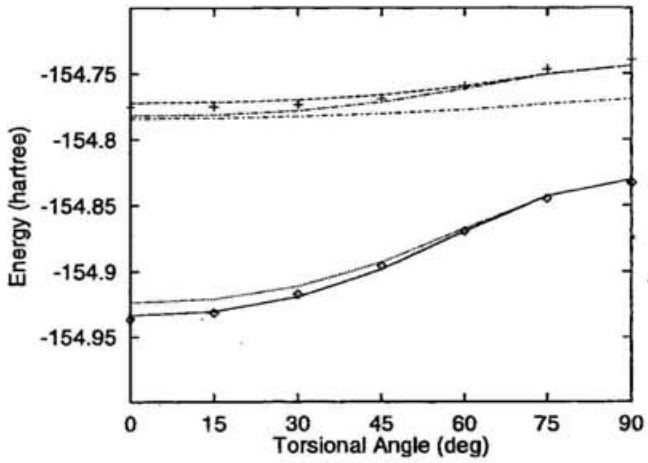

(d) C=C C=C conrotatory twisting

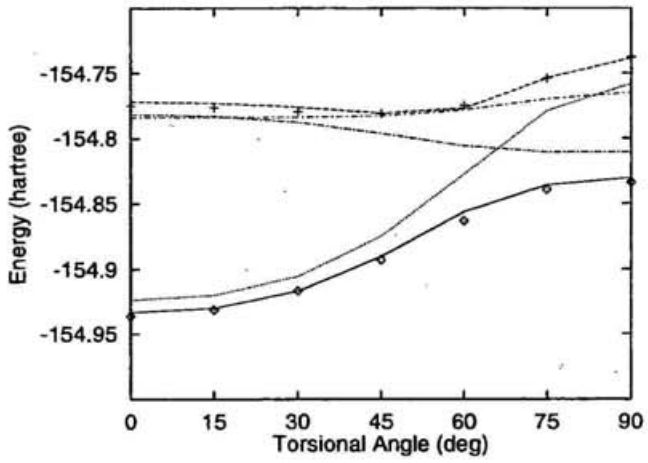

(e) C=C C=C disrotaotry twisting

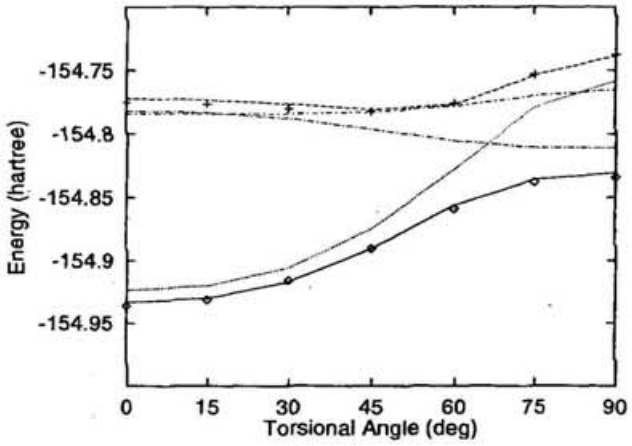

(f) C=C C-C C=C conrotatory twisting

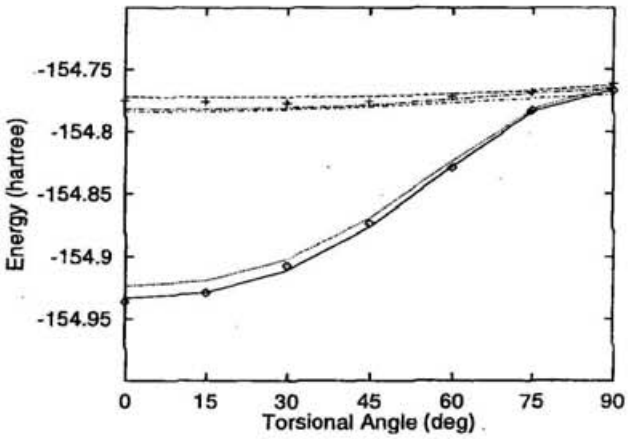

Figure 4.1: Potential energy curves along the various twisting paths. The 1^1Ag state energy from SA-CASSCF calculation (open diamond dot $\diamond$), 2^1Ag SA-CASSCF (+), 1^1Ag Model Hamiltonian (solid line), 2^1Ag Model Hamiltonian (long dashed line), $H_{\pi\,1,1} + V_\sigma$ (dotted line), $H_{\pi\,2,2} + V_\sigma$ (long dashed dotted line), V_σ (short dashed dotted line) The CC bond lengths are optimized along given CC torsions. The bonds angles (H-C-C, H-C-H etc.) and CH bond lengths are fixed as the average of 1^1Ag and 2^1Ag equilibrium values at the planar conformations obtained by SA-CASSCF/DZ+d. (a)C-C twisting (b)C=C twisting (c)C=C C-C simultaneous twisting (d)C=C C=C conrotatory twisting (e)C=C C=C disrotatory twisting (f)C=C C-C C=C conrotatory twisting

Table 4.1: The energy increase of each state by twisting various CC bonds to 90° from the planar s-trans conformation

	CASSCF		Model	
twisted bond	$\Delta E(1^1Ag)$	$\Delta E(2^1Ag)$	$\Delta E(1^1Ag)$	$\Delta E(2^1Ag)$
C-C	0.0329	0.0620	0.0398	0.0501
C=C	0.0617	0.0008	0.0620	-0.0080
C=C C-C	0.1035	0.0357	0.1033	0.0280
C=C C=C^a	0.1024	0.0375	0.1031	0.0336
C=C C=C^b	0.1022	0.0375	0.1029	0.0335
C=C C-C C=C^a	0.1698	0.0138	0.1674	0.0094
C=C C-C C=C^b	0.1698	0.0138	0.1674	0.0094

^{a} Conrotatory Path ^{b} Disrotatory Path

4.2.2 The locus of the degeneracy

Whether two or more states with same symmetry can mutually cross or not is one of the most important informations to understand the mechanism of photochemistry. The non-crossing rule in diatomic molecules (with one dimensional coordinate of the bond length) was first proved by von Neumann and Wigner.[36] One variable (coordinate) can at most satisfy one of two conditions need to have the degeneracy. So, unless the other condition is satisfied by the symmetry, the state energies can not degenerate. For a case of M coordinates, however, two conditions can be always satisfied in $(M-2)$ dimensional space; a molecular geometrical symmetry is not necessarily required. Therefore, Teller,[47] Herzberg and Longuett-Higgins[38] concluded that two state even with same symmetry will intersect along a $(M-2)$ dimensional hyper-line as the energy is plotted against the M nuclear coordinates. Herzberg and Longuett-Higgins demonstrated that in a triangular system of three dissimilar atoms the lowest doublet state is linked with an excited doublet by a conical intersection.

Recently, Olivucci, Celani, Garavelli, and coworkers demonstrated that the 1^1Ag and 2^1Ag states of butadiene, hexatriene and octatetraene degenerate when three CC bonds are partially twisted.[3, 5, 6, 39, 40]

The present model can briefly predict the locus where 2^1Ag states degenerates with 1^1Ag, by considering only the neighbor interactions in the Hamiltonian (Eqs.3.6, 3.7 and 3.8). [21, 24] The condition of the degeneracy is $H^0_{\pi 11} = H^0_{\pi 22}$, $H^0_{\pi 12} = 0$,which is satisfied when

$$\begin{aligned} g_{1,2} &= -g_{3,4} \ , \\ g_{2,3} &= 0 \ . \end{aligned} \tag{4.6}$$

From Eqs. 4.5 and 4.6, it occurs at the triply twisted conformation where all three bonds are twisted to 90°. The energy difference between 1^1Ag

and 2^1Ag states is indeed very small at this conformation; 0.010a.u. in the present model and 0.005a.u. in SA-CASSCF.

Although the twisting of all double bonds to 90° puts the VB energies of 1^1Ag and 2^1Ag closer, the adiabatic curves strongly avoid each other (Figs.4.1(d) and (e)) and it is not expected to causé a very fast nonadiabatic transition. On the other hand, the simultaneous twisting of all double bonds and single bond involves the degeneracy at 90° CC bonds, but the nonadiabatic coupling along the torsion is rather small. Besides, the conformation at 90° is higher in energy in comparison with that with all double bonds twisted to 45°. Therefore the conformation with triple torsion alone is expected not to paly a significant role in the fast internal conversion.

Olivucci and Celani et al. have performed a geometry optimization along the conical intersection seam and found that the 1^1Ag and 2^1Ag degeneracy occurs at local minimum when three carbon atoms get close in distance by forming the "kink" structure.[3, 40]

We here also examine the 2^1Ag potential energy surface along the CCC bending around the triply twisted conformations in our model. In these conformations, the overlaps among the next neighbor localized π orbitals are large (Fig.3.3) and the difference between the diagonal elements of model Hamiltonian is small, and thus the potential energy surfaces are strongly modified by the next neighbor interactions.

The next neighbor interaction expands the hyperspace volume of the degeneracy and lowers the 2^1Ag state energy. Let M be the total number of the internal molecular degrees of freedom. If one considers only the neighbor interactions, the dimensionality of the degeneracy region $M-2$ is accidentally reduced into $M-3$ through the three conditions, $\alpha_1 = 90°$, $\alpha_2 = 90°$, and $\alpha_3 = 90°$ in Eq.4.6, while, if we include the next neighbor interactions, the dimensionality remains to be $M-2$. In other words, the next neighbor

interaction yields the degeneracy at the conformations where the neighbor interaction alone can not cause the degeneracy.

4.2.3 CCC bending

In addition, Eqs.3.10 and 3.12 show that the next neighbor interaction exclusively lowers the energy of φ_2^{VB}. Consequently, 1^1Ag and 2^1Ag potential energy surfaces intersect each other.

We have calculated the potential energy surfaces along CCC bending at a certain geometry with triply twisted CC bonds, which are shown in Fig.4.2. We can see that the system is indeed near crossing at a CCC bending angle of 110°. Along the simultaneous two CCC bendings, the weakly avoided crossing occurs at a larger bending angle (115° as in Fig.4.2(b)). Since the next neighbor interaction contributes to $H_{\pi 1,2}$ in the opposite sign of the neighbor interaction, $H_{\pi 1,2}$ is decreased as reducing the CCC bending angle. It diminishes when the cancelation becomes perfect at a certain CCC bending angle. The accidental degeneracy of 1^1Ag and 2^1Ag states therefore exists when this cancelation occurs at the exact intersection of the φ_1^{VB} and φ_2^{VB} energy curves. Although we have not tried here to find the exact location of such degeneracy, Fig.4.2 shows a very weakly avoided crossing at the intersection point of the VB state energy curves.

(a) C-C-C bending path

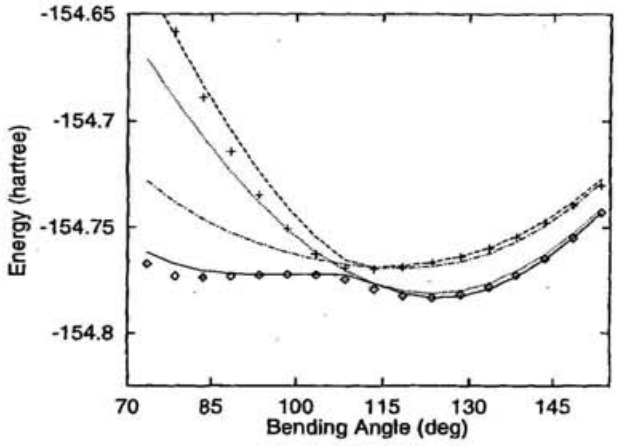

(b) simultaneous two C-C-C bending path

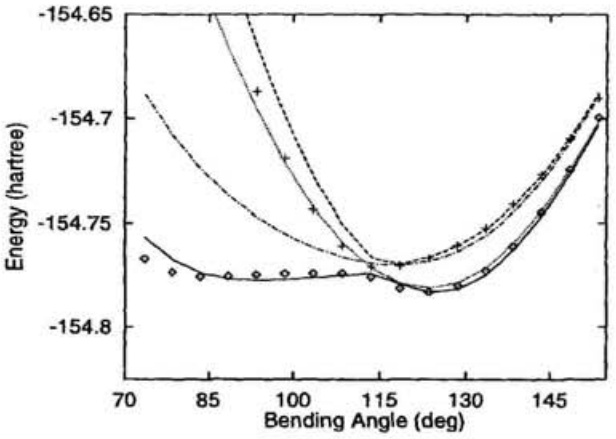

Figure 4.2: Potential energy curves along the CCC bending paths in the neighbor of the conformation with partially twisted CC bonds, $\alpha_1 = 75°$, $\alpha_2 = 90°$, $\alpha_3 = 75°$. The 1^1Ag state energy from SA-CASSCF calculation (open diamond dot $\diamond$), 2^1Ag SA-CASSCF (+), 1^1Ag Model Hamiltonian (solid line), 2^1Ag Model Hamiltonian (long dashed line), $H_{\pi 1,1} + V_\sigma$ (dotted line), $H_{\pi 2,2} + V_\sigma$ (long dashed dotted line) Geometrical parameters other than CCC bending angle are fixed. (a) C-C-C bending path (b) simultaneous two C-C-C bending path

4.3 CC stretching

The potential energy curves for the CC stretching at the planar conformation are shown in Fig.4.3. A double bond stretching alters the energy gap between φ_1^{VB} and φ_2^{VB}, and consequently induces a large excitation energy change, in comparison with a single bond stretching.

(a) single bond stretching around the 2^1Ag equilibrium geometry

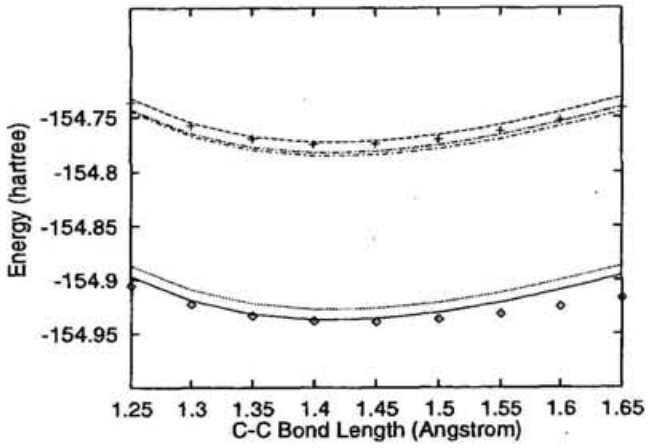

(b) double bond stretching around the 1^1Ag equilibrium geometry

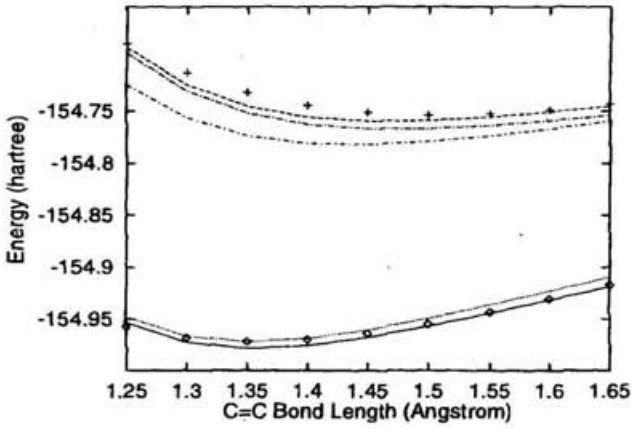

Figure 4.3: Potential energy curves along CC stretching path around the equilibrium structures of 2^1Ag and 1^1Ag. The 1^1Ag state energy from SA-CASSCF calculation (open diamond dot $\diamond$), 2^1Ag SA-CASSCF (+), 1^1Ag Model Hamiltonian (solid line), 2^1Ag Model Hamiltonian (long dashed line), $H_{\pi 1,1} + V_\sigma$ (dotted line), $H_{\pi 2,2} + V_\sigma$ (long dashed dotted line) Geometrical parameters other than the CC bond length are fixed. (a) single bond stretching around the 2^1Ag equilibrium geometry (b) double bond stretching around the 1^1Ag equilibrium geometry

The present simple model certainly has the limitations. Although the present model can produces the basic feature of the 2^1Ag and 1^1Ag state potential energy surfaces, it misses some of their characteristics in compared with the very accurate butadiene potential surfaces calculated by Celani et al.[5] Celani et al has shown that the out-of-plane bending (pyramidalization) is important in the geometry of the lowest conical intersection and in the 2^1Ag relaxed isomerization paths around the "kink" structure. The present model assumes, however, that this out-of-plane bending is not responsible for the electronic character change and does not account for its effect on potential energy surfaces. Celani et al. has also found that there is no metastable 2^1Ag state conformation on the isomerization path toward the conical intersection, although the present model predicts its existence; the conical intersection is the lowest2^1Ag energy configuration in the accurate calculation.[5, 40] The present model includes only a part of the molecular freedoms as the active modes inducing the strong electronic character changes, and thus yields the conical intersection seam energy higher than that obtained with a more accurate calculation.

4.4 Nonadiabatic coupling

The present model Hamiltonian can also reproduces the nonadiabatic coupling in good agreement with those computed by the finite difference of the SA-CASSCF wave function.

The nonadiabatic coupling values along the twisting paths are illustrated in Fig.4.4, where the SA-CASSCF results are calculated by including both 1st (the CI) and 2nd (the orbital and overlap) terms in Eq.4.3. We can see only the significant nonadiabatic coupling between adiabatic 2^1Ag and 1^1Ag states exists along the doubly and the triply torsional path. The nonadiabatic coupling becomes zero at $\alpha_i = 90°$ of any C-C twisting paths. This

is explained from a following simple consideration. The model Hamiltonian can be described mainly by the neighboring interactions, $g_{i,i+1}$, along the CC torsional paths. From Eqs.4.3 and 4.4, the nonadiabatic coupling between the adiabatic 2^1Ag and 1^1Ag states is proportional to $\partial g_{i,i+1}/\partial \alpha_i$. This is zero at $\alpha_i = 90°$ from Eq.4.5.

Along a double bond torsion, the potential energy curves of the VB bases mutually get closer while their coupling $H_{\pi 1,2}$ remains finite, and thus the nonadiabatic coupling between the adiabatic states gradually increases, but is not significant.(Fig.4.4(a))

The simultaneous two double bond torsion induces the intersection of two VB energies, so a nonadiabatic coupling strenth yields a peak at this intersecting point around $\alpha_1 = \alpha_3 = 60°$ (Fig.4.4(b)).

(a) C=C twisting

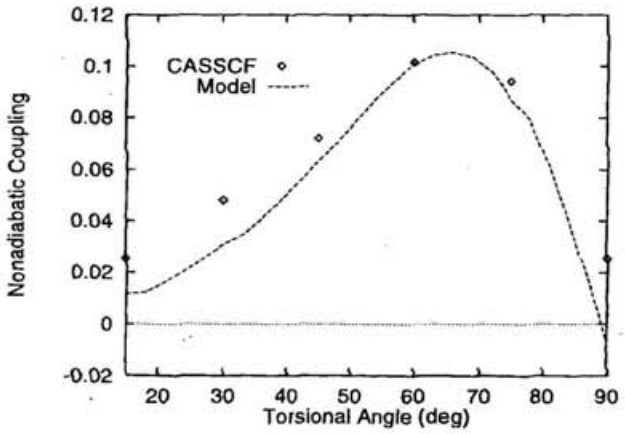

(b) C=C C=C conrotatory twisting

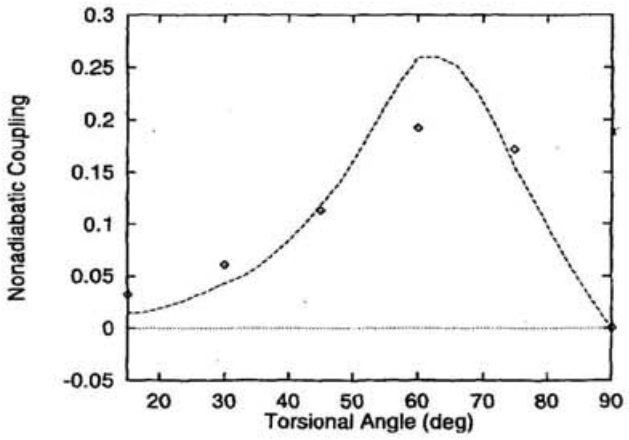

Figure 4.4: Nonadiabatic coupling curve along the twisting path ($amu^{-1/2}bohr^{-1}$). SA-CASSCF calculation (open diamond dot $\diamond$), Model Hamiltonian (solid line) (a)C=C twisting (b)C=C C=C conrotatory twisting

The torsion alone does not cause a large nonadiabatic coupling. The CCC bending is required upon the triple torsion. Fig.4.5 illustrates how the nonadiabatic coupling is enhanced along the CCC bending at a partial triply CC twisted conformation. When the CCC bending angle decreases, the coupling $H_{\pi 1,2}$ in the VB bases gradually decreases and the energy difference between two VB states becomes very small. Hence the wavefunction of each adiabatic state rapidly switches between the VB bases at the intersection points, and the sharp peak of the nonadiabatic coupling appears.

(a) C-C-C bending

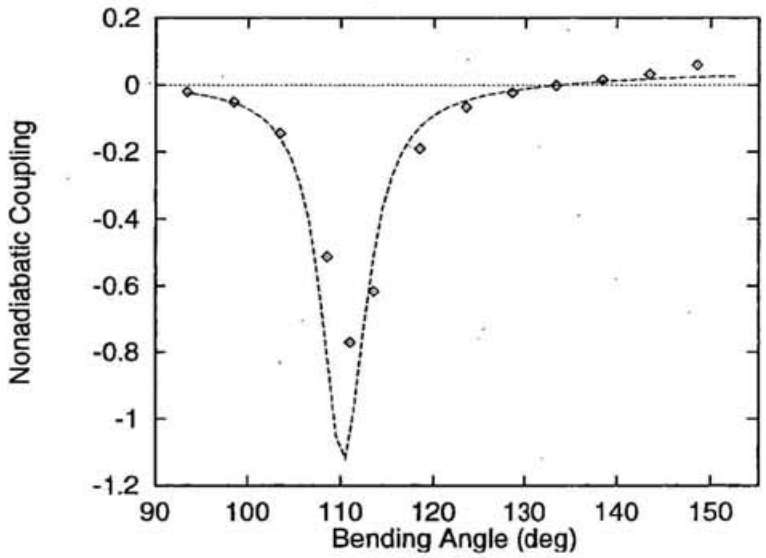

(b) simultaneous two C-C-C bending

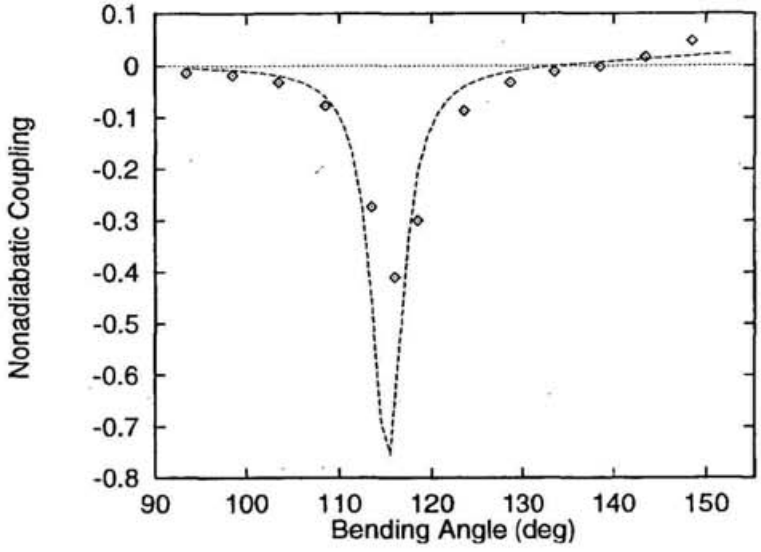

Figure 4.5: Nonadiabatic coupling along the C-C-C bending path ($amu^{-1/2}bohr^{-1}$) in the neighbor of the conformation with partially twisted CC bonds, $\alpha_1 = 75°$, $\alpha_2 = 105°$, $\alpha_3 = -75°$. SA-CASSCF calculation (open diamond dot $\diamond$), Model Hamiltonian (solid line) (a)C-C-C bending (b)simultaneous two C-C-C bending

Chapter 5

trans-hexatriene

Hexatriene has a short fluorescence lifetime due to the facile nonadiabatic transition induced by the isomerization. The ultra fast laser experiment indicates that an internal conversion requires the activation energy between 71.3 and 157.7 cm^{-1}. In this chapter, we investigate the hexatriene internal conversion mechanism by constructing a simplified model Hamiltonian which depends solely on the CC bond torsional angles.

5.1 Model Hamiltonian

As we have discussed above for butadiene, the covalent state 1^1Ag and 2^1Ag can be approximately expanded with neutral VB bases and the effect of ionic VB bases is effectively incorporated into the model Hamiltonian.

The system with six π electrons has more spin couplings to form singlet spin functions than butadiene. We employ the Yamnouchi-Kotani basis set as the VB basis of the model. It consists of five orthogonalized spin functions which provide irreducible representations of the permutation group S_N and are generated by the branching diagram method.(Fig.5.1)

We employ a simplified model Hamiltonian including the neighbor interactions g_i which only depend on the CC bond torsional angles.

$$g_i = \frac{1}{2} + k_i^{c2} \cos 2\alpha_i + k_i^{c4} \cos 4\alpha_i \tag{5.1}$$

The numbering of the torsional angles and the atoms are shown in Fig.5.2

The σ bond potential function is also assumed to depends only on the CC bond torsional angles,

$$V_\sigma = \sum_k V_k^{torsion}(\alpha_k) \tag{5.2}$$

$$V^{torsion}(\alpha_i) = k^{torsion} \cos 2\alpha_i \ , \tag{5.3}$$

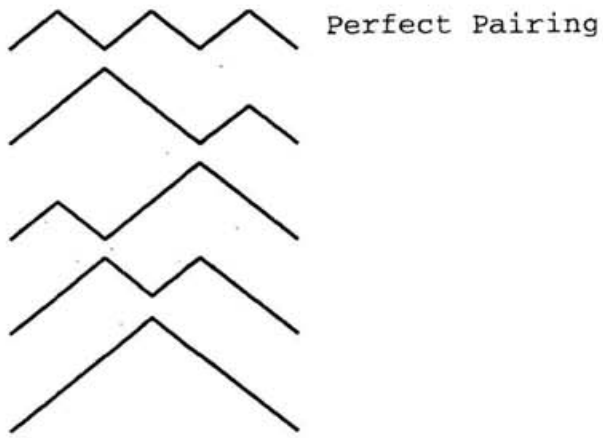

Figure 5.1: The five distinct sequences of the coupling

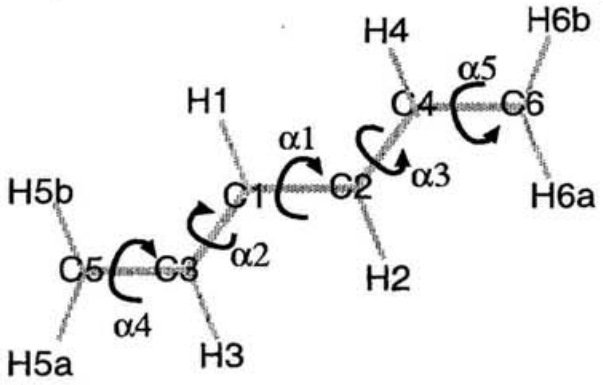

Figure 5.2: Numbering of atoms and torsions

5.1.1 Parameter fitting

We fit the parameter of this simplified model Hamiltonian with the data obtained from the SA-CASSCF/STO-3G calculation along the various isomerization paths. To fit the parameters, a nonlinear least square fitting procedure in the program SALS[32] is employed.

The potential energies at various conformations are calculated by SA-CASSCF with the minimum STO-3G basis set.[42] To calculate numerous samples of various conformational energies of hexatriene, the minimum basis set is used. It is found that this level of calculation can reproduce the characters of the potential energy surfaces obtained from the more extensive calculations.[6] The active space of hexatriene comprises six π electrons and six π orbitals (6e,6o). MOLPRO94 is employed for these calculations. GAUSSIAN94 is mainly employed for the geometry optimization. Sampled conformations are generated by twisting each CC bond by 15°, simultaneously two CC bonds and three CC bonds with all kinds of their combinations; 1733 conformations are generated. We here did not include other internal coordinates (CCC bendings, CC stretchings, CH stretchings, out-of-plane bendings) in hexatriene.

The fitting procedure is the same as that in butadiene. The energies obtained from this model are mostly in the good agreement with those obtained from SA-CASSCF, Their correlation is shown in Fig.5.3. The large deviations are seen in the right below. The seemingly consistent deviation of $1Ag$ and $2Ag$ in Fig.5.3 are due to the relatively high energy conformation with the doubly twisted single bonds and those with triply twisted CC bonds near the Z-isomer. The agreement between the ab-initio energies and the model eigen energies is also rather poor for a single bond torsion. This is because 1^1Ag and 2^1Ag mixes with the ionic character of the upper states as their energies increase along this torsion.

The parameters thus obtained are listed in Table 5.1.

Table 5.1: trans-Hexatriene parameters. Values are in the atomic unit.

g_1^0	-0.0857
g_2^0	-0.1022
g_3^0	-0.0781
k_1^{c2}	0.468
k_2^{c2}	0.502
k_2^{c2}	0.496
k_1^{c4}	-0.090
k_2^{c4}	-0.133
k_3^{c4}	-0.066
$k^{torsion}$	-0.00394

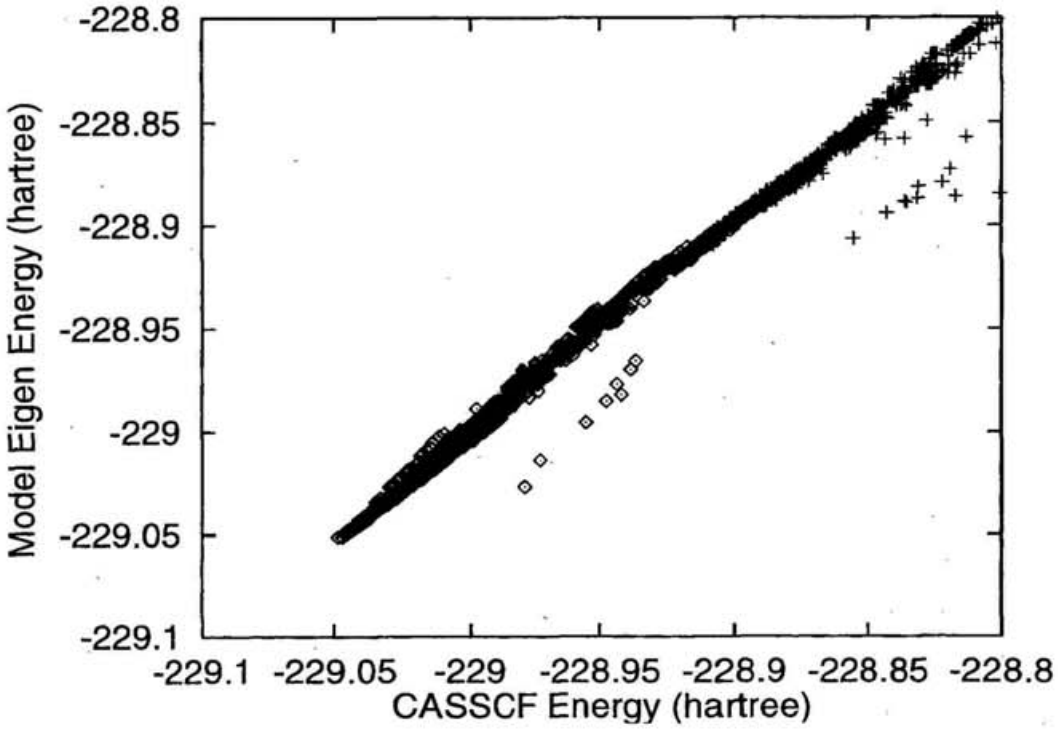

Figure 5.3: The correlation for 1^1Ag and 2^1Ag energies between SA-CASSCF/STO-3G calculation and the present VB model. 1^1Ag(open diamond dot $\diamond$),$2^1Ag(+)$

5.2 Potential Energy Surfaces

The potential energy curves along a single torsion of the terminal C5=C3 are shown in Fig.5.4(a) (see Fig.5.2 for the numbering of atoms). The 2^1Ag state energy is almost unchanged along the isomerization path, while the 1^1Ag state energy is increased. The flat potential energy curve of the 2^1Ag state also means that the planar conformation is not so stabilized. The feature agrees with the experimental investigation.

Along the single bond C3-C1 isomerization path, the 2^1Ag state energy is rapidly increased, while the 1^1Ag state energy is slightly increased. As we discussed about the butadiene, the bonding character of 2^1Ag is opposite to that of 2^1Ag. It reflects on the different behavior of the state energies along a single torsion.

Along the central double bond C1=C2 isomerization path, both the 1^1Ag and 2^1Ag state energies are monotonically increased. In contrast to the butadiene, the 2^1Ag state of a longer polyene has remaining anti-parallel spin pairs. Hence the isomerization in the 2^1Ag state of a polyene is not so facile. Later we see the same tendency of the octatetraene.

The potential energy curves along the double torsional paths are shown in Fig.5.5. Along the double torsional paths the 2^1Ag and 1^1Ag state energies are increased, though the 2^1Ag isomerization barriers of double torsions of the C=C bonds are lower than that of single torsion of the C-C bond.

5.2.1 Degeneracy

Olivucci et al. found that the degeneracy occur at the C5=C3 C3-C1 C1=C3 twisted conformation.[6] Added to this, we show that there are another symmetry distinct way of twisting which induce a degeneracy and other way of twisting does not induce a degeneracy. The triple torsion, which divides the π electron conjugation into four parts consisting odd carbon atoms, yields

the degeneracy between the 1^1Ag and 2^1Ag states.(see Fig5.6(a) and (c)) These kind of triple torsions induce the tetra-radical character.[3, 6] On the other hand, the other way of triple torsion does not induce a degeneracy as shown in Fig.5.6(b) and (d).

5.2.2 Internal conversion

The present model qualitatively represents the ab-initio potential energy surfaces whose global feature gives the intuitive interpretation of the internal conversion mechanism of hexatriene. The planar conformation of the 2^1Ag state is not stable against the terminal C=C torsion. And if the molecule has a certain excess energy, the facile nonadiabatic transition is induced.

5.2.3 Further improvement of the model

The activation energy obtained from the present model is too high to reproduce the experimental internal conversion rate through the nonadiabatic dynamics simulation. The present model has three unsatisfactory points. First, the CASSCF with the minimum basis set is employed to determine the parameters and the geometry relaxation effect is not fully incorporated. More extensive ab-initio calculation and the geometry optimization lowers the degenerated energy level and the resultant conformation inducing the degeneracy has the kink $-(CH)_3-$ structure. Secondly, the Hamiltonian should depend on other important nuclear coordinates, i.e. CC bond lengths, out-of-plane bendings, and CCC bendings. It is also required for the model to follow the ab-initio optimized geometry. Thirdly, the next neighbor interaction and more higher interaction involving more than two electrons are required to reproduce the more quantitative energies.

(a)Terminal C5=C3 twisting

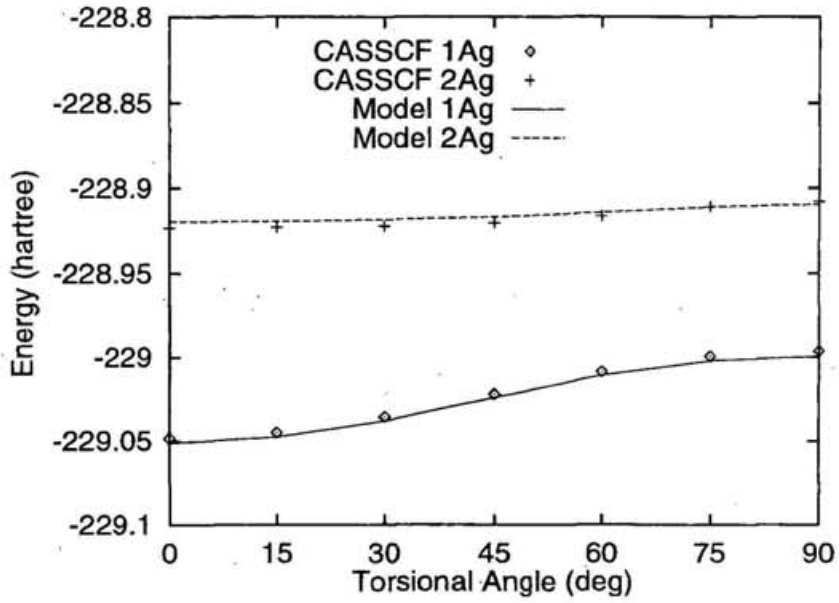

(b)C3-C1 twisting

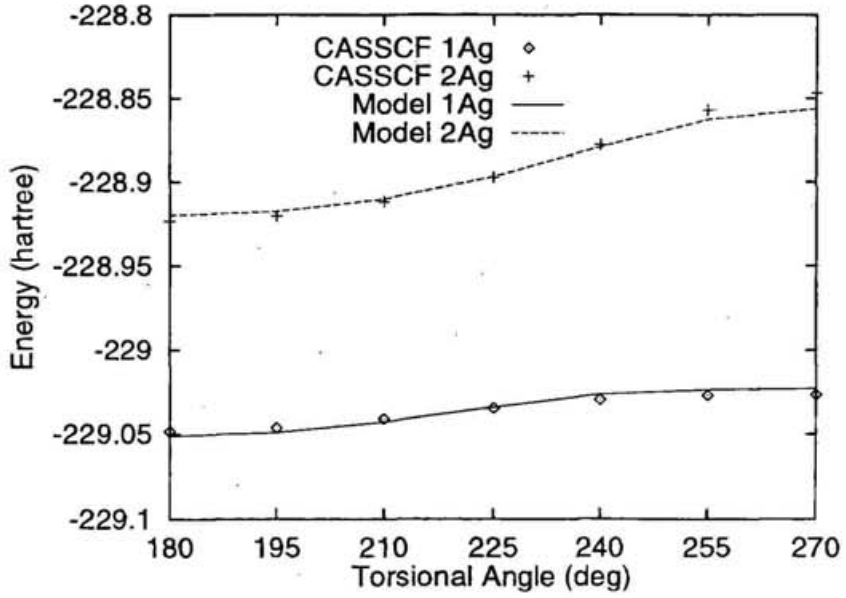

(c)Central C1=C2 twisting

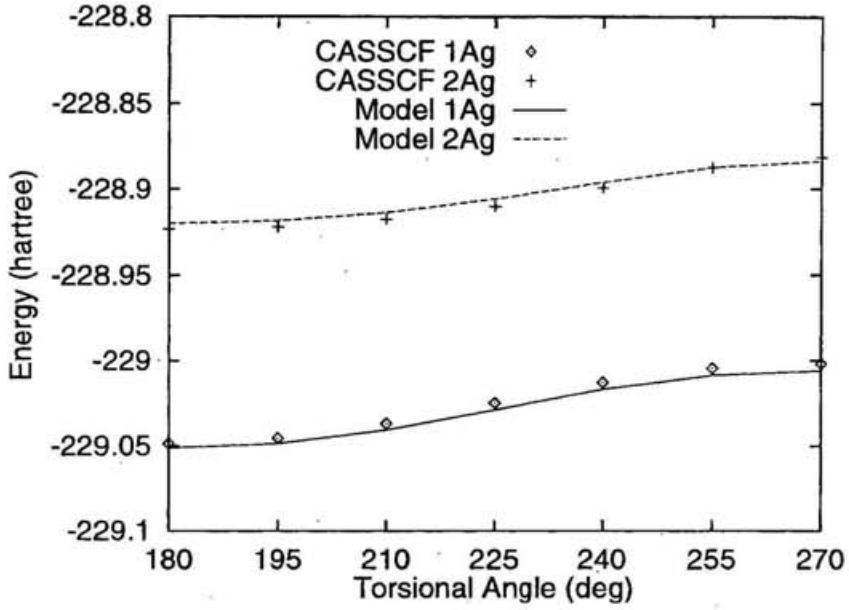

Figure 5.4: Potential energy curves along the singly torsional paths. The 1^1Ag state energy from SA-CASSCF calculation (open diamond dot ◇), 2^1Ag SA-CASSCF (+), 1^1Ag Model Hamiltonian (solid line), 2^1Ag Model Hamiltonian (long dashed line), (a)Terminal C5=C3 twisting (b)C3-C1 twisting (c)Central C1=C2 twisting

(a)C5=C3 C1=C2 twisting

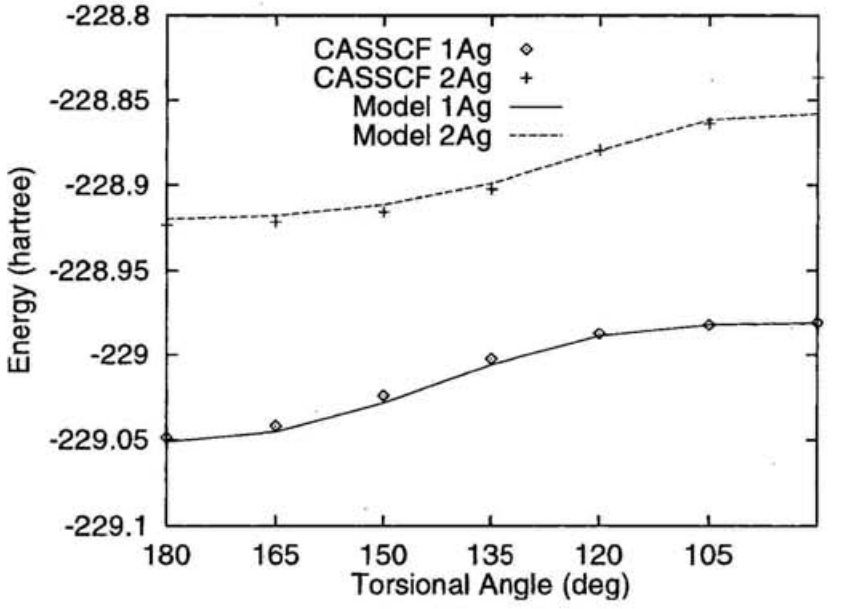

(b)C5=C3 C3-C1 twisting

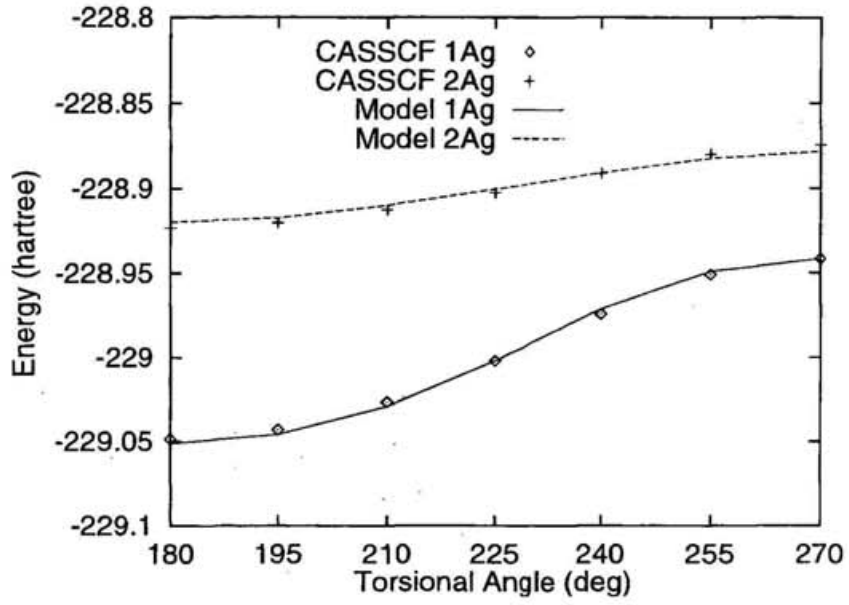

(c)C5=C3 C2-C4 twisting

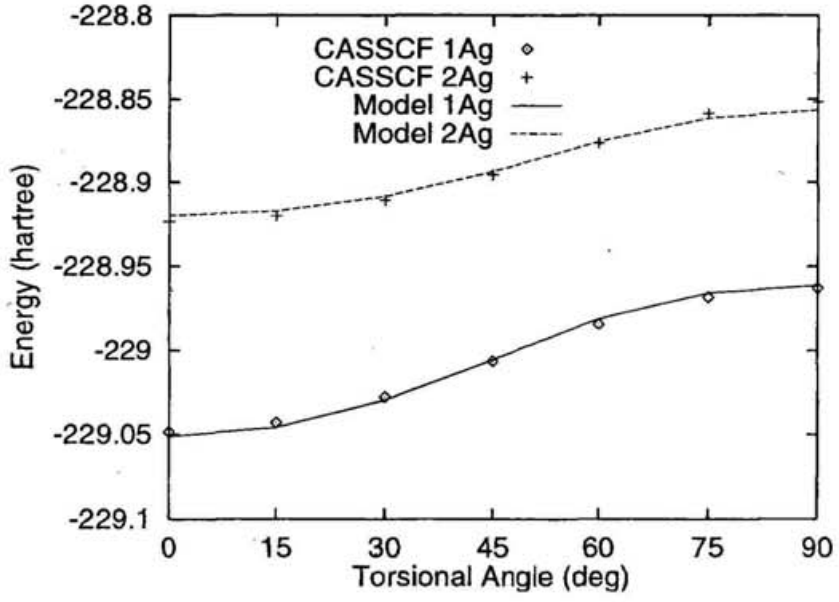

(d)C5=C3 C4=C6 twisting

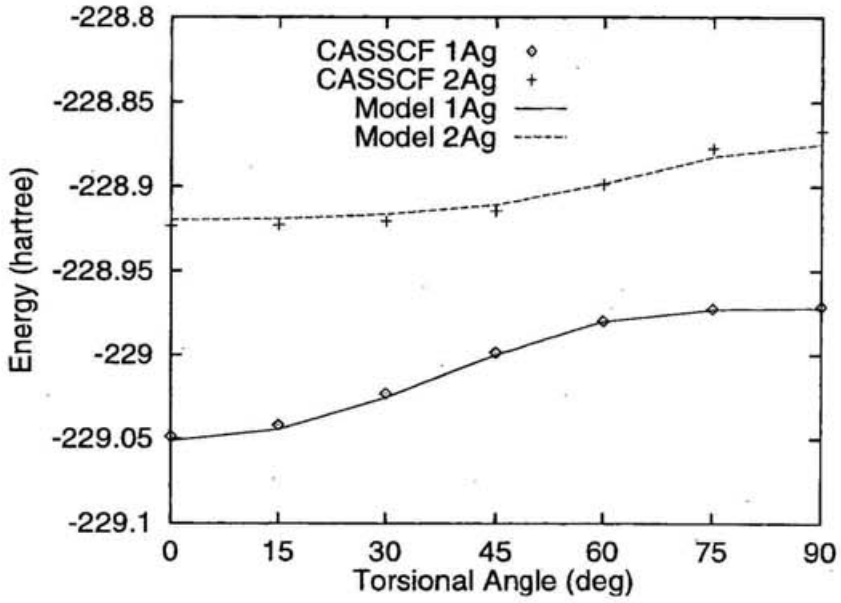

(e)C3-C1 C2-C4 twisting

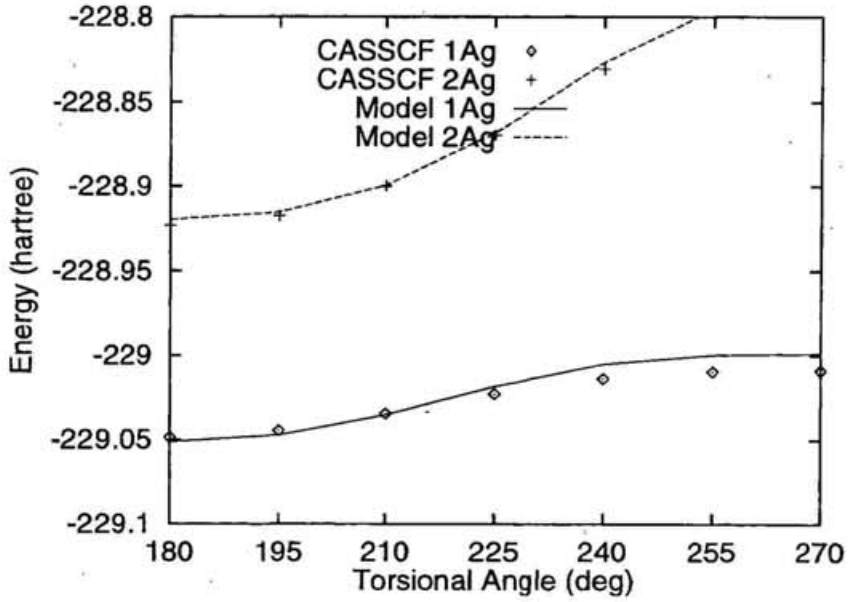

Figure 5.5: Potential energy curves along the doubly torsional paths. The 1^1Ag state energy from SA-CASSCF calculation (open diamond dot $\diamond$), 2^1Ag SA-CASSCF (+), 1^1Ag Model Hamiltonian (solid line), 2^1Ag Model Hamiltonian (long dashed line), (a)C5=C3 C1=C2 twisting (b)C5=C3 C3-C1 twisting (c)C5=C3 C2-C4 twisting (d)C5=C3 C4=C6 twisting (e)C3-C1 C2-C4 twisting

(a)C5=C3 C3-C1 C1=C2 twisting

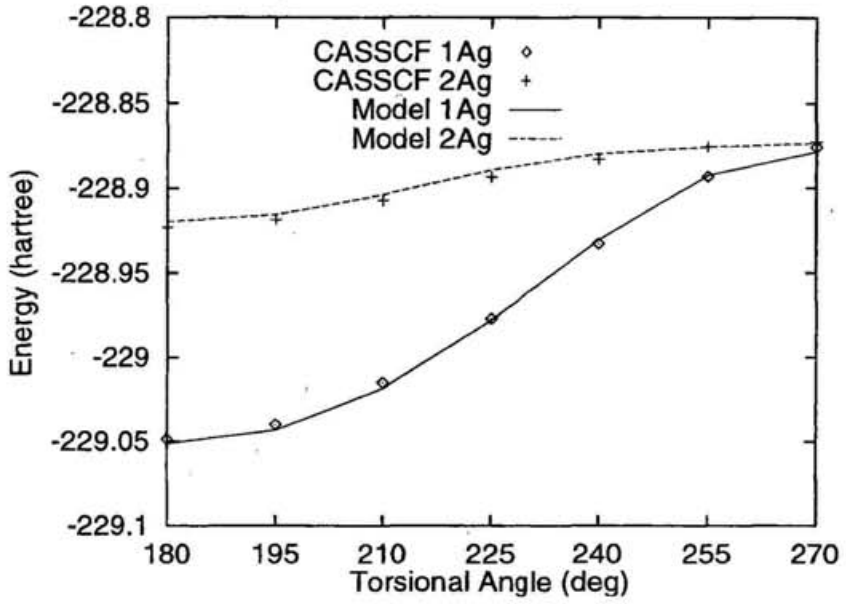

(b)C5=C3 C1=C2 C2-C4 twisting

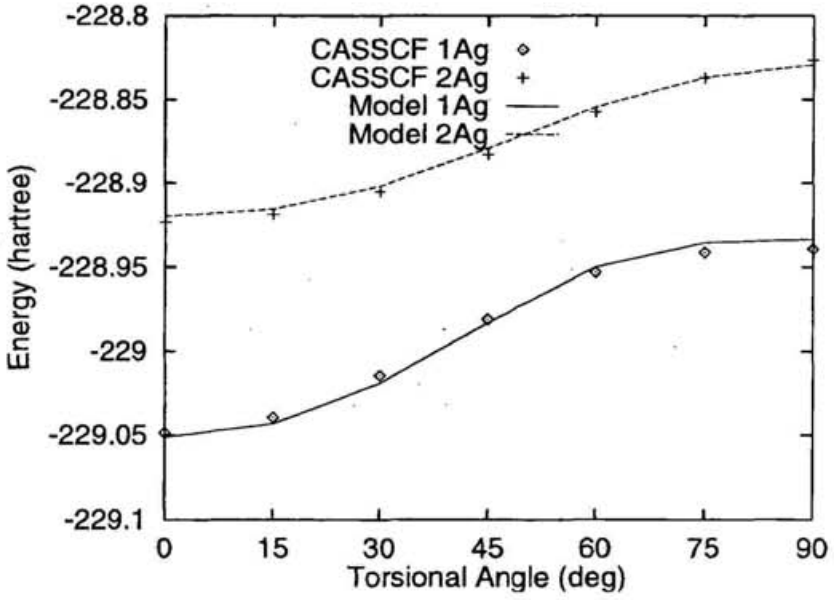

(c)C5=C3 C2-C4 C4=C6 twisting

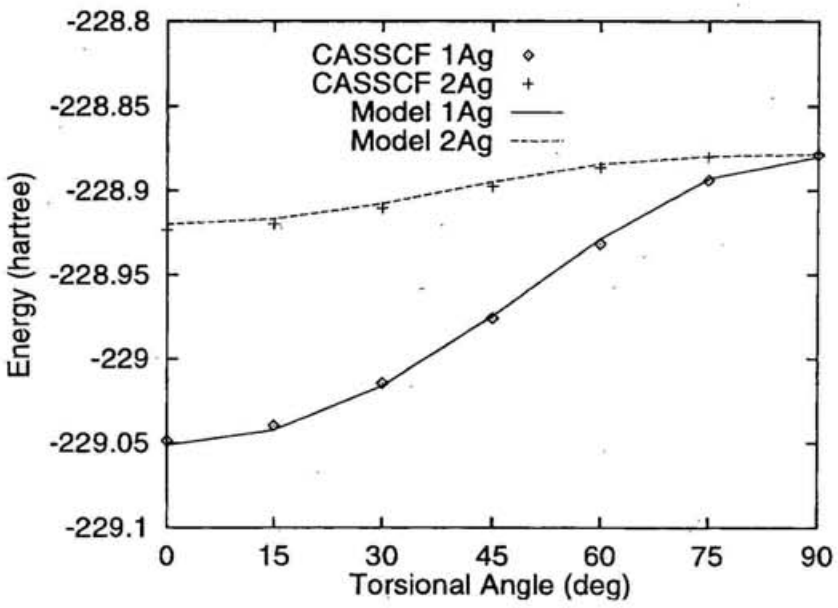

(d)C5=C3 C1=C2 C4=C6 twisting

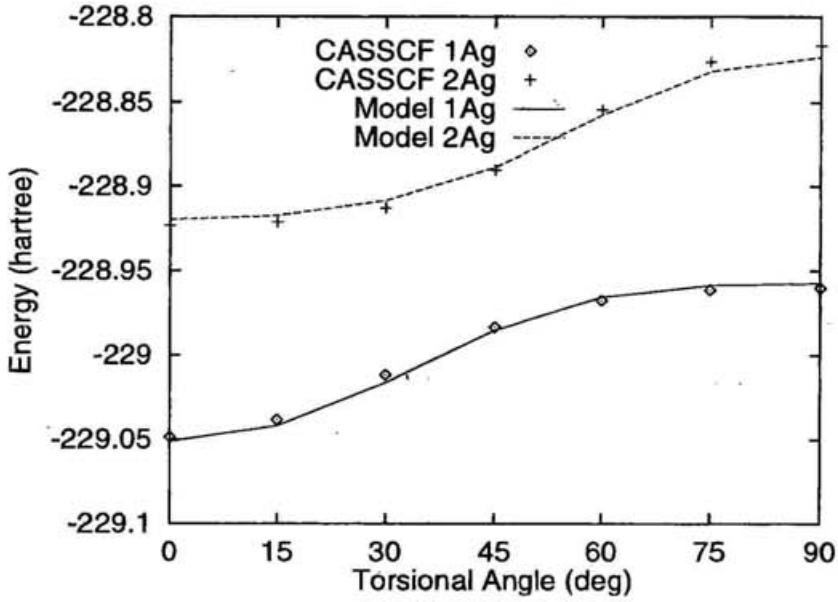

Figure 5.6: Potential energy curves along the triply torsional paths. The 1^1Ag state energy from SA-CASSCF calculation (open diamond dot $\diamond$), 2^1Ag SA-CASSCF (+), 1^1Ag Model Hamiltonian (solid line), 2^1Ag Model Hamiltonian (long dashed line), (a)C5=C3 C3-C1 C1=C2 twisting (b)C5=C3 C1=C2 C2-C4 twisting (c)C5=C3 C2-C4 C4=C6 twisting (d)C5=C3 C1=C2 C4=C6 twisting

Chapter 6

all trans-octatetraene

Octatetraene is known to yield the longest fluorescence life time among polyenes. Extensive experimental studies have been performed on this molecule including the measurement of the Z/E-photoisomerization yield and the fluorescence decay rates of vibrational modes in the 2^1Ag state.[8, 7] In this section, we have performed the ab-initio calculation to investigate the photoisomerization and the internal conversion mechanism of octatetraene.

6.1 Computational Details

The CASSCF method in GAMESS[41] is used to calculate the potential energy surfaces of octatetraene 1^1Ag, 2^1Ag, and 1^1Bu states. The complete active space (CAS) is generated by occupying eight electrons in eight active orbitals for CASSCF wavefunction in all possible way. The total number of CSF's are 1764. These CASSCF eight orbitals are the π orbitals delocalized over the whole molecule. The basis set we employed are the minimal STO-3G[42] and the Dunning/Hay double zeta basis set (DH). The STO-3G set was used for both the geometry optimization and the force constant calculation. The geometry optimization were carried out by using the analytic gradient method for the CASSCF wavefunction. The force constants were obtained from the numerical differentiation of the energy gradients. The

optimization within the (avoided) crossing seam is performed by employing GAUSSIAN94.[35]

In order to get more reliable estimation of the energies and to incorporate the $\sigma - \pi$ electron correlation, we performed the MRSDCI calculation whose reference configurations are selected from those of the CASSCF wavefunctions. MELD[43] is used. The natural orbitals of the CASSCF wavefunctions are used as the one-particle basis functions in the MRDCI calculation. A set of configurations are chosen as a zeroth order space so that they compromise more than 85% of the MRDCI wave functions at all conformations in order to achieve the balanced description of the low-lying state PES along the isomerization paths. The electronic Hamiltonian is diagonalized over this small set of configurations and the first 3 roots are chosen.

All single excitations (σ and π) and all double excitations, each of which involves at least one π electron, from the reference configurations are included in the CI.(See Fig.6.1) The second order Rayleigh-Schödinger perturbation energies to the average (i.e. one third of the sum) of the eigen vectors of these three lowest roots from all configurations outside the zeroth order space on these roots were calculated and those configurations having large values of the second order energies were selected as CSF's included in CI.[45] The threshold value for this second order Rayleigh-Schödinger perturbation selection of CSF's is $3.7\mu hartree$ and the number of selected CSF's are $31000 \sim 44000$. Inclusion of the remaining configurations is made in an extrapolation procedure.

6.2 Properties of the representative isomers at each equilibrium geometry

The equilibrium bond lengths and angles of three isomers in 2^1Ag state are listed in Table6.1. We can see that their values are almost same among all

isomers, indicating the 2^1Ag electronic characters in these isomer conformations are essentially mutually same. The C-C single bonds are longer than the double bonds by 0.04 $\sim$ 0.06 Å. The central single bond is a slightly longer than the other single bonds. All bond angles are almost equal to 120° with the carbon sp^2 hybridization. The CCC bond angles are slightly larger and the CCH bond angles are less than 120°.

Table 6.1: 2Ag optimized geometries of representative isomers

coordinate	all-trans[a]	cis,trans	cis,cis
C2-C1	1.416	1.426	1.416
C3-C1	1.456	1.460	1.461
C4-C2	1.456	1.457	1.461
C5-C3	1.392	1.392	1.391
C6-C4	1.392	1.391	1.391
C7-C5	1.453	1.454	1.453
C8-C6	1.453	1.452	1.453
C3-C1-C2	123.51	126.0	125.5
C4-C2-C1	123.51	122.9	125.5
C5-C3-C1	123.70	126.2	126.4
C6-C4-C2	123.70	123.7	126.4
C7-C5-C3	123.81	123.3	123.2
C8-C6-C4	123.81	123.8	123.2
H9-C1-C2	118.72	117.6	118.6
H10-C2-C1	118.72	119.7	118.6
H11-C3-C1	117.40	116.0	115.9
H12-C4-C2	117.40	117.4	115.9
H13-C5-C3	118.70	119.6	119.7
H14-C6-C4	118.70	118.7	119.7
H15-C7-C5	120.84	120.9	120.9
H16-C8-C6	120.84	120.9	120.9
H17-C7-C5	120.99	121.0	121.0
H18-C8-C6	120.99	121.0	121.0

Bond lengths are in angstrom, and bond angles and torsional angles are in degree.

[a]Aoyagi,M.; Ohmine,I.;Kohler,B.E. J.Phys.Chem.1990,94,3922.

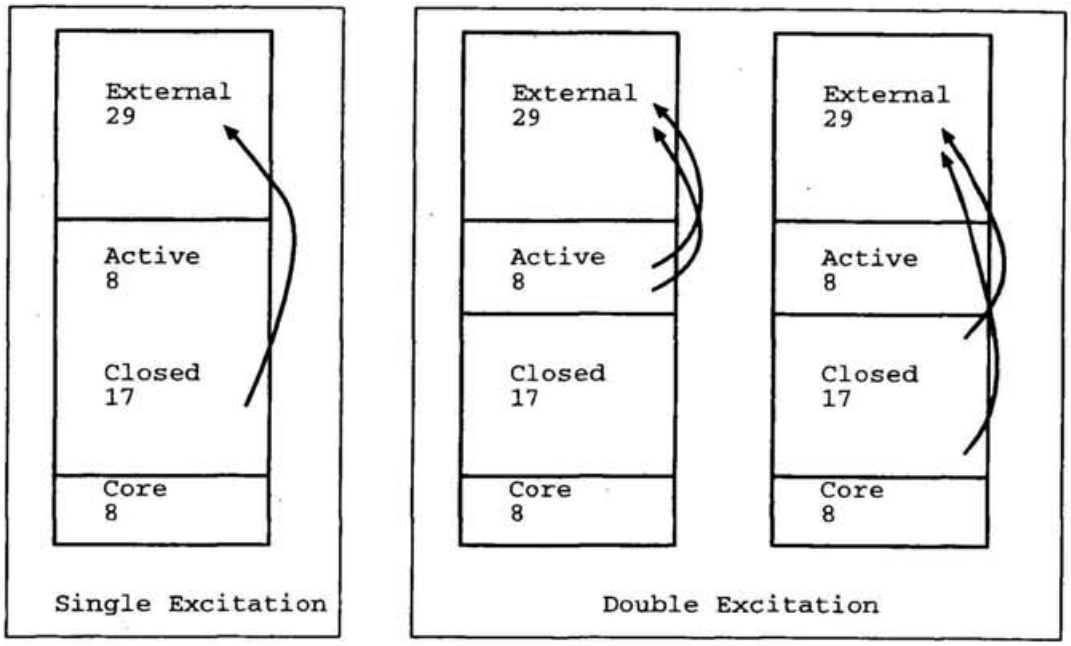

Figure 6.1: Configurations included in the CI

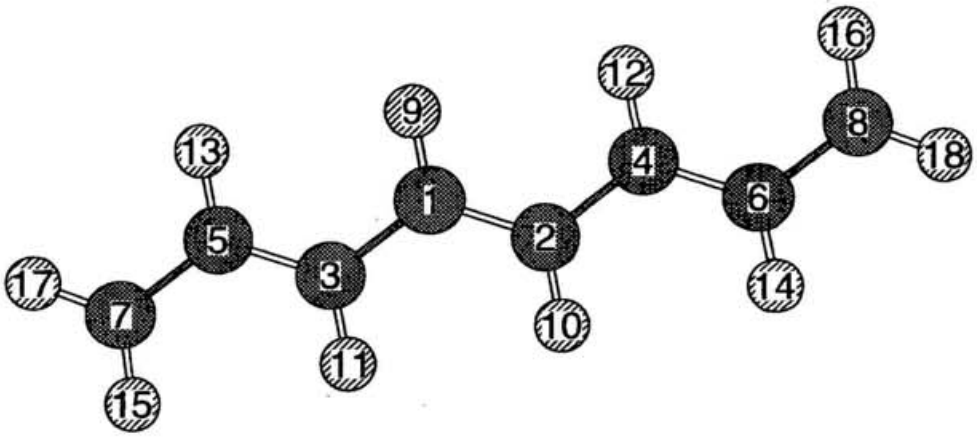

Figure 6.2: Numbering of atoms

The vibrational frequencies of the 2^1Ag electronic state are calculated for all-trans and cis,trans-isomers and listed in Table6.2. The frequencies are almost same for these two isomers, since their electronic structures are almost same. The calculated frequencies yields the best fit (giving the least deviation) to the experimental values by scaling them by a factor,0.905.

Table 6.2: 2Ag vibrational frequencies (cm^{-1}) of all-trans and cis,trans-isomers

sym	all-trans[a]		cis,trans		expl.[b]	
a'	3836	1490	3836	1520		1509
	3836	1464	3836	1475		1499
	3715	1419	3729	1454		1479
	3713	1415	3720	1379		
	3713	1371	3711	1355		
	3710	1303	3709	1261		1226
	3708	1157	3695	1124	3583	
	3702	1107	3691	1093		1080
	3659	1072	3649	1056		
	3650	1014	3648	996		968
	2290	601	2281	732		628
	1861	580	1850	533	1789	538
	1738	403	1746	430		364
	1732	359	1738	353		338
	1688	234	1723	228	1662	210
	1572	92	1585	100	1621	
	1503		1553		1516	
a"	1124	681	1009	327		
	1117	653	996	278		236
	1087	349	878	174		
	1057	218	771	156		
	891	169	758	139		
	891	135	658	121	623	49
	847	56	420	84	448	33
	821		411			

[a]Aoyagi,M.; Ohmine,I.;Kohler,B.E. J.Phys.Chem.1990,94,3922.
[b]Buma W.J.;Kohler B.E.;Shaler T.A. J.Chem.Phys.1992,96,399.

Table6.2 lists the the total and relative energies of the lowest singlet states at the 1^1Ag, 2^1Ag, and 1^1Bu equilibrium geometries. CASSCF/DH and

MRSDCI/DH methods were used. The energies are compared with those of Cave and Davidson.

One particle orbital basis used in the present MRSDCI calculation are generated from the CASSCF calculation for a certain state indicated in the third column (the 1^1Ag, 2^1Ag, or 1^1Bu). The CASSCF orbitals are transformed to the natural orbitals and then used in the MRSDCI. They are thus not so called state averaged orbitals. The state energies in MRSDCI depends on for which state CASSCF is converged and the natural orbitals are generated.

The 1^1Ag-2^1Ag 0-0 transition energies of CASSCF/DH and MRDCI calculations (3.68eV and 3.24eV, respectively) are in a reasonable agreement with the experimental energy (3.60 eV), yielding almost same quality with much more sophisticated Cave and Davidson calculation (4.15 ev).

There is a large difference in the equilibrium geometry between the 1^1Ag and 2^1Ag states, and the 1^1Ag-2^1Ag vertical transition energy (5.72 eV in CASSCF and 4.31 eV in MRSDCI) is much larger than the 0-0 transition energy (3.68eV and 3.24eV, respectively) and is also far off from the experimental value. Without including either of the diffuse or the Rydberg basis, MRSDCI calculation can not lower the absolute 2^1Ag state energy drastically. On the other hand, the 1^1Ag-1^1Bu vertical transition energy is drastically improved by including the dynamical correlation through MRSDCI (6.79eV in CAS to 5.71 eV in MRSDCI).

Table 6.3: Total and Relative Energies of the lowest singlet states at the 1Ag,2Ag,1Bu equilibrium geometries.

CASSCF/DH results

state	geometry[a]	MO's[b]	energy (hartree)	ΔE (eV)[c]	expl (eV)
1Ag	1Ag	1Ag	-308.7300		
2Ag	1Ag	1Ag	-308.5201	5.72	
1Bu	1Ag	1Ag	-308.4804	6.79	4.40
2Ag	2Ag	2Ag	-308.5946	3.68	3.60
1Bu	1Bu	1Bu	-308.5021	6.20	4.40

[a]CASSCF/STO-3G optimized geometries are used. [b]Converged State. [c]Relative to the 1Ag result at the ground state equilibrium geometry.

MRSDCI/DH results

state	geometry	MO's[d]	energy (hartree)	ΔE (eV)	expl (eV)
1Ag	1Ag	1Ag	-308.9729		
2Ag	1Ag	1Ag	-308.8145	4.31	
1Bu	1Ag	1Ag	-308.7632	5.71	4.40
2Ag	2Ag	2Ag	-308.8538	3.24	3.60
1Bu	1Bu	1Bu	-308.7979	4.76	4.40

[d]CASSCF Natural Orbital.

Cave R.J.;Davidson R.E. J.Phys.Chem.1988,92,2173

MRCI/Basis set C(3s2p),H(2s) + C(d) exp:0.55 + C(p) exp: 0.021

state	geometry	MO's	energy (hartree)	ΔE (eV)	expl (eV)
1Ag	1Ag	1Ag KO	-309.0470		
1Bu	1Ag	1Bu ANO	-308.8708	4.79	4.40
2Ag	2Ag	1Ag KO	-308.6103[e]	4.15	3.60
1Bu	1Bu	1Bu KO	-308.8794	4.56	4.40

[e]πQCI Calculation

6.3 Adiabatic isomerization in the 2^1Ag state

The measurements of the Z/E-photoisomerization by Kohler et.al suggests that the isomerization is adiabatic.[8] On the other hand, the florescence measurement of all trans-octatetraene and its derivatives t by Petek et al. shows that there exists a very fast internal conversion channel about $\sim 2000cm^{-1}$ above the 2^1Ag planar minimum.[7] We show here that the isomerization along a double bond isomerization does not induce the nonadiabatic transition where as the triple twisted conformations can induce the facile nonadiabatic transition in octatetraene, as we have seen in butadiene and hexatriene.

The potential energy curves along a single torsion of the central C1=C3 are shown in Fig.6.3(a) (see Fig.3.2 for the numbering of atoms). All geometrical parameters other than the dihedral angle C5-C3=C1-C2 are optimized for the 2^1Ag state. The geometry change along the isomerization is shown in Table6.4. The CC single bonds are stretched, the CC double bonds shorten, and consequently the bond alternation becomes indistinct at the transition state on this isomerization path. The bond angles are almost unchanged except the C3-C1-C2 bending angle adjacent to the twisted CC bond. All dihedral angles other than C5-C3=C1-C2 are also almost unchanged, whereas the out-of-plane bending of the terminal $-CH_2$ by 7.6° is induced. The energies of 1^1Ag, 2^1Ag, and 1^1Bu states are monotonically increased along this single C=C isomerization. The energy gap between 1^1Ag and 2^1Ag is slightly decreased but can not become small enough to induce the facile nonadiabatic transition.

In Fig.6.3(b), we plot the potential curves along the same single C=C torsional motion but the geometrical parameters other than the dihedral angle C5-C3=C1-C2 are optimized for the 1^1Bu state. The 1^1Bu state energy is gradually decreased along the isomerization, while the energies of the other

two states are increased. Consequently there is a weakly avoided crossing between the 1^1Bu and 2^1Ag states at 105°. Unlike ethylene the 1^1Bu state and the 1^1Ag state does not get close each other to form so called sudden polarized states, and the facile nonadiabatic transition can not take place at the 90° twisted conformation.

The potential energy curves along the terminal C=C torsional path are shown in Fig.6.3(c). All geometrical parameters other than the dihedral angle H17-C7=C5-C3 are optimized for the 2^1Ag state. The barrier height of the terminal C=C bond isomerization in 2^1Ag state is the lowest among all isomerization paths. The nonadiabatic transition is not significantly induced along this isomerization path.

The potential energy curves along the simultaneous two central C=C bond torsional path are shown in Fig.6.3(d). All geometrical parameters other than the dihedral angles, C5-C3-C1-C2 and C6-C4-C2-C3, are optimized for the 2^1Ag state. This isomerization drastically decreases the energy gap between 1^1Ag and 2^1Ag states. The double torsional motion thus might play a significant role in the internal conversion.

Table 6.4: Optimized Geometric Parameters of all-trans isomer and the Transition State for C1=C3 isomerization.

coordinate	all-trans	TS	coordinate	all-trans	TS
C2-C1	1.416	1.465	C4-C2-C1-C3	180.00	-176.61
C3-C1	1.456	1.500	C5-C3-C1-C2	180.00	-93.54
C4-C2	1.456	1.415	C6-C4-C2-C1	180.00	-179.60
C5-C3	1.392	1.408	C7-C5-C3-C1	180.00	-179.82
C6-C4	1.392	1.414	C8-C6-C4-C2	180.00	178.95
C7-C5	1.453	1.397	H9-C1-C2-C3	180.00	173.61
C8-C6	1.453	1.461	H10-C2-C1-C4	180.00	-179.29
C3-C1-C2	123.51	122.57	H11-C3-C1-C5	180.00	-179.65
C4-C2-C1	123.51	123.39	H12-C4-C2-C6	180.00	-179.79
C5-C3-C1	123.70	123.40	H13-C5-C3-C7	180.00	-179.94
C6-C4-C2	123.70	123.88	H14-C6-C4-C8	180.00	-178.45
C7-C5-C3	123.81	124.02	H15-C7-C5-C3	0.00	0.06
C8-C6-C4	123.81	123.56	H16-C8-C6-C4	0.00	6.69
H9-C1-C2	118.72	118.40	H17-C7-C5-H15	180.00	-179.98
H10-C2-C1	118.72	117.89	H18-C8-C6-H16	180.00	166.76
H11-C3-C1	117.40	118.02			
H12-C4-C2	117.40	118.05			
H13-C5-C3	118.70	117.92			
H14-C6-C4	118.70	118.59			
H15-C7-C5	120.84	121.26			
H16-C8-C6	120.84	120.39			
H17-C7-C5	120.99	121.44			
H18-C8-C6	120.99	120.48			

Bond lengths are in angstroms, and bond angles and torsional angles are in degree.

(a)The C1=C3 torsion minimum energy path in 2Ag state

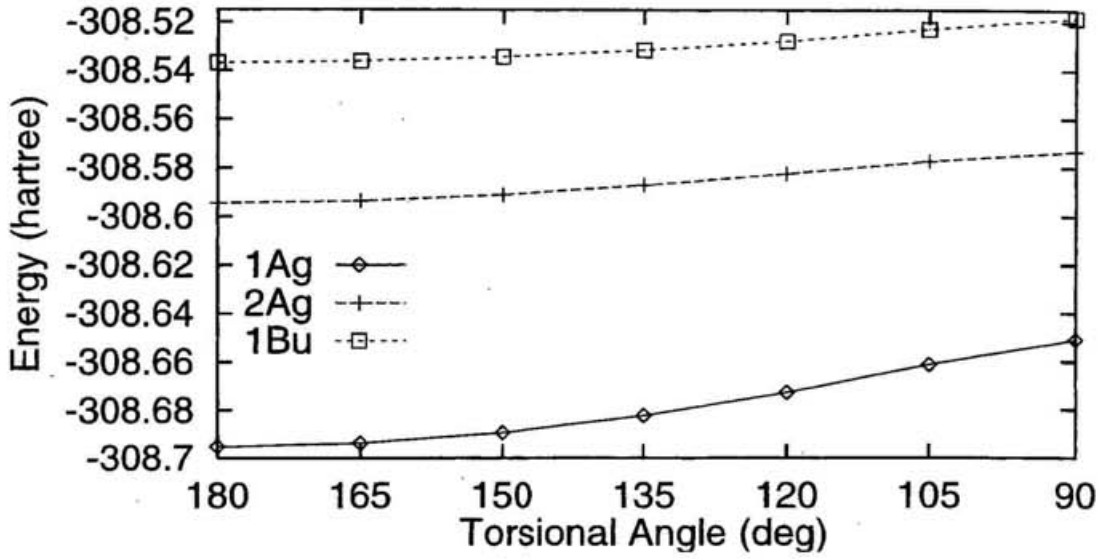

(b)The C1=C3 torsion minimum energy path in 1Bu state

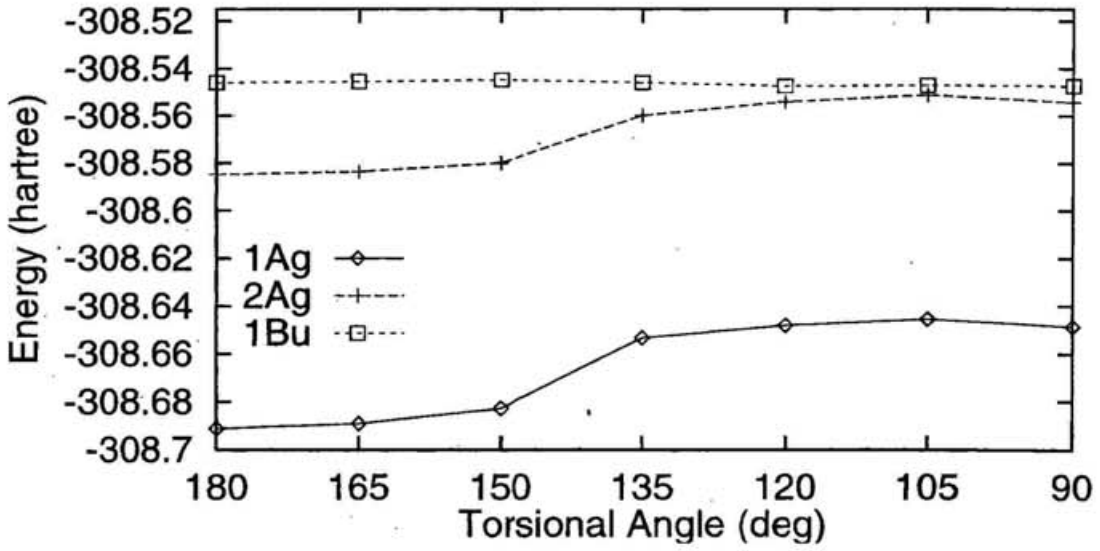

(c)The C5=C7 torsion minimum energy path in 2Ag state

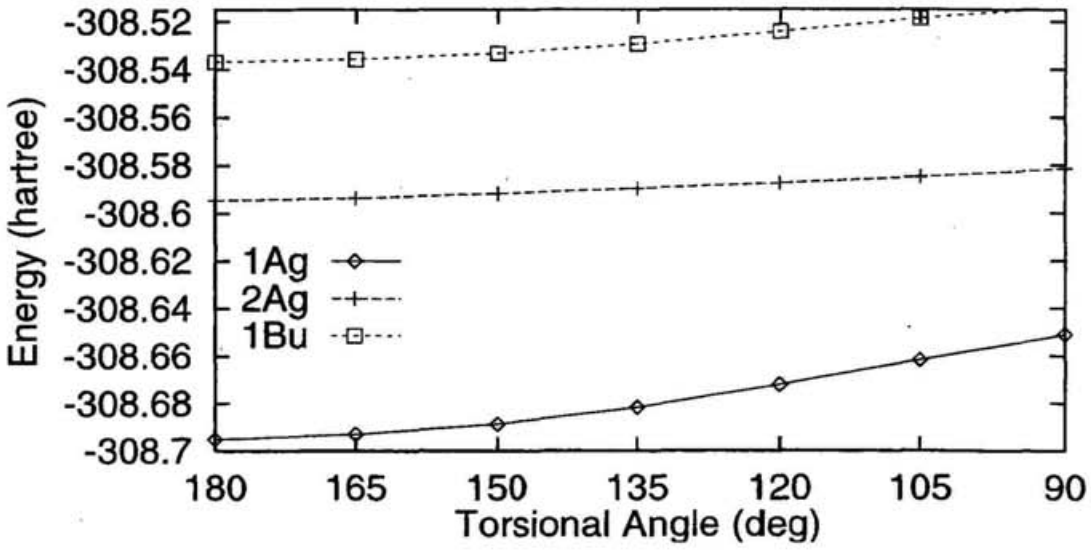

(d)The C1=C3 C2=C4 double torsion minimum energy path in 2Ag state

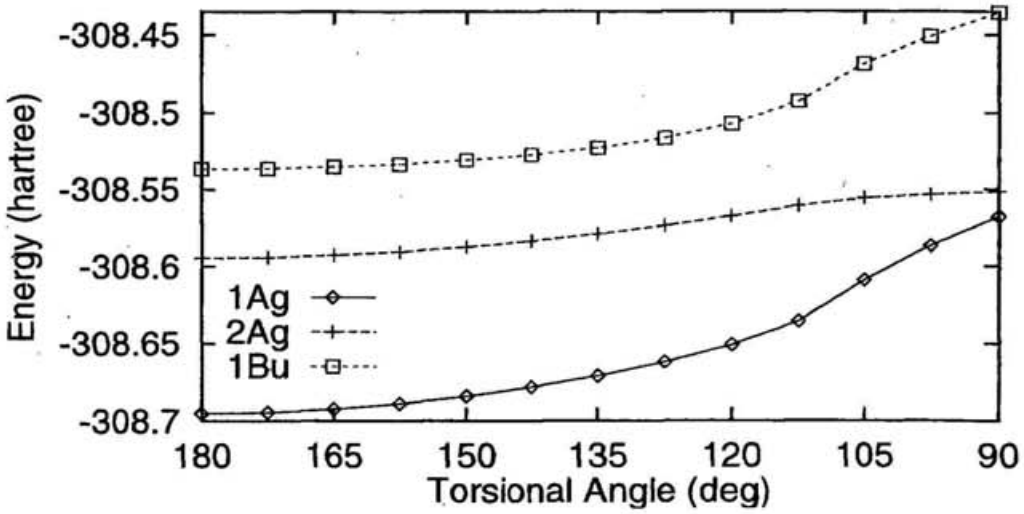

Figure 6.3: Potential energy curves along the isomerization paths (CASSCF/DH). (a)The C1=C3 torsion minimum energy path in 2Ag state (b)The C1=C3 torsion minimum energy path in 1Bu state (c)The C5=C7 torsion minimum energy path in 2Ag state (d)The C1=C3 C2=C4 double torsion minimum energy path in 2Ag state

Table6.5 summarizes the barrier height of the 2^1Ag adiabatic isomerization and the energy gap between the 2^1Ag and 1^1Ag states. Any isomerization along a double bond can not bring the 2^1Ag and 1^1Ag state potential energy curves close enough to cause the facile nonadiabatic isomerization, thus is 'adiabatic'. The single bond isomerization in the 2^1Ag state involves a considerably higher barrier as we have seen in butadiene and hexatriene. The experiments of Kohler et. al and Petek et. al suggest that the adiabatic isomerization barrier is lower than the internal conversion channel ($\sim 2400cm^{-1}$). Our calculation agrees with these experiments in that the barrier for the central double bond (C1=C3) isomerization is relatively lower than the barrier for the internal conversion. The isomerization barrier is decreased by including the dynamic correlation through MRSDCI calculation, while the energy gap between 2^1Ag and 1^1Ag is unchanged.

Table 6.5: Total and Relative Energies of the lowest excited state at the 90° C=C twisted geometries[a].

CASSCF/DH results

twisted bond	energy	ΔE(2Ag)[b]	ΔE(1Ag)[c]
C1=C3	-308.5733	0.0213(4670)[d]	0.0777
C1=C3(1Bu)[e]	-308.5542	0.0306(6720)	0.0944
C5=C7	-308.5815	0.0131(2880)	0.0695
C1=C3,C2=C4	-308.5514	0.0432(9480)	0.0163

[a]CASSCF/STO-3G Optimized excited state geometry used in the calculation. [b]Relative to the 2Ag energy at the planer equilibrium geometry. [c]Relative to the 1Ag energy at the twisted geometry. [d]In cm^{-1}. [e]Optimized in the 1Bu state.

MRSDCI/DH results

twisted bond	energy	ΔE(2Ag)[b]	ΔE(1Ag)[c]
C1=C3	-308.8454	0.0129(2830)	0.0688
C1=C3(1Bu)	-308.8413	0.0084(1840)	0.0734
C5=C7	-308.8453	0.0098(2150)	0.0708
C1=C3,C2=C4	-308.8120	0.0418(9170)	0.0342

6.4 The isomerization inducing the nonadiabatic transition to 1^1Ag

As we discussed earlier in butadiene and hexatriene, the triple torsion, which divides the π electron conjugation into four parts consisting odd carbon atoms, yields the degeneracy between the 1^1Ag and 2^1Ag states in octatetraene. The potential energy curves along two such isomerization paths are shown in Fig.6.4, and the lowest energy conformation in the crossing seam between the 1^1Ag and 2^1Ag states is shown in Fig.6.5. Other types of the triple torsion, which results in the molecular segments with even carbon atoms, yield the strongly avoided crossing.

(a)The C1-C2 C1=C3 C2=C4 torsion

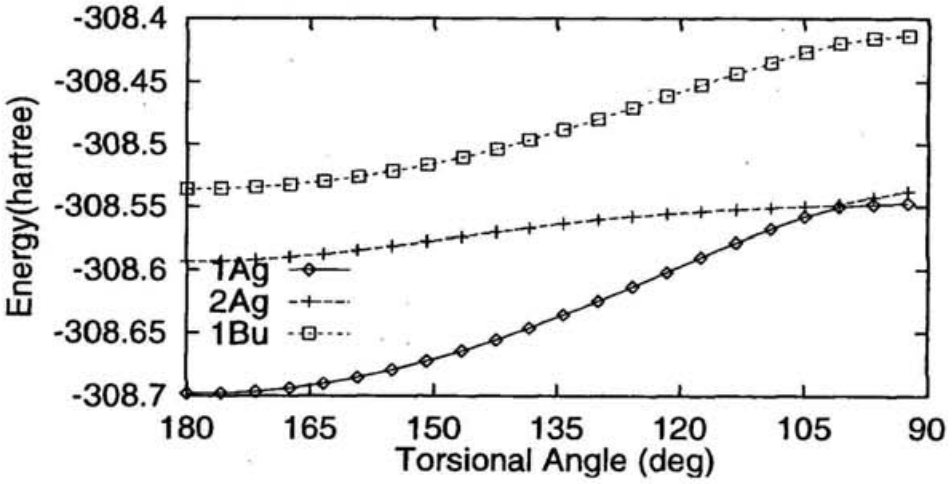

(b)The C1-C2 C2=C4 C5=C7 torsion

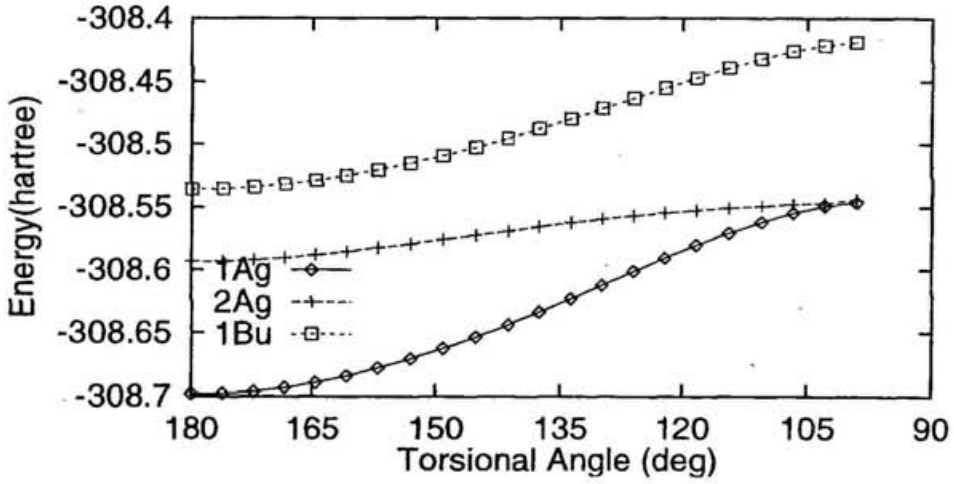

Figure 6.4: Potential Energy Curves along the Path to the Lowest Energy Conformation in the Avoided Crossing Seam. (CASSCF/DH) (a)The C1-C2 C1=C3 C2=C4 torsion (b)The C1-C2 C2=C4 C5=C7 torsion

(a)The C1-C2 C1=C3 C2=C4 torsion

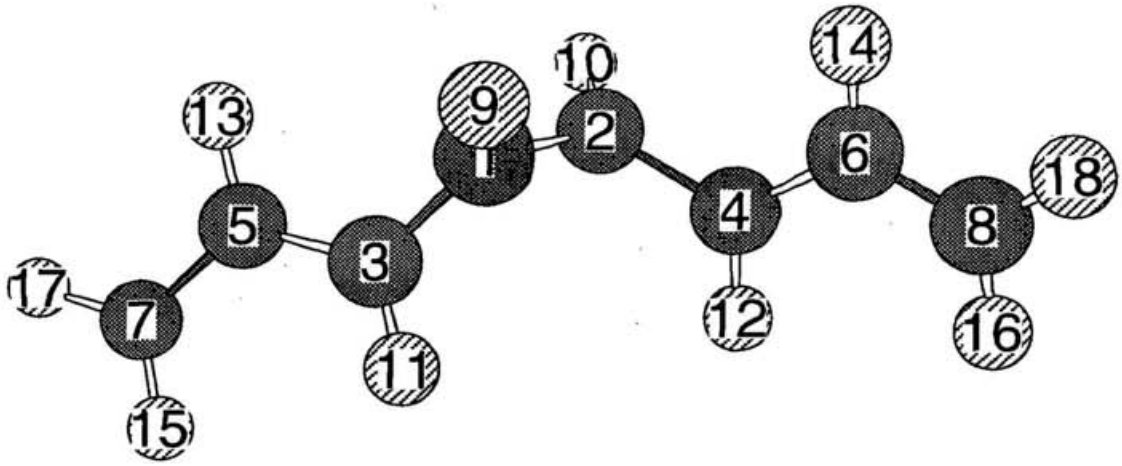

(b)The C1-C2 C2=C4 C5=C7 torsion

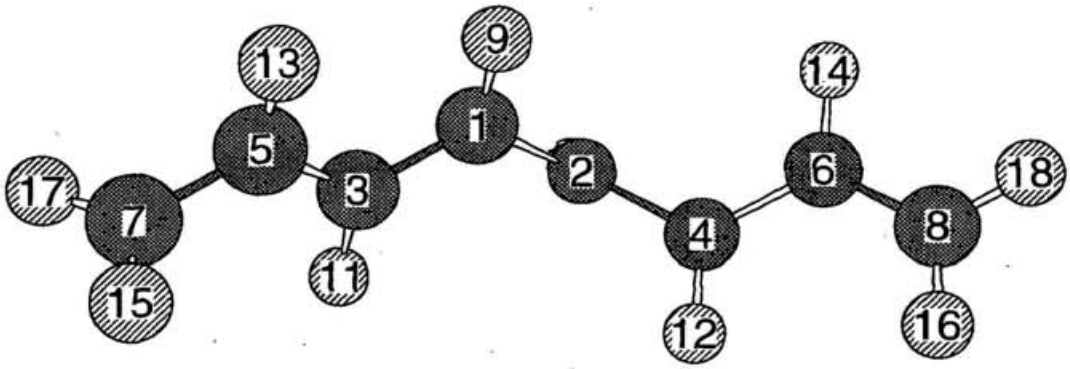

Figure 6.5: The Lowest Energy Conformations in the Crossing Seam. (a)The C1-C2 C1=C3 C2=C4 torsion (b)The C1-C2 C2=C4 C5=C7 torsion

6.5 Fluorescence decay

From the global feature of the potential energy surfaces calculated here, we may predict the internal conversion mechanism involved in the octatetraene photoisomerization. After the very fast internal conversion from 1^1Bu to 2^1Ag, which is expected to take place within some tens of femto seconds. a near planar octatetraene begins to undergoes the isomerize on the 2Ag surface. If it has only small excess energy not enough to induce the triple torsion at this stage, the molecule must stay on 2^1Ag state around all trans-isomer which is most stable in the 2^1Ag state for long time. If it has the excess energy high enough to induce the triple torsion, the facile nonadiabatic transition can take place.

The fluorescence life time of 2^1Ag thus must show the strong excess energy dependence; the steep rise of the internal conversion rates in the free jet expansion experiment is attributed to this nonadiabatic transition at the triply twisted conformation. The low Z/E-photoisomerization yield of the condensed phase experiments is also explained in the same manner. As the excess energy is dissipated in the condensed phase, the system can not induce the the triple torsion causing the facile nonadiabatic transition.

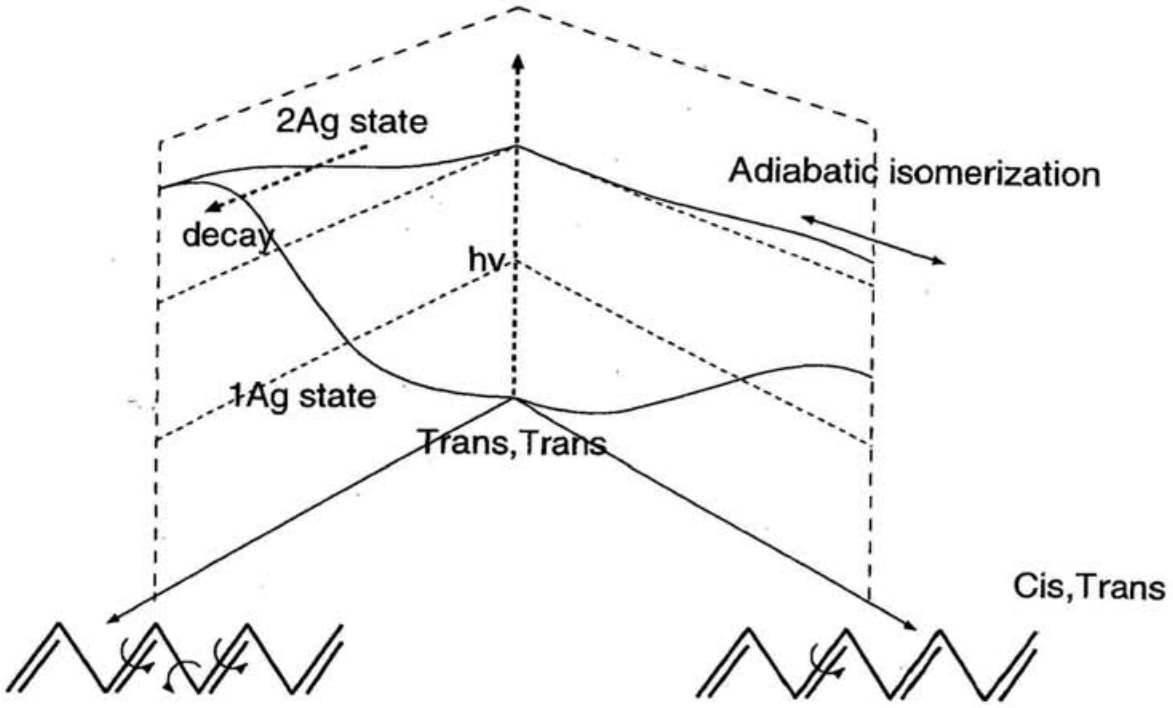
2Ag state
Adiabatic isomerization
decay
hv
1Ag state
Trans,Trans
Cis,Trans

Chapter 7

Conclusion

We have developed the model Hamiltonian based on VB picture, which reproduces the potential energy surfaces and nonadiabatic coupling of the 1^1Ag and 2^1Ag states of butadiene along various isomerization paths. The agreement between the model and SA-CASSCF calculation is remarkable and the first-principle nonadiabatic dynamics simulation could be performed with this model Hamiltonian. The model also provides a simple interpretation for the electronic structures of the 1^1Ag and 2^1Ag states of butadiene. At the planar conformation, the VB state with the perfect pairing character dominates the 1^1Ag state and that of the double triplet character dominates 2^1Ag. The mixing of VB states is taken place by the change of π bonding character along isomerization paths. The intense nonadiabatic coupling occurs when the energies of two VB states get mutually close and the Hamiltonian off-diagonal element between the VB states becomes small. The model can also predict the locus of the degeneracy between 1^1Ag and 2^1Ag states in a simple manner. The degeneracy occurs, when the isomerization induces the exact cancelation between the effective spin interaction contributions to the Hamiltonian off-diagonal element and the energies of two VB states agree with each other exactly.

The present model was shown to be also applicable for hexatriene. The ab-initio potential energy surface of hexatriene is reproduced qualitatively

by the present simplified model, although the quantitative accuracy is not enough to be employed in a dynamics simulation yet. Further improvement of the hexatriene model is in progress.

Although the present model calculation explains the qualitative feature of the PES's of the 1^1Ag and 2^1Ag states and their nonadiabatic couplings, a more elaborate model is required for quantitative analysis of the photoisomerization dynamics. As expected from that no fluorescence has been detected in experiments, t he decay of the 2^1Ag state occupation probability should be much faster than that calculated by the present model.[46] This is due to that only CC bond stretching, bending and torsion are treated to induce the electronic character change of the 1^1Ag and 2^1Ag states in the present model and other coordinates must involves the nonadiabatic transitions.

Bibliography

[1] M.Aoyagi, Y. Osamura and S. Iwata, J. Chem. Phys. 83, 1140 (1985)

[2] F. Zerbetto and M. Z. Zgierski, J. Chem. Phys. 93, 1235 (1990)

[3] M. Olivucci, I. N. Ragazos, F. Bernardi and M. A. Robb, J. Am. Chem. Soc. 115, 3710 (1993)

[4] I. Ohmine, J. Chem. Phys. 83, 2348 (1985)

[5] P. Celani, F. Bernardi, M. Olivucci and M. A. Robb, J. Chem. Phys. 102, 5733 (1995)

[6] M. Olivucci, F. Bernardi, P. Celani, I. Ragazos and M. A. Robb, J. Am. Chem. Soc. 116 , 1077 (1994)

[7] H. Petek, A.J. Bell, R.L. Christensen and K. Yoshihara, J. Chem. Phys. 96, 2412 (1992); H. Petek, A.J. Bell, K. Yoshihara, B.A. Tounge and R.L. Christensen, ibid. 98, 3777 (1993);

[8] B. E. Kohler, Chem. Rev. 93, 41 (1993);

[9] J. Michl and V. Bonačić-Koutecký, Electronic aspects of organic photochemistry (Wiley, New York, 1990)

[10] W. M. Gelbart, K. F. Freed and S. A. Rice, J. Chem. Phys. 52, 2460 (1970)

[11] B. Bagchi, G. R. Fleming and D. W. Oxtoby, J. Chem. Phys. 78, 7375 (1983)

[12] A. Warshel, Z. T. Chu and J. K. Hwang, Chem. Phys. 158, 303 (1991)

[13] G. J. M. Dormans, G. C. Groenenboo and H. M. Buck, J. Chem. Phys. 86, 4895 (1987)

[14] M. Perisco, J. Am. Chem. Soc. , 102 , 7839 (1980)

[15] L. Seiner and W. Domcke Chem. Phys. 186, 27 (1994) ; H. Köppel, W. Domcke and L. S. Cederbaum, Advan. Chem. Phys. 57, 59 (1984) ; R. Schnider, W. Domcke and H. Köppel, J. Chem. Phys. 92, 1045 (1990)

[16] R.B. Woodward and R. Hoffman, The Conservation of Orbital Symmetry, Verlag Chemie, Weinheim/Deerfield Bearch, 1970; K. Fukui, Angew. Chem., Int. Ed. Engl. 21,801 (1982)

[17] J.P. Marlrieu and D. Maynau, J.Am.Chem.Soc. 104,3021 (1982); D. Maynau and J.P. Malrieu, ibid. 104, 3029 (1982)

[18] M. Said, D. Maynau, J.P. Malrieu and M.A.G.Bach, J.Am.Chem.Soc. 106, 571 (1984); M. Said, D. Maynau and J.P. Malrieu, ibid. 106, 580 (1984)

[19] G. Treboux, D. Maynau and J.P. Malrieu, J.Phys.Chem. 99 , 6417 (1995)

[20] A. Warshel in, 'MODERN THEORETICAL CHEMISTRY',Vol. 7, p133, eds.G. A. Segal, PLENUM PRESS,NEW YORK AND LONDON

[21] F. Bernardi, M. Olivucci, J. J. W. McDouall and M. A. Robb, J. Chem. Phys. 89, 6365 (1988)

[22] F. Bernardi, M. Olivucci and M. A. Robb, J. Am. Chem. Soc. 114, 1606 (1992)

[23] P.Durand and J.P. Malrieu, Adv.Chem.Phys. 76,321(1987)

[24] F. Bernardi, S. De, M. Olivucci and M.A. Robb, J.Am.Chem.Soc. 112,1737 (1990)

[25] B.R. Smith, M.J. Bearpark, M.A. Robb, F. Bernardi and M. Olivucci, Chem.Phys.Lett. 242, 27 (1995)

[26] M.J. Bearpark, F. Bernardi, S. Clifford, M. Olivucci, M.A. Robb, B.R. Smith and T. Vreven, J.Am.Chem.Soc. 118, 169 (1996)

[27] A. Warshal and M. Karplus, J.Am.Chem.Soc. 94,5612 (1972); A.C. Lasaga, R.J. Aerni and M. Karplus, J.Chem.Phys. 73,5230 (1980)

[28] R.Pauncz, 'Spin Eigenfunctions Construction and Use',Plenum Press, New York 1979

[29] N.L.Allinger, J.Am.Chem.Soc. 99, 8127 (1977); J.T.Sprague, J.C. Tai, Y. Yuh and N.L. Allinger, J.Comput.Chem. 8, 581 (1987); N.L. Allinger, Y.H. Yuh and J.-H. Lii, J.Am.Chem.Soc. 111, 8551 (1989)

[30] A. K. Rappé, C. J. Casewit, K. S. Colwell, W. A. Goddard III and W. M. Skiff, J. Am. Chem. Soc. 114, 10024 (1992)

[31] W.D.Cornell, P.Cieplak, C.I. Bayly, I.R. Gould, K.M. Mertz Jr., D.M.Ferguson, D.C.Spellmeyer, T. Fox, J.W. CaldWell and P.A.Kollman, J.Am.Chem.Soc. 117, 5179 (1995)

[32] T. Nakagawa and Y. Oyanagi, "Program System SALS for Nonlinear Least Square Fitting in Experimental Science" in Recent Developments in Statistical Inference and Data Analysis, K. Matusita, editor, p. 221-225 (North Holland Publishing Company, Amsterdam, 1980)

[33] T.H. Dunning and P.J. Hay, in Methods of Modern Theoretical Chemistry edited by H. F. Schaefer (Plenum, New York, 1977), Vol.3, pp 1-27.

[34] MOLPRO is a package of ab initio programs written by H.-J. Werner and P.J. Knowles, with contributions form J. Almolöf, R.D. Amos, M.J.O. Deegan, S.T. Elbert, C. Hampel, W.Meyer, K. Peterson, R. Pitzer, A.J. Stone and P.R. Taylor; H.-J. Werner and P.J. Knowles, J.Chem.Phys. 82, 5053 (1985); P.J. Knowles and H.-J. Werner, Chem.Phys.Lett. 115, 259 (1985); H.-J. Werner and W. Meyer, J.Chem.Phys. 73, 2342 (1980); ibid. 74, 5794 (1981); H.-J. Werner, Adv. Chem. Phys. LXIX, 1 (1987)

[35] Gaussian 94, Revision B.3, M. J. Frisch, G. W. Trucks, H. B. Schlegel, P. M. W. Gill, B. G. Johnson, M. A. Robb, J. R. Cheeseman, T. Keith, G. A. Petersson, J. A. Montgomery, K. Raghavachari, M. A. Al-Laham, V. G. Zakrzewski, J. V. Ortiz, J. B. Foresman, C. Y. Peng, P. Y. Ayala, W. Chen, M. W. Wong, J. L. Andres, E. S. Replogle, R. Gomperts, R. L. Martin, D. J. Fox, J. S. Binkley, D. J. Defrees, J. Baker, J. P. Stewart, M. Head-Gordon, C. Gonzalez, and J. A. Pople, Gaussian, Inc., Pittsburgh PA, 1995.

[36] J. von Neumann and E. Wigner, Physik. Z. 30, 467 (1929)

[37] E. Teller, J. Chem. Phys. 41, 109 (1937)

[38] G. Herzberg and H. C. Longuett-Higgins, Transact. Faraday Soc. 35, 77 (1963)

[39] M. Garavelli, P. Celani, N. Yamamoto, F. Bernardi, M.A. Robb and M. Olivucci, J.Am.Chem.Soc. in press

[40] P. Celani, M. Gravelli, S. Ottani, F. Bernardi, M.A. Robb and M.Olivucci, J.Am.Chem.Soc. 117, 11584 (1995)

[41] M.W.Schmidt, K.K.Baldridge, J.A.Boatz, J.H.Jensen, S.Koseki, M.S.Gordon, K.A.Nguyen, T.L.Windus, S.T.Elbert QCPE Bulletin, 10, 52-54 (1990).

[42] W.J.Hehre, R.F.Stewart, and J.A.Pople, J.Chem.Phys. 51, 2657-2664(1969)

[43] The MELD siries of electronic structure codes was developed by L.E. McMurchie, S.T. Elbert, S.R. Langhoff, and E.R. Davidson and was extensively modified by D. Feller and D.C. Rawlings. We use these codes at IMS computer center.

[44] K. Morihashi and O. Kikuchi, Theoret. Chim. Acta 67,293 (1985)

[45] R.J. Cave and E.R. Davidson, J. Phys. Chem, 91, 4481 (1987); ibid, 92, 614 (1988); ibid, 92, 2173 (1988)

[46] V. Vaida, Acc. Chem. Res. 19, 114 (1986); J.B. Snow, Ph.D. Thesis, Wesleyan University, 1980; R. M. Gavin Jr., S. Risemberg, S.A. Rice, J.Chem.Phys. 58, 3160 (1973)

[47] E. Teller, J. Chem. Phys. 41, 109 (1937)

Part II

Internal Conversion Mechanism of s-trans Butadiene

Chapter 8

Introduction

The fluorescence decay of butadiene and hexatriene is very fast, whereas octatetraene and longer polyenes yield the intense fluorescence. Their fast decay is due to the C-C torsional isomerization involving the efficient nonadiabatic transition to the ground state. As we discussed earlier, the polyene molecules have the electronic structure and the shape of potential energy surfaces essentially different from ethylene.

A few models have been proposed to deal with the internal conversion from the 2^1Ag to 1^1Ag state, which are based on the analysis of the potential energy surfaces obtained from the ab-initio calculations. By using a model calculation, Zerbetto and Zgierski have proposed that a nonadiabatic transition from 2^1Ag to 1^1Ag is induced by the CC torsions.[1] Robb and his coworkers have proposed that the triple CC torsion is the major path to yield a very fast nonadiabatic transition.[2, 3, 4] Their CASSCF/4-31G calculation have scanned an entire conformational space over all three CC bond torsional degrees.[2]

A considerable number of investigations of the polyene photoisomerization processes have been performed on the basis of the intuitive picture of the ethylene isomerization. [6, 7, 8, 9, 10, 11] ; the Golden-rule model of Gelbert, Freed and Rice [6], the phenomenological damped oscillator model of Bagchi, Fleming and Oxtoby [7], and the surface-hopping trajectory of rhodopsin by

Warshel and his coworkers [8]. Since these treatments are often based on models which only include a part of internal molecular degrees of freedom, they might not fit to treat the irreversible character in the nonadiabatic transitions of the polyene photoisomerization processes, as indicated by the study of Domcke and collaborators. [11]

For simulating a nonadiabatic dynamics of the photoisomerization, we use employ the model Hamiltonian based on the Heisenberg Hamiltonian. As we discussed earlier, it can well describe the multidimensional feature of the 2^1Ag and 1^1Ag potential energy surfaces and their nonadiabatic coupling. In order to investigate various isomerization paths, this model is simple enough for the efficient evaluation of the potential energy surfaces and the nonadiabatic coupling. Besides, the model can includes all internal degrees of the molecule in order to treat the energy relaxation dynamics properly.

In the present work, we focus our attention on the dynamical aspects of this internal conversion process from 2^1Ag to 1^1Ag of s-trans butadiene, especially the intramolecular mode dynamics promoting this conversion. We have chosen here the photoisomerization of butadiene by three reasons; We already have obtained the set of parameters which reproduce fairly realistic potential energy surface and nonadiabatic coupling term along various intramolecular degrees of freedom. The short time scale dynamics of butadiene internal conversion [12] makes it possible to perform extensive molecular dynamics simulations. The 1^1Ag and 2^1Ag potential surfaces of butadiene, hexatriene, and octatetraene have the common feature that they degenerate at the triple twisted CC conformations.[4]

Chapter 9

Method of Nonadiabatic Dynamics Simulation

9.1 Propagation of the classical and quantum subsystems

A semiclassical surface hopping treatment is applied to investigate the nonadiabatic transition and the relaxation dynamics in the photoisomerization of butadiene. The nuclei are assumed to follow a classical equation of motion, and represented by coordinates $\mathbf{R}(t)$. The electronic Hamiltonian $\mathbf{H}(\mathbf{r}, \mathbf{R}(t))$ parametrically depends on time through $\mathbf{R}(t)$. The electronic wave function $\psi(\mathbf{r}, t)$ of the system is nonstationary and satisfies the time dependent Schrödinger equation. It is expanded in terms of a set of instantaneous adiabatic states $\phi_n(\mathbf{r}, \mathbf{R})$,

$$\psi(\mathbf{r}, t) = \sum_n a_n(t)\phi_n(\mathbf{r}, \mathbf{R}(t)) \ , \tag{9.1}$$

$$i\hbar\frac{\partial}{\partial t}\psi(\mathbf{r}, t) = \mathbf{H}(\mathbf{r}, \mathbf{R}(t))\psi(\mathbf{r}, t) \tag{9.2}$$

where we assume only two states, 1^1Ag and 2^1Ag (n=1 and 2, respectively), are involved in the dymanics. The adiabatic bases are the eigenstates of the electronic model Hamiltonian specified by the classical coordinates $\mathbf{R}(t)$ at time t.

Substituting this expansion of the electronic wavefunction $\psi(\mathbf{r},t)$ into the time-dependent Schrödinger equation results in the evolution of the expansion coefficients $a_n(t)$,

$$\dot{\mathbf{a}}(t) = \mathbf{U}(t)\mathbf{a}(t) \ , \tag{9.3}$$

$$\mathbf{U}(t) = \begin{bmatrix} E_1 & -i\hbar\langle\phi_1|\frac{\partial}{\partial\mathbf{R}}|\phi_2\rangle\cdot\dot{\mathbf{R}} \\ -i\hbar\langle\phi_2|\frac{\partial}{\partial\mathbf{R}}|\phi_1\rangle\cdot\dot{\mathbf{R}} & E_2 \end{bmatrix} . \tag{9.4}$$

The nuclear coordinates are driven by the Hellmann-Feynman force of either instantaneous adiabatic state $\phi_n(\mathbf{r},\mathbf{R}(t))$,

$$\mathbf{m}\ddot{\mathbf{R}}(t) = -\sum_i\sum_j C_{in}^* \frac{\partial H_{ij}}{\partial\mathbf{R}} C_{jn} \ , \tag{9.5}$$

Here $H_{i,j}$ is a Hamiltonian matrix element between two VB bases, $\varphi_i^{VB}(\mathbf{R}(t))$ and $\varphi_j^{VB}(\mathbf{R}(t))$.

9.2 A semiclassical surface hopping trajectory method

The adiabatic state whose force drives the nuclear coordinates is switched on the way of the trajectory calculation, so that the averaged dynamics satisfies the statistical requirement.

Since the average of dynamical quantities of the system is obtained by propagating swarm of N trajectories, the number of trajectories on the surface of adiabatic state n at time t must be equal to $a_n^*(t)a_n(t)N$ from the statistical requirement. In order to satisfy this condition, we employ so called the "Fewest Switch" algorithm. [13] The system intermittently makes the stochastic hops between the 2^1Ag and the 1^1Ag states depending on the occupation probability change.

When a hop occurs, the velocity components parallel to the nonadiabatic coupling vector are adjusted to conserve the total energy. [14, 15, 16] In the case when the transition occurs to the upper state, it requires a velocity

reduction and thus restricts a hop. If the velocity change cannot compensate for the adiabatic energy difference, the velocity components are just reversed.[16]

The force vectors driving the nuclear coordinates are given in the internal coordinates and are transformed into the Cartesian vectors. The equation of motion for the nuclear coordinates in the Cartesian coordinate are integrated by the Verlet method. This method conserves the total energy in the second order of the time step Δt.

On the other hand, Webster et al. argued that the integration of the quantum force conserves the energy only through the first order in Δt [17]. The total energy of the system is

$$E = \langle \phi_n | \mathbf{H} | \phi_n \rangle + \sum_i \frac{1}{2} m_i \dot{R}_i^2 . \tag{9.6}$$

Applying the Hellmann-Feynman theorem and assuming that the electronic state is always n'th state, we have $dE/dt = 0$. In the simulation, however, a time-stepping algorithm is employed, hence the total energy is only approximately conserved. To demonstrate the total energy change for a finite time step size, we consider the following time-dependent Hamiltonian.

$$\mathbf{H}(\mathbf{r}, \mathbf{R}(t_{i+1})) = \mathbf{H_Q}(\mathbf{r}, \mathbf{R}(t_i)) + \Delta t \mathbf{H}'(\mathbf{r}) \tag{9.7}$$

for small $\Delta t = t_{i+1} - t_i$. Since the $\mathbf{H}'$ is assumed to be independent of $\mathbf{R}$, the Hellmann-Feynman force is time-independent. The energy change of the nuclei due to this force is

$$-\Delta t \left\langle \phi_n \left| \frac{\partial \mathbf{H_Q}}{\partial \mathbf{R}} \right| \phi_n \right\rangle \cdot \dot{\mathbf{R}} = -\Delta t \langle \phi_n | \mathbf{H}' | \phi_n \rangle . \tag{9.8}$$

This corresponds to the first-order perturbation energy. Thus, for finite time steps the simulation conserves the total energy only through the first order in Δt . It is largely due to neglect of changes of the wavefunction of the electronic state. We thus use a very small time step, Δt =0.01fs, to trace

the rapidly varying nonadiabatic coupling and conserve the total energy up to the fifth decimal.

At each time t evolving the classical coordinates, the wave function is propagated to determine the switch probability between two adiabatic states. Since the expansion coefficients $a_n(t)$ rapidly oscillate, a smaller time step is required to integrate its equation of motion accurately. So we divide the classical time step Δt into four parts δt and approximate the system propagator by the linear interpolation.

$$\mathbf{U}(t + k\delta t) = \mathbf{U}(t) + \frac{k\delta t}{\Delta t}(\mathbf{U}(t + \Delta t) - \mathbf{U}(t)) \ , \tag{9.9}$$

$$k = 1 \cdots 4 \ .$$

The quantum time step δt is $1/48$ of the smallest period calculated from the maximum energy fluctuation($\sim$0.2 hartree) by the uncertainty principle.

We use the split time operator method by dividing the propagator $\mathbf{U}(t)$ (Eq.9.4) into the diagonal (energy) part and the off-diagonal (nonadiabatic) part in order to avoid the numerical error in diagonalization of the propagator. [18, 19, 20]. This method is known to well conserve the norm; the error due to the non-commutability of the energy and the nonadiabatic coupling is of the second order of δt in this method.

Chapter 10

Nonadiabatic Transition and Energy Relaxation Dynamics

The semiclassical calculation is performed to simulate the butadiene photoisomerization process, including nonadiabatic coupling.

The initial configurations of the trajectories are prepared by performing a classical trajectory of the ground state, 1^1Ag, where the averaged kinetic energy of the system is equal to the room temperature $T = 298K$. The system is then excited at randomly chosen time t_{init} from the ground state to 2^1Ag state through the Frank-Condon transition, by keeping the positions and velocities of all atoms in butadiene unchanged. Numerous initial configurations (geometries and velocities) on the 2^1Ag state potential surface are generated by choosing different t_{init}. Among them, we select the configurations whose total energies are 0.0311 $\sim$ 0.0361 hartree higher than the 2^1Ag potential energy at the planar equilibrium structure.

Then we monitor the following semiclassical surface hopping trajectories in 5 ps. The total number of the trajectories calculated in the present work is 515.

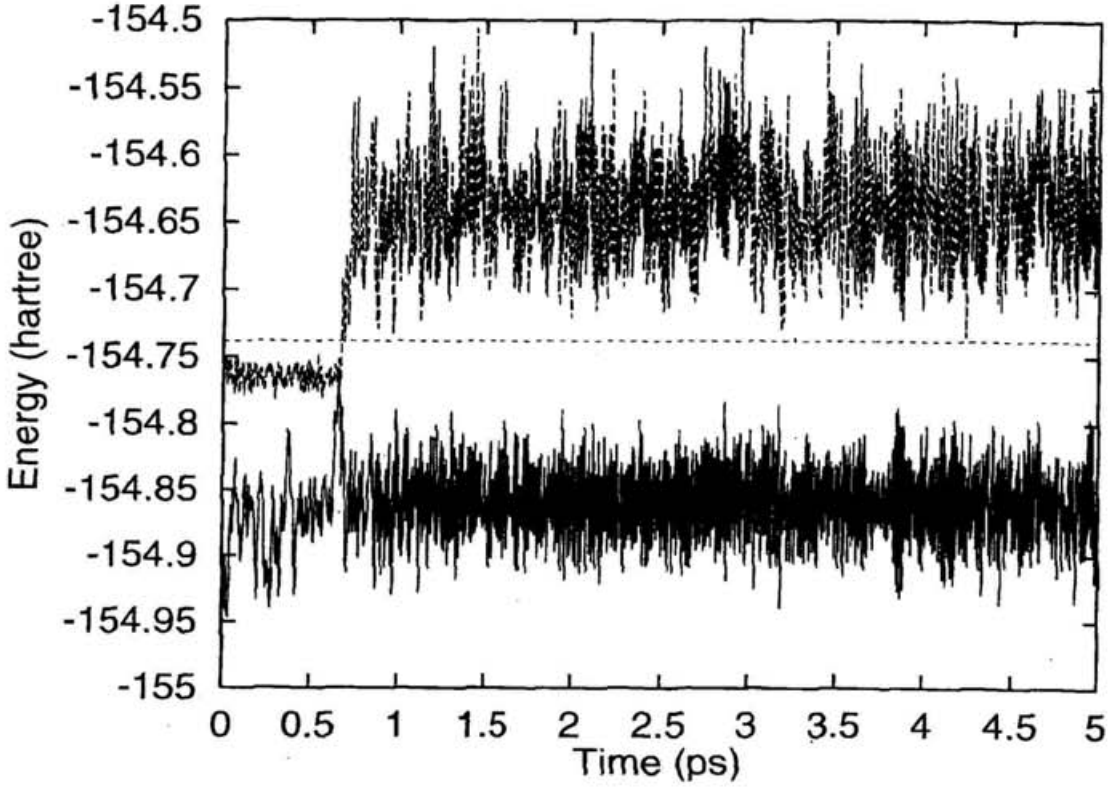

Figure 10.1: State energies and the total energy as functions of time after excitation into 2^1Ag state in a nonadiabatic dynamics trajectories. The 1^1Ag potential energy (solid line), 2^1Ag (long dashed line), the total energy (short dashed line) The total energy is shown to indicate the accuracy of the energy conservation.

10.1 Nonadiabatic transitions in the representative trajectories

The time evolution of the wavefunction is sensitive to the difference of the energy gap and the nonadiabatic coupling. We have found two typical types of the nonadiabatic transitions in the trajectories.

In the first type (shown in Fig.10.2), the trajectory passes through a crossing point between 1^1Ag and 2^1Ag potential energy surfaces and then the occupation probability $|a_2(t)|^2$ of the 2^1Ag adiabatic state in wavefunction and that of the second VB state suddenly diminish within 20 fs (Figs.10.2(b) and (c), respectively). The surface hop between the adiabatic states occurs in this 20 fs. As seen in Fig.10.2(c), the occupation probability of the second VB state yields large oscillation as the coupling between the VB states alters along the isomerization before the surface hop takes place. The oscillation then becomes faster due to the complex phase difference change between $a_1(t)$ and $a_2(t)$ as the wavefunction becomes the superimposed state of ϕ_1 and ϕ_2. The phase change rate is proportional to the energy of the adiabatic states(Eq.9.4). When the CCC bending is enhanced (Fig.10.2(d)), the large peak of the nonadiabatic coupling appears (Fig.10.2(e); the inner product of the nonadiabatic coupling and the velocity vector is plotted.)

In the second type (shown in Fig. 10.3), the occupation probability of 2^1Ag adiabatic state in the wavefunction and that of the second VB state only gradually decrease, since the difference between the 1^1Ag and 2^1Ag potential energies does not get so small by their strong avoiding. The occupation probability of the second VB state exhibits also a rapid oscillation (Fig.10.3(c)) as in the first type after the wavefunction becomes the superimposed state of ϕ_1 and ϕ_2. The nonadiabatic coupling also appears when the CCC bending is enhanced (Fig.10.3(d) and (e)). But the enhancement

is not so large as in the first type and the 2^1Ag state occupation probability change is small due to the finite energy gap.

(a) The state energies and the total energy (in hartree)

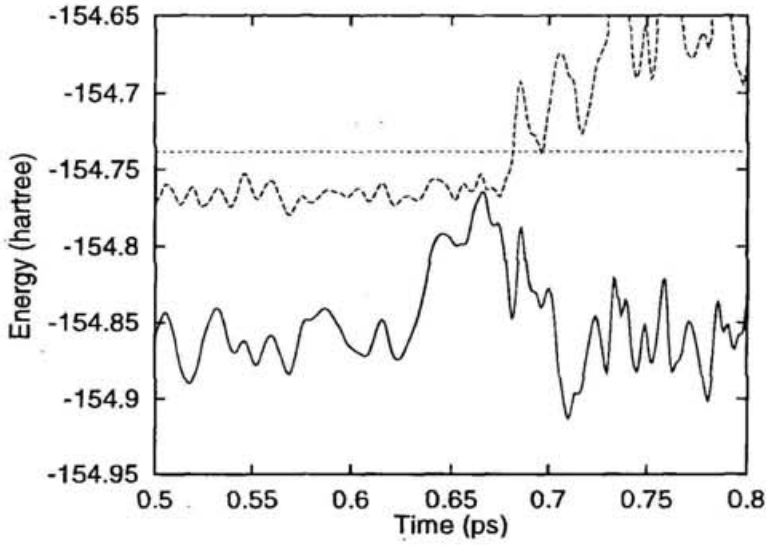

(b) The occupation probability of 2^1Ag in the wavefunction

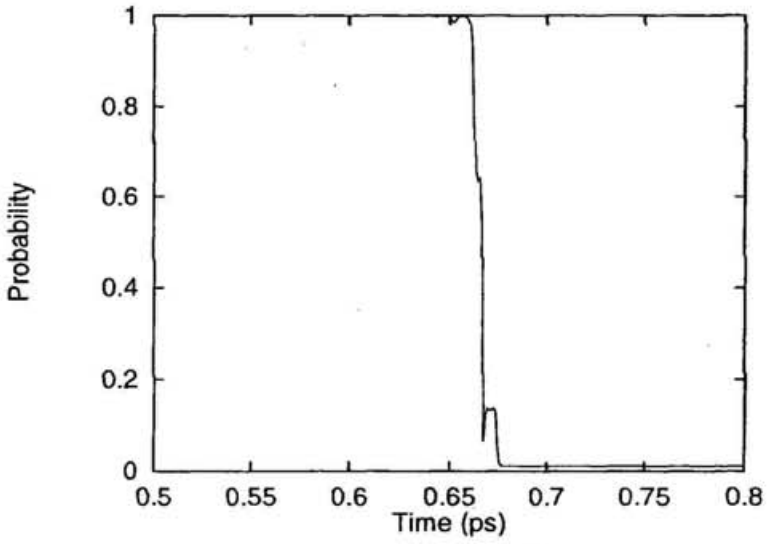

(c) That of second VB state in the wavefunction

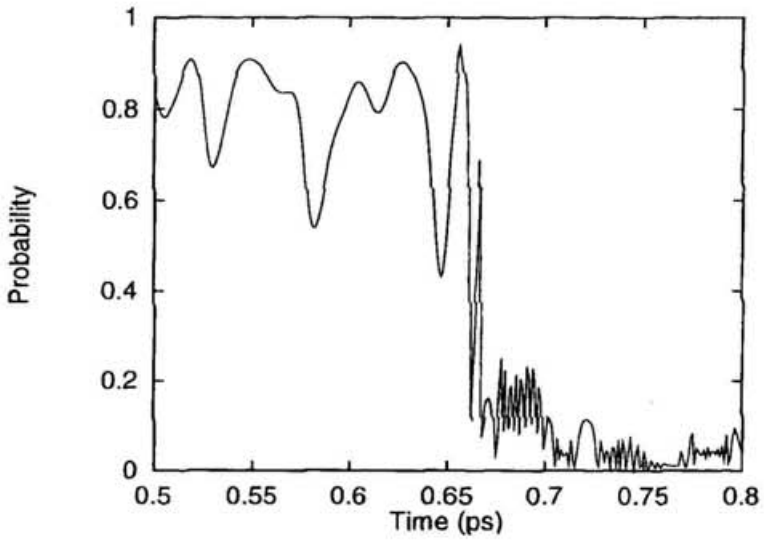

(d) The CCC bending angles (in deg)

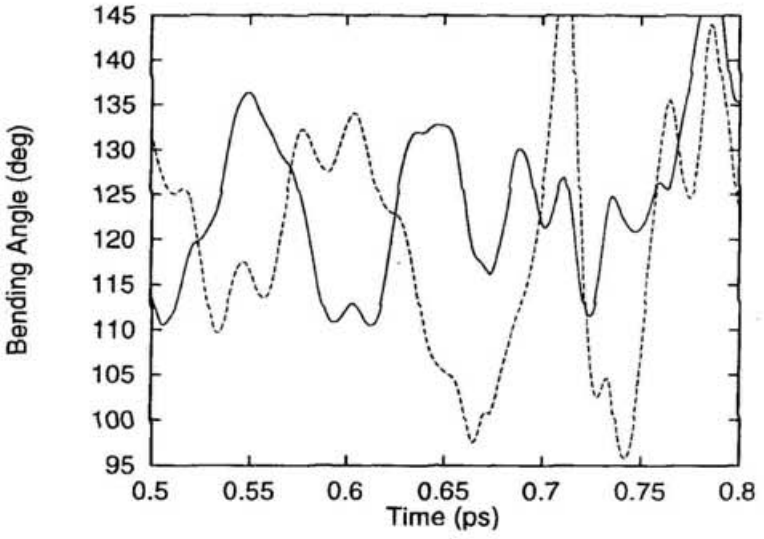

(e) The inner product of the nonadiabatic coupling and the velocity vectors as functions of time after excitation into 2^1Ag state, in a trajectory

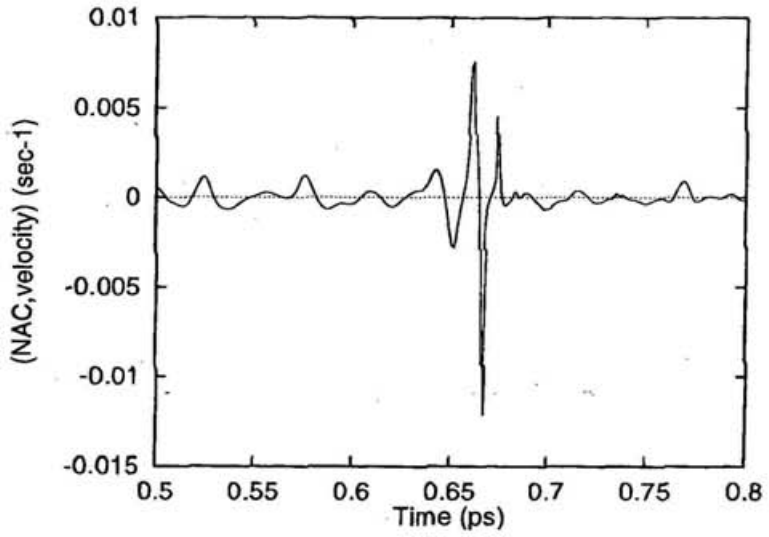

Figure 10.2: (a)The state energies and the total energy (in hartree), The 1^1Ag potential energy (solid line), 2^1Ag (long dashed line), the total energy (short dashed line) (b)the occupation probability of 2^1Ag in the wavefunction, (c)that of second VB state in the wavefunction, (d)the CCC bending angles (in deg), θ_1(solid line), θ_2(long dashed line), and (e)the inner product of the nonadiabatic coupling and the velocity vectors as functions of time after excitation into 2^1Ag state, in a trajectory.

(a) The state energies and the total energy (in hartree)

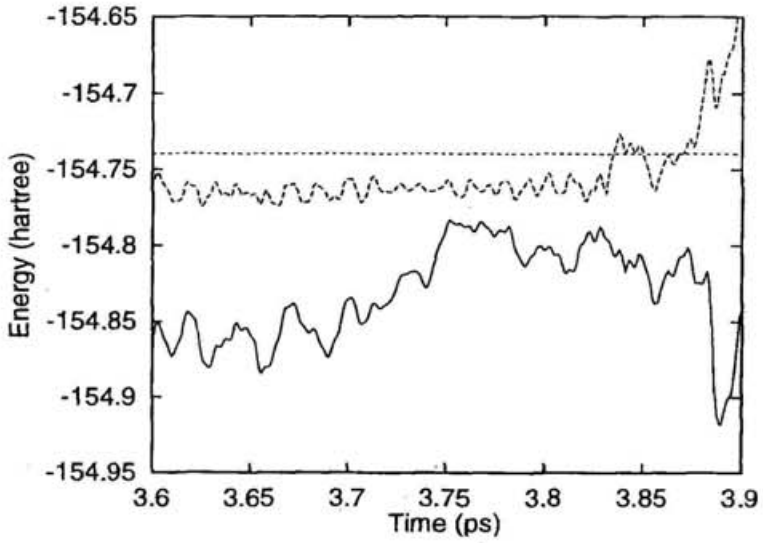

(b) The occupation probability of 2^1Ag in the wavefunction

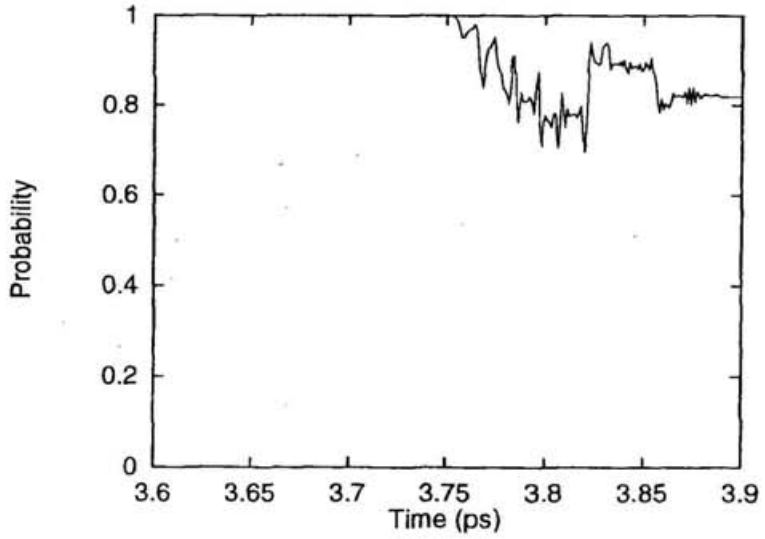

(c) That of second VB state in the wavefunction

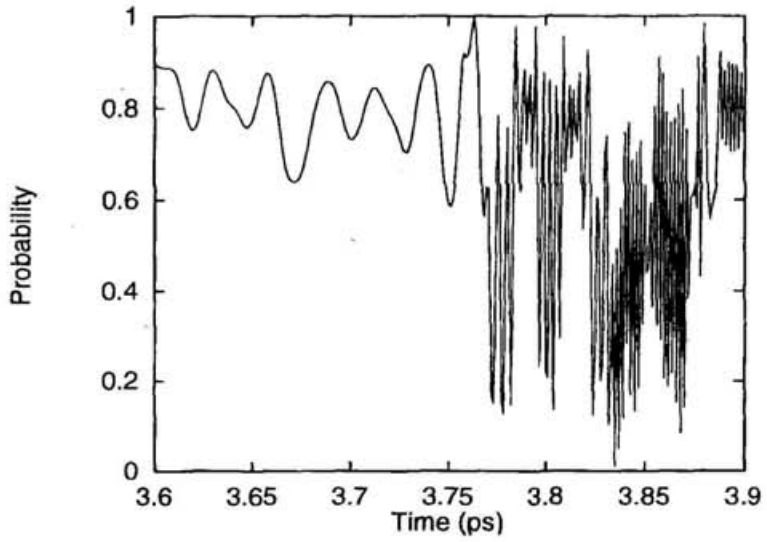

(d) The CCC bending angles (in deg)

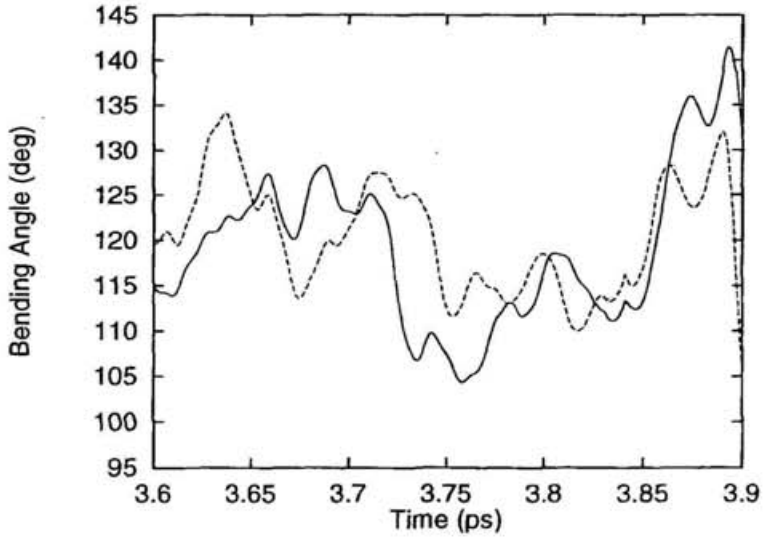

(e) The inner product of the nonadiabatic coupling and the velocity vectors as functions of time after excitation into 2^1Ag state, in a trajectory

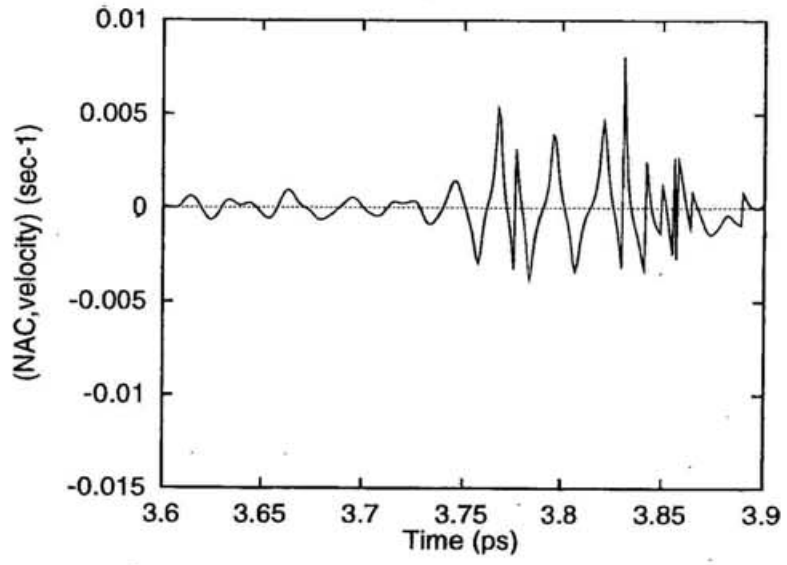

Figure 10.3: (a)The state energies and the total energy (in hartree), The 1^1Ag potential energy (solid line), 2^1Ag (long dashed line), the total energy (short dashed line) (b)the occupation probability of 2^1Ag in the wavefunction, (c)that of second VB state in the wavefunction, (d)the CCC bending angles (in deg), θ_1(solid line), θ_2(long dashed line), and (e)the inner product of the nonadiabatic coupling and the velocity vectors as functions of time after excitation into 2^1Ag state, in a trajectory.

10.2 Swarm dynamics

Let us consider the averaged behavior of the system as the swarm dynamics of all trajectories in the conformational space of the CC bond torsions. The probability density of the molecular conformations of the i'th state being at given CC bond torsional angels in trajectories is defined as

$$\Gamma_i(\alpha_1,\alpha_2,\alpha_3,t) = \frac{\Delta\alpha}{\sqrt{\pi}}\left\langle |\, a_i(t)|^2 \exp\left(-\frac{1}{\Delta\alpha^2}\left((\alpha_1(t)-\alpha_1)^2+ (\alpha_2(t)-\alpha_2)^2+(\alpha_3(t)-\alpha_3)^2\right)\right)\right\rangle \quad (10.1)$$

The Gaussian function with the exponent $-1/\Delta\alpha^2$ is used instead of Dirac's delta function for drawing contour surfaces with finite number of grid points. The contour surface of $\Gamma_i(\alpha_1,\alpha_2,\alpha_3,t)$ is shown in Figs.10.5 and 10.6, where a window width $\Delta\alpha = 5.0°$ is used. The coordinates system of $(\alpha_1,\alpha_2,\alpha_3)$ is indicated in Fig.10.4.

The swarm dynamics can be divided into three parts.

In the first stage of the dynamics (about 100 fs), the swarm is quickly diffused over the CC double bond torsions (Fig.10.5(a), (b) and (c)). This double bond isomerization induces the π electron energy decay and the weight of φ_2^{VB} state rapidly decreases (Fig.10.8(a) and (b)).

Along various C=C torsional paths, the avoided crossing between the 1^1Ag and 2^1Ag states produces local minima, as we have seen in Fig.4.1(d) and (e). Fig.10.5(d), (e) and (f) show that the swarm spreads over this low energy region of 2^1Ag in the next 600 fs (the second stage). This double bond isomerization induces the π electron energy decay and the weight of φ_2^{VB} state gradually decreases (Fig.10.8(a) and (b)).

In the third stage, after 700 fs from the Frank-Condon excitation, the swarm starts spreading over the region of the partially twisted three CC bonds (The left hand side of Fig.10.6), and this leads to the decrease of the occupation probability of the adiabatic 2^1Ag state (Fig.10.8(a)) The swarm

of the ground state $\Gamma_1(\alpha_1, \alpha_2, \alpha_3, t)$ is shown in the right hand side of Fig.10.6. We can see that the swarms initially appear around the triply twisted CC conformations. Although butadiene in 2^1Ag state travels through the large conformational space, the nonadiabatic transition to 1^1Ag state exclusively takes place near this three partially twisted CC bond conformations. Other nonplanar conformations, which was considered to be responsible for the internal conversion in previous studies, scarcely induce the nonadiabatic transition.

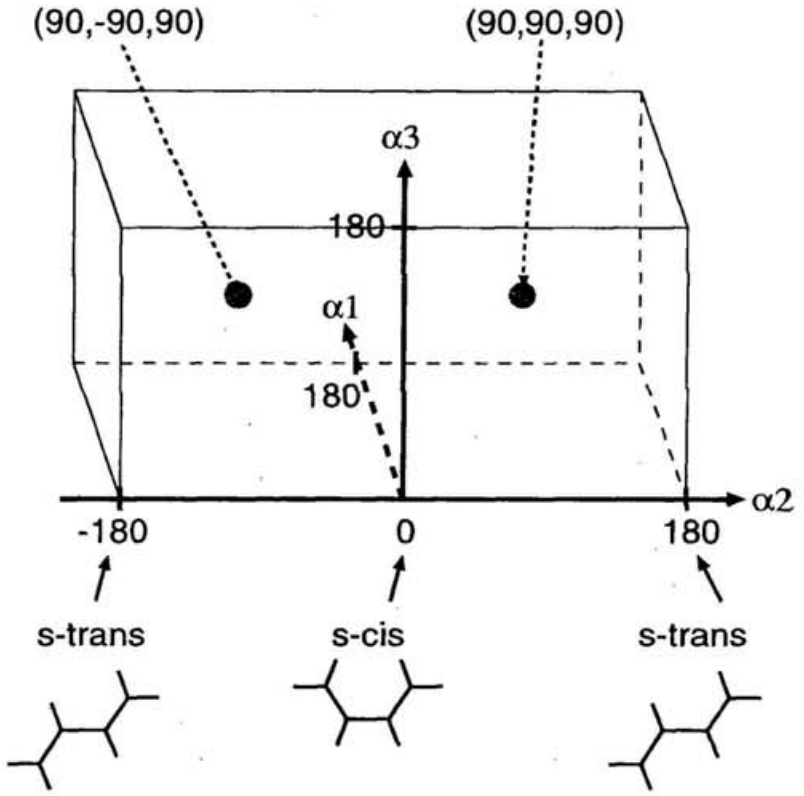

Figure 10.4: Conformational space over all three CC bond torsional degrees, $(\alpha_1, \alpha_2, \alpha_3)$ used to plot the contour surface of probability change in Fig.10.5-10.7. 1/4 of the entire region is shown. The coordinates α_1,α_3 (C=C torsion) span a half of the full range $[-180°, 180°]$.

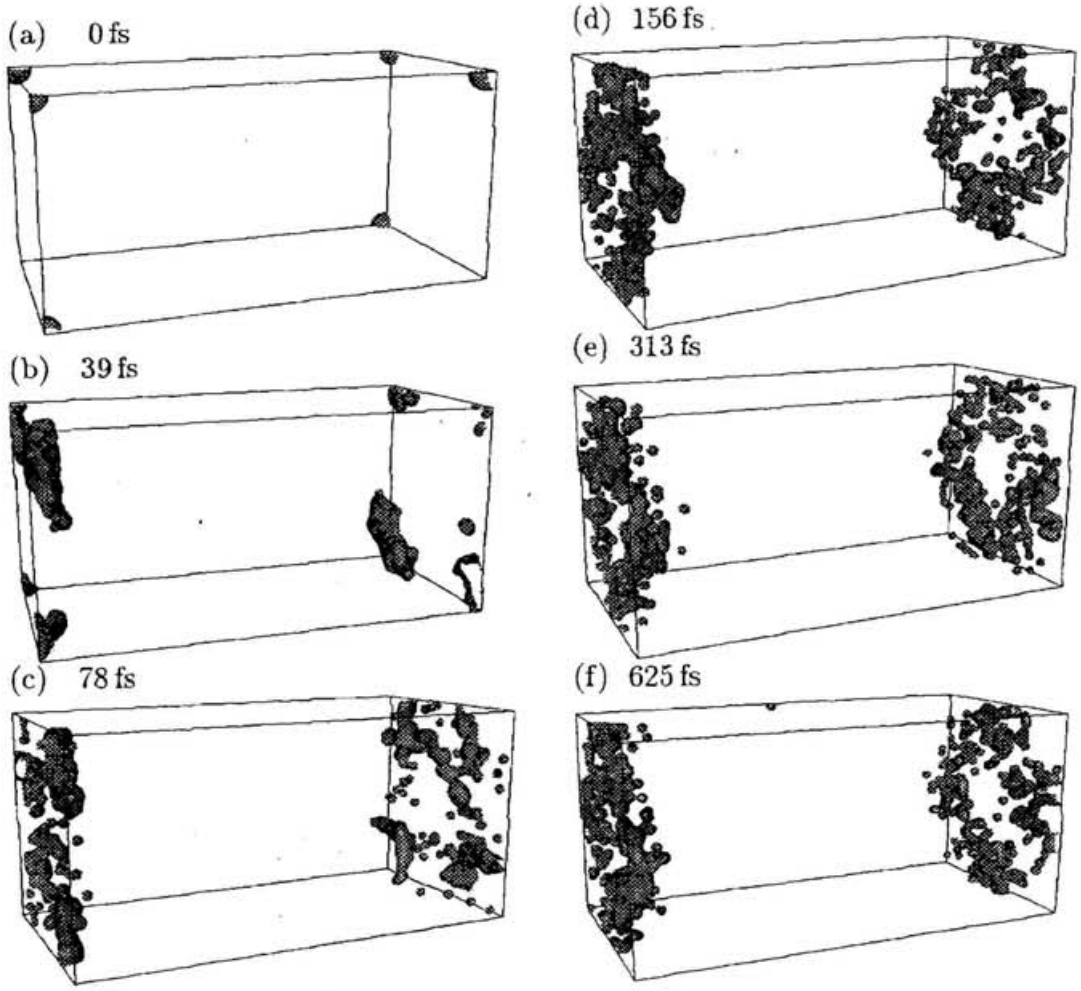

Figure 10.5: The time evolution of the 2^1Ag state occupation probability density $\Gamma_2(\alpha_1, \alpha_2, \alpha_3, t)$. See Fig.10.4 for the coordinates. (a)$t = 0\,fs$, (b)$t = 39\,fs$, (c)$t = 78\,fs$, (d)$t = 156\,fs$, (e)$t = 313\,fs$, (f)$t = 625\,fs$

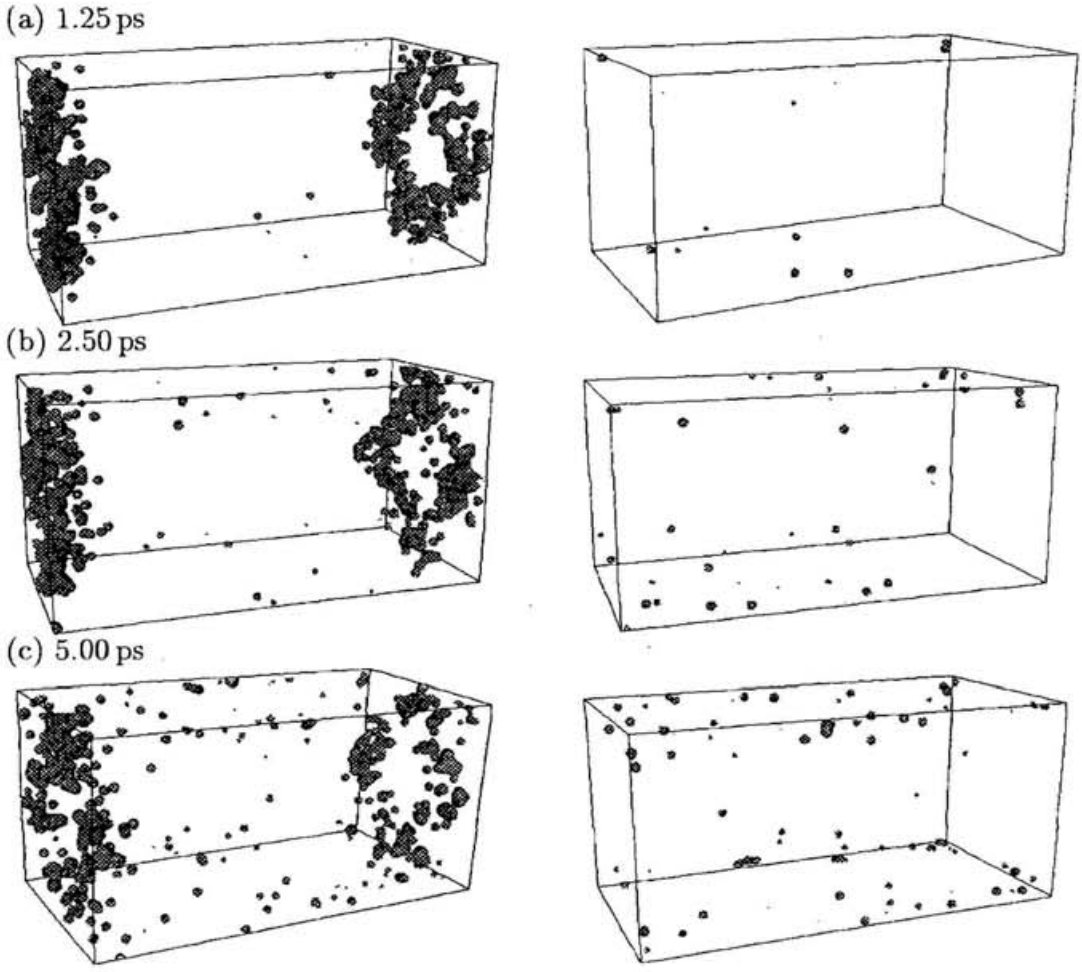

Figure 10.6: The time evolution of the 2^1Ag and 1^1Ag state occupation probability densities $\Gamma_2(\alpha_1, \alpha_2, \alpha_3, t)$, $\Gamma_1(\alpha_1, \alpha_2, \alpha_3, t)$. See Fig.10.4 for the coordinates. (a)$t = 1.25\,ps$, (b)$t = 2.50\,ps$, (c)$t = 5.00\,ps$ The figures in the left hand side are for 2^1Ag and those in the right hand side are for 1^1Ag.

In order to determine the exact locus where the facile nonadiabatic transition takes place, we define the transition density function $J_i(\alpha_1, \alpha_2, \alpha_3)$ for the CC bond torsional angles α_i as

$$J_i(\alpha_1, \alpha_2, \alpha_3) = \frac{\Delta\alpha}{\sqrt{\pi}} \left\langle \int_0^T \left(\frac{d}{dt} |a_i(t)|^2 \right) \exp\left(-\frac{1}{\Delta\alpha^2} \left((\alpha_1(t) - \alpha_1)^2 + (\alpha_2(t) - \alpha_2)^2 + (\alpha_3(t) - \alpha_3)^2 \right) \right) dt \right\rangle , \quad (10.2)$$

which indicates the molecular geometries where the system makes an nonadiabatic transition from an adiabatic state to the other in the trajectories. Here, $\alpha_i(t)$ is the torsional angle of the molecular conformation in a trajectories. The Gaussian function with $\Delta\alpha = 3.0°$ is used instead of Dirac's delta function. The contour surface of $J_1(\alpha_1, \alpha_2, \alpha_3)$ averaged over all 515 trajectories is plotted in Fig.10.7. We can see that 73 % of the state transition mainly occurs around at three partially twisted CC bonds conformations and only occasionally takes place at two CC double bonds twisted conformations. At the latter conformations, although a significant nonadiabatic coupling exists, the energy gap is not small (see Figs.4.1(d) and (e)). Hence, the phase of the expansion coefficients $a_i(t)$ changes so rapidly that the total effect of the nonadiabatic coupling becomes small, $a_i(t + \delta t) - a_i(t) \sim 0$.

(a) 96.3 %

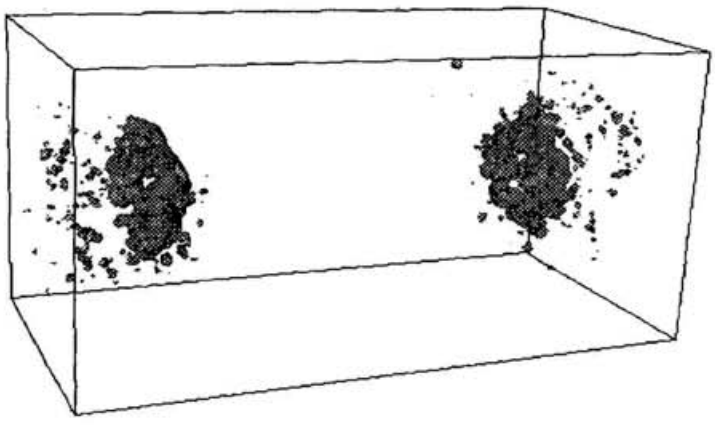

(b) 76.6 %

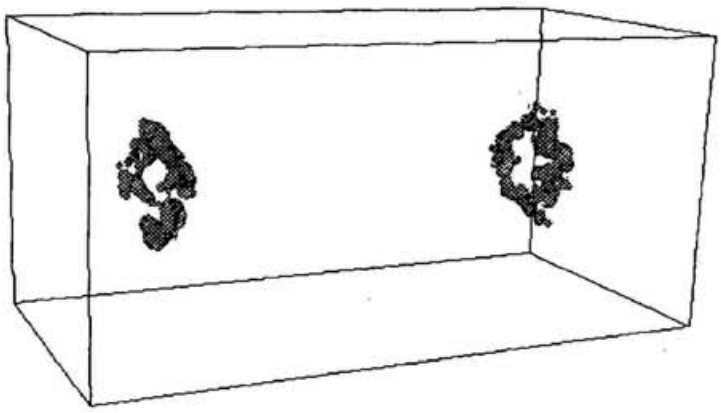

Figure 10.7: The contour surface of $J_1(\alpha_1, \alpha_2, \alpha_3)$. See Fig.10.4 for the coordinates. (a)The threshold value is 1.0×10^{-5} . The summation of the probability change within the iso-surface is 96.28 % of the total probability change. (b)5.0×10^{-5}, 72.62 %

10.3 Energy Relaxation

The energy flow among various modes in the nonadiabatic trajectories is shown in Fig.10.8(b). We here deal with the energies averaged over all 515 trajectories. The relaxation process can be divided into three stages and each of them corresponds to that of the swarm dynamics.

In the first stage, the weight of φ_2^{VB} state in the total wave function rapidly decreases in the first 100 fs as shown in Fig.10.8(a). The excited π electron energy flows into the bendings and the CC stretching potential, as well as its small portion goes to the σ torsions.

In the second stage of the next 600 fs, the remaining π electron energy flows into the σ bond energies. The CC stretching potential energies shown in Fig.10.8(b) oscillates rapidly during the first and the second stages when the vibrations of all trajectory are almost in phase. While the CH stretching shows the monotonic increasing in that period.

After these induction periods ($t > 700$ fs), the third stage starts. The occupation probability of the 2^1Ag state gradually and monotonically decreases; the CC stretching, CCC bending and torsional modes are the promoting modes enhancing the nonadiabatic transitions. The CH stretching and the CCH and HCH bending modes act as the accepting modes, not directly inducing the nonadiabatic transition. The irreversibility of the state occupation decay arises from the multidimensional nature of the nonadiabatic transition dynamics. Although the hopping from 2^1Ag to 1^1Ag state can take place whenever the probability change, $|a_i(t+\delta t)|^2 - |a_i(t)|^2$, exceeds a certain random number generated in the surface hopping method, the hopping back to the higher energy 2^1Ag state hardly occurs, since it requires that the energy gap should be compensated with the velocity components change parallel to the nonadiabatic coupling vector. Besides, the kinetic

energy is very swiftly distributed among many internal degrees of freedom in the ground state, and the volume of the conformational space where the system can travel through is expanded. Consequently the probability that the system pass through the region of the strong nonadiabatic coupling is relatively reduced. so that the nonadiabatic transition scarcely occurs.

(a)

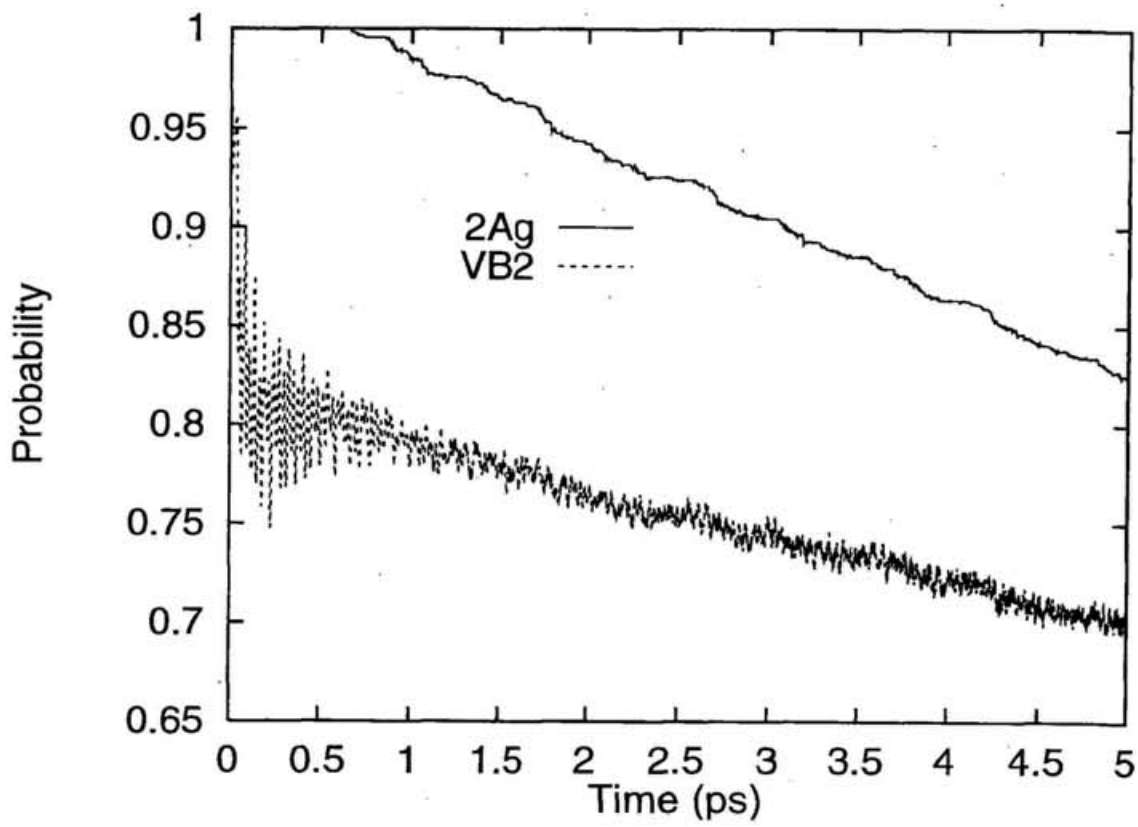

(b)

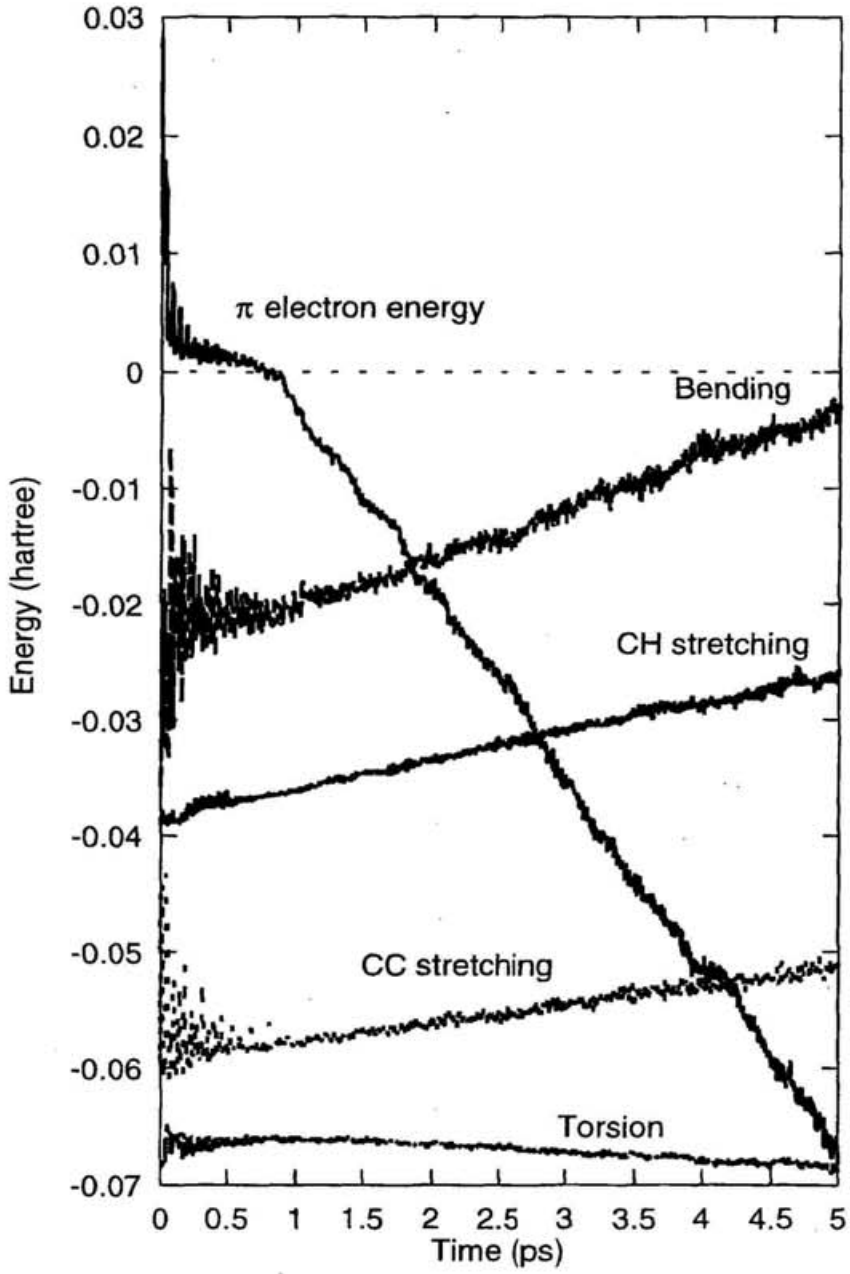

Figure 10.8: (a)The averaged occupation probabilities of 2^1Ag and second VB state, and (b)the π electrons energy of the occupied state, the stretching potential, the bending potential and the torsional potential energies as functions of time after excitation into 2^1Ag state averaged over all 515 trajectories. Energy values are arbitrary shifted in (b).

Chapter 11

Conclusion

The energy distribution relaxation among various modes and the mechanism of the nonadiabatic transition were carefully analyzed. The photoisomerization through the partially triply twisted conformations assisted by the CCC bendings, which brings the system close to the conical intersection, is confirmed to be the dominant channel of the internal conversion from the 2^1Ag state to the 1^1Ag state, and the π electron energy is shown to flow to other modes preceding the decay of the 2^1Ag state occupation probability.

Although the present model calculation explains the qualitative behavior of the relaxation process, a more elaborate model is required for quantitative analysis of the photoisomerization dynamics. The decay of the 2^1Ag state occupation probability should be much faster than that calculated by our model, as expected from that no fluorescence has been detected in experiments.[12] This is due to that only CC bond stretching, bending and torsion can induce the electronic character change of the 1^1Ag and 2^1Ag states in the present model. This restriction acquires the 2^1Ag state potential energy surface higher than that obtained from the CASSCF calculation with the fully geometry relaxation near the triply twisted CC conformations.

Bibliography

[1] F. Zerbetto and M. Z. Zgierski, J. Chem. Phys. 93, 1235 (1990)

[2] M. Olivucci, I. N. Ragazos, F. Bernardi and M. A. Robb, J. Am. Chem. Soc. 115, 3710 (1993)

[3] P. Celani, F. Bernardi, M. Olivucci and M. A. Robb, J. Chem. Phys. 102, 5733 (1995)

[4] P. Celani, M. Gravelli, S. Ottani, F. Bernardi, M.A. Robb and M.Olivucci, J.Am.Chem.Soc. 117, 11584 (1995)

[5] J. Michl and V. Bonačić-Koutecký, Electronic aspects of organic photochemistry (Wiley, New York, 1990)

[6] W. M. Gelbart, K. F. Freed and S. A. Rice, J. Chem. Phys. 52, 2460 (1970)

[7] B. Bagchi, G. R. Fleming and D. W. Oxtoby, J. Chem. Phys. 78, 7375 (1983)

[8] A. Warshel, Z. T. Chu and J. K. Hwang, Chem. Phys. 158, 303 (1991)

[9] G. J. M. Dormans, G. C. Groenenboo and H. M. Buck, J. Chem. Phys. 86, 4895 (1987)

[10] M. Perisco, J. Am. Chem. Soc. , 102 , 7839 (1980)

[11] L. Seiner and W. Domcke Chem. Phys. 186, 27 (1994) ; H. Köppel, W. Domcke and L. S. Cederbaum, Advan. Chem. Phys. 57, 59 (1984) ; R. Schnider, W. Domcke and H. Köppel, J. Chem. Phys. 92, 1045 (1990)

[12] V. Vaida, Acc. Chem. Res. 19, 114 (1986); J.B. Snow, Ph.D. Thesis, Wesleyan University, 1980; R. M. Gavin Jr., S. Risemberg, S.A. Rice, J.Chem.Phys. 58, 3160 (1973)

[13] J. C. Tully, J. Chem. Phys. 93, 1061 (1990)

[14] W. H. Miller and T. F. George, J. Chem. Phys. 56 , 5637 (1972)

[15] M. F. Herman, J. Chem. Phys. 81 , 754 (1984)

[16] S. Hammes-Schiffer and J. C. Tully, J. Chem. Phys. 101 , 4657 (1994)

[17] F.Webster, P.J.Rossky and R.A. Friesner, Comput.Phys.Commun. 63,494(1991)

[18] M.D. Feit, J.A. Fleck Jr.,A. Steiger, J.Comput.Phys. 47 , 412 (1982)

[19] M.D. Feit, J.A. Fleck, J.Chem.Phys. 78,301(1982)

[20] M.D. Feit, J.A. Fleck, J.Chem.Phys. 80,2578(1984)